PROJECTED CHANGES IN EXTREME PRECIPITATION AT SUB-DAILY AND DAILY TIME SCALES

by

Alex Morrison

A thesis submitted in partial fulfillment
of the requirements for the Master of Science
degree in Civil and Environmental Engineering in the
Graduate College of
The University of Iowa

August 2019

Thesis Supervisor: Associate Professor Gabriele Villarini

To my amazing friends in the SWD Crew who have been along with me on this difficult journey.
To my endlessly supportive parents and the rest of my great family who have always been there even when I didn't know I needed them.
To Kyle Scherner for keeping me grounded during my most stressful days.
To my cat Bella for keeping me company during my all-nighters working on homework, research, or studying for exams.

ACKNOWLEDGEMENTS

I would like to thank Gabriele Villarini for the opportunity to work with him and others at IIHR. Thank you for all the help along the way and teaching me how to be a better researcher and scientist. I appreciate your honesty and patience. It has been a great privilege to work with such an amazing engineer and researcher. I would like to also thank the rest of my thesis committee for this opportunity and for their support and feedback. I would like to also acknowledge Wei Zhang for all his help. This work would not have been possible without his help and assistance throughout this project.

I would like to acknowledge The College of Engineering for the Dean's Fellowship and their support throughout my research. I would also like to acknowledge The Graduate College for the Recruitment Fellowship and for their support throughout my research. Without their generous funding and resources, I would not have been able to accomplish everything I have in these two year in this program.

ABSTRACT

In recent decades, extreme meteorological events have become more frequent and more severe. Flooding, heavy precipitation and droughts, in particular, are a few of these extreme events that can cause widespread property damage and loss of life. The climate is always changing and there is a general agreement that the changes will be more amplified and occur more rapidly due to anthropogenic influences. As a result, it is expected that the societal and economic impacts of heavy precipitation, floods, and droughts will increase as the climate continues to rapidly change. For these reasons, continued research to improve extreme precipitation predictions and long-term projections is vital. With improved projections, society will be able to improve their efforts to prepare for and implement better management practices to effectively adapt to the changing climate and help reduce the impacts of a changing climate.

A great deal of progress has already been made in extreme precipitation research in relation to climate change. Overall, the tendency for dry areas to get drier and wet areas to get wetter has been identified. However, much of the work has focused on the daily timescale, and much less is known about sub-daily precipitation. It is becoming increasingly more important to consider this time scale because of evidence that climate change could have more of an impact on sub-daily (e.g., 3-hourly) rather than daily precipitation. To complicate the matter, there is still a need to evaluate the performance of global climate models in reproducing the precipitation statistics at the sub-daily time scales.

The goal of this work is to evaluate the projected changes in precipitation at both the daily and sub-daily time scales and, more specifically, understand whether daily or sub-daily precipitation extremes will change more through the end of this century. However, to understand future projections it is first vital to analyze model accuracy and determine how well global

climate models can reproduce the extreme precipitation statistics across the historical past. This is accomplished by comparing the historical runs for each model to observations during the same time period using several different methods, including a skill score analysis, using Taylor diagrams to visualize accuracy, and meridional plots that show intermodel variability.

The results from this analysis show model performance for daily extreme precipitation is higher than that of the 3-hourly extreme precipitation. Although there are few models that do an adequate job of producing reliable results at the sub-daily time scale, there is an overall significant increase in skill as the temporal resolution becomes coarser. Variability also exists among models, with sub-daily precipitation having more widespread variability across every latitude, but daily precipitation has a wider range in potential extreme precipitation that is focused more in the tropics. Model performance also varies by season, resulting in higher performance and less variability among models for individual seasons. These results also point to several models that consistently perform well for both sub-daily and daily extreme precipitation, but it is still worth remembering that there is no guarantee that a good performance during the historical period ensures a good performance in the futures as well.

The next part of the work focuses on the models with the highest performance in reproducing the observations. From there, it was possible to determine locations with the greatest changes in precipitation, the magnitude of changes, and whether sub-daily or daily extreme precipitation will be impacted more by climate change. Overall, extreme precipitation at both sub-daily and daily times scales is projected to increase globally. At the regional scale, precipitation is projected to primarily increase in the tropics, with smaller changes towards the poles. Areas of decreases in precipitation vary by model with the exception of a decrease in precipitation near the tropical Pacific Ocean that is seen in almost every model.

PUBLIC ABSTRACT

In the fall of 2012, Hurricane Sandy devastated the East Coast of the United States with widespread flooding, storm surge, and wave damage. It was one of the costliest hurricanes to ever strike the United States with recovery efforts struggling to provide sufficient relief. At least 72 deaths resulted directly from the storm with drowning being the most common cause of death. This same year, what would become one of worst droughts on record in California was just beginning, lasting from 2012 to 2015. Although several years of drought conditions are not unusual for California, this drought was the worst one seen in the last 1,200 years and resulted from exceptionally low precipitation and record-breaking high temperatures.

As the climate continues to change, events like these are projected to become more common: how much will extreme precipitation change through the end of the century? The objective of this work is to explore different precipitation projections and gain a better understanding of how precipitation is projected to change during the 21st century. The focus is on precipitation at both the sub-daily and daily scales, with regional and global analyses performed at the annual and seasonal scales. The results can be used to understand how the public and decision makers will need to adapt and plan for these changes. In addition, accuracy of the models is also examined to gain an understanding of how models need to be improved.

TABLE OF CONTENTS

LIST OF TABLES

LIST OF FIGURES

CHAPTER 1: INTRODUCTION

In the fall of 2012, Hurricane Sandy devastated the East Coast of the United States with widespread flooding, storm surge, and wave damage. It was one of the costliest hurricanes to ever strike the United States with recovery efforts struggling to provide enough relief. The death toll reached 117 people and the associated costs totaled $62 billion (Abramson 2013). Coastal states experienced widespread flooding from storm surge, with heavy precipitation experienced across many other states (Carbone et. al. 2015). At least 72 deaths resulted directly from the storm, with drowning being the most common cause of death.

The same year Hurricane Sandy occurred, California was just starting to experience one of the worst droughts on record, ultimately lasting until 2015 (Swain 2015). Although several years of drought conditions are not unusual for California, this drought was the worst one seen in the last 1,200 years and resulted from exceptionally low precipitation and record-breaking high temperatures (Seager 2015). Water resources became severely depleted resulting in multiple emergency drought proclamations being issued and in 2015 alone this devastating drought costed California's economy $2.7 billion and nearly 21,000 jobs (Rice 2015).

Overall, the aforementioned events are not isolated cases, but there has been an increasing amount of extreme meteorological events in recent decades. These extreme events have been both expensive and have caused great losses of life (Jenkins 2013). The 2014 report on climate change from the Intergovernmental Panel on Climate Change (IPCC) indicates that heavy precipitation events have largely increased over land and there are more regions where heavy precipitation has increased than decreased (IPCC 2014). Global trends in droughts, on the other hand, have been more difficult to track, with some studies indicating an increasing trend and others indicating little change in drought frequency since 1950 (Dai 2013; Sheffield et al.

2012). Precipitation has continued to increase in frequency and intensity through the first two decades of the 21st century, with annual maximum daily precipitation continuing to increase (Westra et al. 2012). In general, models are predicting a continued increase in global precipitation, with some specific regions such as the western United States, Southern Africa, and Australia experiencing a decrease in precipitation. Projections of mean precipitation indicate a general increasing trend in the deep tropics and extratropics, while a decreasing trend is expected in the subtropics. There is a general agreement among scientists that changes will be amplified by anthropogenic influences and stories like Hurricane Sandy and record-breaking droughts will become more common not just for the United States, but globally as the frequency and intensity of meteorological extremes change. More research is necessary to better understand these events and properly prepare to live in a rapidly changing climate.

1.1 Literature Summary

A great deal of progress has already been made in extreme precipitation research in relation to climate change, focusing on precipitation at the daily or longer time scales at both regional and global scales (e.g., Trenberth 2005; Zhu 2012; Chou 2012). Research focusing on global precipitation over the past several decades has shown a clear increasing trend in the intensity of global annual precipitation (e.g., Westra et al. 2012; Greve et al. 2014). The greatest increases have been in the tropics, mainly over the oceans due to an increase in atmospheric moisture from warming sea surface temperatures, and precipitation has also increased at higher latitudes in places such as Europe, Northern Asia, North America and South America (Trenberth 2011; Groisman 2012). Globally, consecutive dry days have decreased since the 1950s (Alexander 2015). However, in some regions, such as the western United States, droughts have increased in intensity and frequency since the 1970s (Dai et al. 2004; Chiang 2018). These

increases in droughts have also been largely occurring over land in the tropics and subtropics and some specific locations where there have been the greatest increases in drought conditions include the southwestern United States, southern Asia, and all throughout Africa and the Mediterranean region.

Extreme precipitation has increased globally, with record-breaking events becoming more frequent and severe. Research indicates this increase is due to global warming and climate change (Lehmann 2015). Specific regions are seeing greater increases in extreme precipitation, such as the tropics and northern subtropics, while some regions, such as the southern subtropics, have not experienced a large change (Lehmann 2015). With the climate continuing to rapidly change, this trend in increasing extreme precipitation is likely to continue as well.

Models are projecting an averaged global increase in precipitation (Kao et al. 2011; Sillman et al. 2013). Projections of mean precipitation generally indicate an increasing trend in the deep tropics and extratropics, a decreasing trend is expected in the subtropical regions (Kharin 2007; O'Gorman and Schneider 2009), and, more specifically, areas prone to drought conditions are expected to experience more severe droughts from climate change (Wang 2016; Rajsekhar 2017; Carrao 2017). These areas are also primarily located in the subtropics, including Australia, Central Americas, and parts of southern Asia.

However, there is still a great deal of uncertainty with these projected changes in precipitation. Uncertainty primarily comes from three sources: model uncertainty, scenario uncertainty, and internal variability of the climate system. For global precipitation through the 21st century, internal variability contributes to most of the total uncertainty for the first decade, model uncertainty generally dominates afterwards, and scenario uncertainty tends to be small

and almost negligible over land areas (Hawkins 2010). Ultimately this means that understanding and improving models is a vital part in the analysis of precipitation projections.

There are several well-known problems that exist for models, including difficulties with atmospheric-ocean coupling leading to a double Intertropical Convergence Zone (ITCZ) pattern, and research has shown this precipitation pattern is very common with global models (Lin 2007). In general, the greatest variability among models is in the tropics (Long et. al. 2015). Considering the tropics is also where the greatest changes in precipitation have already occurred, we will likely continue to see the greatest changes in precipitation in that region, and therefore it is a significant issue that this is also where models struggle the most.

1.2 Motivation

Research has shown changes in extreme weather are due to anthropogenic climate change (e.g., Anderegg 2010; Jankovic 2016; Mann 2017; Ornes 2018). Of all the expected changes, extreme precipitation is one of the costliest and most dangerous with the resulting flooding causing widespread damage and threat to both property and life (Doocy 2013). For these reasons, continued research to improve extreme precipitation predictions and long-term projections is vital, and with improved projections, society will be able to make efforts to prepare for and implement better management practices to effectively adapt to the rapidly changing climate, thus reducing the impacts of anthropogenic climate change.

Most of the research that has already been done has focused on precipitation at daily and longer time scales, and there has been little focus on the sub-daily scale. Three-hourly precipitation has not been as extensively looked at on a global scale as daily precipitation, and it is still often not evaluated in regional studies. Despite this limited knowledge, there is now evidence that the increase in CO_2 expected with climate change has more of an impact on sub-

daily precipitation extremes than daily ones (Zhang et al. 2017). In addition, research on 3-hourly and daily precipitation, specifically over Europe, has also shown there are important differences between the time scales that cannot be ignored (Scoccimarro et al. 2014). More specifically, Scoccimarro et al. (2014) found the differences in intense precipitation projections to be up to 40% between the two time scales, and whether there is a larger intensification of precipitation at the sub-daily or daily scale varies by location. Although this was a regional study, this new evidence has highlighted the importance of further research on the impacts of climate change at temporal resolutions finer than daily.

For these reasons, my work looks further into sub-daily and daily precipitation by exploring the impacts of climate change on global precipitation extremes at 3-hourly and daily time scales through the end of the century. The lack of research on sub-daily precipitation also means there has been little work on the capability of global climate models (GCMs) in reproducing the precipitation extremes' statistics at the shorter scales; this is a research question I will address in my thesis to gain a better understanding of the GCMs' performance, highlighting their strengths and weaknesses in reproducing precipitation extremes at the 3-hourly time scale.

1.3 Objective and Approach

The main objective of this thesis is to understand precipitation projections at the sub-daily and daily scale. To accomplish this, my work is divided into two parts. The first part of the research focuses on model verification. Building on the insights gained from the first part, the second part then focuses on the projections of extreme precipitation for each model, with a specific focus on models that performed the best based on the results in part one.

The analysis on model accuracy is accomplished by comparing the model output to observational data using a decomposition of the mean square error to produce a Skill Score for

each model (e.g., Hashino et al. 2007). From there, maximum precipitation for three different time periods (1985-2005, 2026-2045, and 2081-2100) for 16 GCMs from the Climate Model Intercomparison Project Phase 5 (CMIP5) are analyzed. Several maps and plots are made for each model, summarizing extreme precipitation projections for the models used in this study. For each model output, both the 3-hourly and daily time scales are used. The maximum value of precipitation at each grid point for every year or season was extracted, and then I computed the median of these maxima. The median was computed over computing the average to reduce the impact of outliers, it is considered to be more robust, and is easy to understand. This was done for the time periods of interest (1985-2005, 2026-2045, and 2081-2100) and for both 3-hourly and daily outputs. Representative Concentration Pathways (RCP) are used to understand possible precipitation projections. Some of the models do not have outputs for every RCP. A list of models used in this study and which RCPs are available for each model is shown in Table 1. To quantify the projected changes in extreme precipitation, I compare the future time slices (2026-2045 and 2081-2100) for the different RCPs to the historical period (1985-2005) for each model by subtracting the projections from the historical output. In addition to analyses at the annual scale, I also consider the four seasons: December-January-February (DJF), March-April-May (MAM), June-July-August (JJA), and September-October-November (SON).

Further analysis of the global change was conducted by taking each map and averaging precipitation horizontally to get a single value at each latitude. This was then plotted as a single meridional line on one plot to compare the historical run to each available RCP output. Similar to the global maps, this was done for annual sub-daily and daily precipitation and then broken down by season.

	Research Center	Country	Resolution	Reference	Available RCPs			
Models	-	-	-	-	2.6	4.5	6	8.5
ACCESS1-0	Research Organization/Bureau of Meteorology	Australia	192×145	http://www.bom.gov.au	N	Y	N	Y
ACCESS1-3					N	Y	N	Y
BCC-CSM1-1	Beijing Climate Center	China	128×64	http://bcc.ncc-cma.net/	Y	Y	Y	Y
CNRM-CM5	Centre National de Recherches Meteorologiques	France	256×128	https://www.umr-cnrm.fr/?lang=fr	Y	Y	N	Y
FGOALS-g2	State Key Laboratory of Numerical Modeling for Atmospheric Sciences and Geophysical Fluid Dynamics	China	128×60	http://www.lasg.ac.cn/english/	Y	Y	N	Y
GFDL-CM3	Geophysical Fluid Dynamic Laboratory (NOAA)	United States	144×90	https://www.gfdl.noaa.gov/	N	Y	N	Y
GFDL-ESM2G					Y	Y	Y	Y
GFDL-ESM2M					Y	Y	Y	Y
IPSL-CM5A-LR	Institute Pierre Simon Laplace	France	96×96	https://www.ipsl.fr/en/	Y	Y	Y	Y
IPSL-CM5A-MR			144×143		Y	Y	Y	Y
MIROC5	Atmosphere and Ocean Research Institute and Japan Agency for Marine-Earth Science and Technology	Japan	256×128	https://www.jamstec.go.jp/e/	Y	Y	Y	Y
MIROC-ESM			128×64		N	Y	N	Y
MIROC-ESM-CHEM					Y	Y	Y	Y
MRI-CGCM3	Meteorological Research Institute	Japan	320×160	http://www.mri-jma.go.jp/index_en.html	Y	Y	Y	Y
MRI-ESM1					N	N	N	Y
NorESM1-M	Norwegian Climate Center	Norway	144×96	https://cicero.oslo.no/no	Y	Y	Y	Y

Table 1: A list of CMIP5 models used in this study and the corresponding RCP output available for each model. ("Y" indicates the RCP was available for the model and "N" indicates the RCP was not available).

CHAPTER 2: DATA AND METHODOLOGY

2.1 Data Summary

The models used in this study are 16 GCMs that come from the CMIP5 (Table 1). The main goal behind creating the CMIP5 project was to better understand climate variability and major gaps in understanding of past and future climate change. CMIP5 provides a multimodel context for examining the ability to predict climate focusing on the forecast ability on decadal time scales, why models with similar forcings result in a range of responses, and assess the mechanisms responsible for model differences in feedbacks associated with the carbon cycle and with clouds that are poorly understood. Included in CMIP5 are four scenario runs or RCP that are based on a range of projections of population growth, technological development, and societal responses. The first scenario, RCP2.6, has radiative forcing increasing through the middle of the century before decreasing to 2.6 W/m^2, RCP4.5 and RCP6 are two intermediate scenarios with a low peak and decay in forcings, and RCP8.5 is the highest scenario with continual increases in radiative forcing through the 21^{st} century reaching a peak of 8.5 W/m^2 (Taylor 2012).

The GCMs used in this study include: two Commonwealth Scientific and Industrial Research Organization/Bureau of Meteorology (CSIRO-BOM) models (ACCESS1-0 and ACCESS1-3); the Beijing Climate Center Climate System Model version 1.1 (BCC-CSM1-1); the Centre National de Recherches Meteorologiques (CNRM-CM5); the Flexible Global Ocean Atmosphere-Land System model Grid-point Version 2 (FGOALS-g2); two National Oceanic and Atmospheric Administration (NOAA) Geophysical Fluid Dynamics Laboratory (GFDL) Earth System Models (GFDL-ESM2G and GFDL-ESM2M), and the GFDL Coupled Physical Model Version 3 (GFDL-CM3); Institute Pierre Simon Laplace (IPSL) low resolution model (IPSL-

CM5A-LR) and high resolution model (IPSL-CM5A-MR); the Model for Interdisciplinary Research On Climate Version 5 (MIROC5), an earth system model (MIROC-ESM), an atmospheric chemistry coupled version of MIROC-ESM (MIROC-ESM-CHEM); the Meteorological Research Institute (MRI) earth system model Version 1 (MRI-ESM1), MRI's upgraded Coupled Global Climate Model Version 3 (MRI-CGCM3); and the Norwegian Earth System Model (NorESM1-M).

For observations, data from the Multi-Source Weighted-Ensemble Precipitation (MSWEP) Version 2 dataset were used. This is a dataset that spans from 1979-2017 and is available as 3-hourly and daily precipitation. It gives a full global coverage, similar to the models, by merging observations from gauges, satellites, and reanalyses. Observations from 76,747 rain gauges were used and to help correct for gauge under-catch and orographic effects, additional observations from 13,762 streamflow stations were used to infer catchment-average precipitation. This method was used to determine both 3-hourly and daily precipitation observations (Beck et al. 2018).

2.2 Methodology

The quantity of interest is the median of the annual/seasonal maximum over the historical period (1985-2005) and the 21st century (2026-2045 and 2081-2100), for both the 3-hourly and daily time scales. Observations and model outputs were compared pixel by pixel after regridding the former to the resolution of each of the GCMs. As stated in Chapter 1.3, the capability of the GCMs in reproducing the historical records was quantified using a decomposition of the mean square error to obtain a Skill Score, SS_{MSE}, for the median maximum precipitation annually and seasonally and the sub-daily and daily scale (e.g., Hashino et al. 2007; Murphy 1987):

$$SS_{MSE} = 1 - \frac{MSE}{\sigma_o^2} \quad (1)$$

SS_{MSE} can then be broken down into three parts to better understand model accuracy and help identify areas the models might be lacking (e.g., Hashino et al. 2007; Bradley at al. 2016; Murphy 1987):

$$SS_{MSE} = \rho_{mo}^2 - \left[\rho_{mo} - \frac{\sigma_m}{\sigma_o}\right]^2 - \left[\frac{\mu_m - \mu_o}{\sigma_o}\right]^2 \quad (2)$$

$$SS_{MSE} = PS - SREL - SME \quad (3)$$

where ρ_{mo}^2 represents the potential skill (PS or the square of the correlation coefficient) which is the skill that could be obtained in the absence of biases and ranges from 0 to 1; μ_m and μ_o signify the means of modeled and observed precipitation, respectively; σ_m and σ_o are the standard deviation of modeled and observed precipitation, respectively. The second term of Equation (2) in the right side of the equation represents the conditional bias, which is known as slope reliability (SREL). The last term of Equation (2) is the unconditional bias or the standardized mean error (SME). The decomposition of the SS (SS_{MSE} or SS) allows me to pinpoint potential issues and quantitatively analyze the capability of the GCMs in reproducing the observations. Equation (3) shows a rewritten form of Equation (2) with PS, SREL, and SME written in their proper locations.

An SS_{MSE} value of 1 represents a perfect agreement, and as the value decreases, the accuracy of the model decreases. For a model to obtain a high SS_{MSE} we want PS to be high and

SREL and SME to be low. A model can have a high PS, but if biases are also high, it will not perform well.

Taylor diagram was used as an alternative analysis of model performance, which allows us to compare several models to observations in terms of their correlation, their root-mean-square (RMS) difference (through the root-mean-square error), and the ratio of their variance (Taylor 2001). The correlation coefficient is commonly used to quantify pattern similarity, but it is not possible to determine whether the two patterns have the same amplitude of variation. RMS difference is used to quantify differences in two fields, but it is not possible to determine how much of the error is due to a difference in structure and phase and how much is due to difference in the amplitude. In other words, the correlation coefficient and the RMS difference provide complementary statistical information. This diagram ultimately allows the viewer to determine how much of the overall RMS difference is attributed to difference in variance and how much is due to poor pattern correlation.

In this diagram, the standard deviation is proportional to the radial distance from the origin, the correlation coefficient is related to the azimuthal angle, and the RMS error is centered on the reference point. The distance from the observational reference point and each model point represents the root mean square difference. Essentially, if a model were to fall exactly on the reference point, this would represent a "perfect" model with output identical to the observations. In addition to these synthetic and global measures, I also plotted maps directly comparing observations and model outputs for the historical time period to gain a better understanding of specific locations where models are underestimating or overestimating precipitation.

Past research has also shown that great variability exists among climate models (Lin 2007; Long et al 2015). To understand variability, the meridional plots for each model were used

to produce a composite plot of all the results. Individual plots were created for the historical run, annually and seasonally, and observations were provided again to understand overall model performance. In addition, the mean of all the models was calculated and plotted.

As stated previously in Chapter 1.3, projected trends in extreme precipitation were examined by taking the maximum value of precipitation at each grid point for every year or season and then computing the median of these maxima. The historical reference period used in this study was 1985-2005, and the two future time slices used were 2026-2045 and 2081-2100. Global maps were created showing the difference between the projected changes in extreme precipitation and extreme precipitation during the historical reference period for each model. From there, extreme precipitation was averaged horizontally to create a new set of meridional plots giving a single value for each latitude. Projected precipitation was again compared to the historical reference period and this was done for both annual and seasonal precipitation at both the sub-daily and daily times scales.

CHAPTER 3: MODEL EVALUATION

In this chapter, I will provide a quantitative evaluation of the performance of each of the models in reproducing the statistics of precipitation extremes across the globe both at the annual and seasonal time scales. These analyses are done for both 3-hourly and daily time scales. Global maps are also created for each model comparing model output to observations. Additional figures can be found in Appendix A-F.

3.1 Sub-daily Scale

3.1.1 Skill Score Analysis

The results from the SS analysis indicate model skill is rather low for sub-daily precipitation (Figures 1 and 2). Many of the models have SS values below zero, indicating a performance that is worse than what would have been obtained using climatology. Only eight of the 16 models have an SS value greater than 0, and only one model has a value greater than 0.5. Based on these results, the model with the greatest accuracy is FGOALS-g2, with an SS value just over 0.5. The model with the next highest value of SS is MRI-ESM1 (~0.4). MRI-CGCM3 and CNRM-CM5 also have values of SS that fall close behind 0.4.

Accuracy improves slightly for individual seasons. For DJF and MAM (JJA and SON), ten (nine) of the 16 models have positive SS values and the same models with positive values of SS annually perform comparably seasonally. IPSL-CM5-MR and MIROC5 are the two models that switch from negative SS annually to positive SS when broken into seasons; however, IPSL-CM5-MR still has a negative SS in JJA and SON. MIROC5 improves slightly more seasonally, starting with an SS that is equal to -0.05 annually and a positive value between 0.1 and 0.2 seasonally. However, like the results for the annual analyses, the values of SS remain fairly low seasonally, with most of them being less than 0.5. FGOALS-g2 consistently performs better than

the other models for every season. In addition, MRI-ESM1 also continues to do well seasonally, with ACCESS1-3 that performs comparatively well.

Figures 1 and 2 also show the breakdown of the SS, giving each model's results for PS, SREL, and SME. PS values range from 0.2 to 0.7 at the annual and seasonal scales. Models with high skill scores would need to have high values of PS to start with, and this is exactly what I found: FGOALS-g2 has the highest value of PS annually (~ 0.7), with seasonal values ranging from 0.5 to 0.7. However, for JJA FGOALS-g2 does not have the highest PS and instead BCC-CSM1-1 takes its place, with a PS value of about 0.6. Several other models with high PS values annually and seasonally include CNRM-CM5, MRI-CGCM3, MRI-ESM1, ACCESS1-0 and ACCESS1-3.

When I examine SREL and SME (i.e. conditional and unconditional biases, respectively), I find that conditional biases are generally lower than unconditional biases both annually and seasonally. Models with the highest SS have low biases, including FGOALS-g2. A few of the models that have moderate PS also have high biases, resulting in an overall low SS values. In general, models that ended with negative or low SS also had low PS and high SREL and SME.

Model accuracy is also shown using Taylor diagrams (Figures 3 and 4). Points that fall on the dashed line from the reference point will have the correct standard deviation and therefore have the correct variability. The results of the analysis are for annual (Figure 3) and seasonal (Figure 4) 3-hourly precipitation. Of the models analyzed, FGOALS-g2 falls the closest to the reference value, just outside the 10.0 mm root-mean-square (RMS) contour with a standard deviation (SD) just over 7.5 mm and correlation coefficient of about 0.7. However, based on this diagram, there are several other models that are performing about as well as FGOALS-g2 annually, including CNRM-CM5, MRI-ESM1, and MRI-CGCM3.

Like FGOALS-g2, CNRM-CM5 has a correlation coefficient of about 0.7, but has a lower SD that is farther away from the reference value with a value just under 7.5 mm. The RMS for this model is also near the 10-mm line. MRI-ESM1 and MRI-CGCM3, on the other hand, have a correlation coefficient lower than FGOAL-g2 at about 0.6 and have about the same value for SD of ~8.75 mm. These models have a slightly higher RMS value compared to the other high performing models, with a value of about 11 mm.

Another important note is the SD for all the models for sub-daily precipitation falls below the reference standard deviation (dashed line). This indicates the range of values seen in the models is much smaller (i.e. have a smaller variability) than observations. The correlation coefficient is also low for most models with the exception of a few with values greater than 0.6. Otherwise, most models have a correlation coefficient of about 0.4 or less. As a result, many of the models also have high MSE values (~13.0 mm). One interesting outlier is the MIROC-ESM-CHEM model which has a value of SD the closest to the reference; however, this model also has a low value of the correlation coefficient, resulting in the highest MSE of about 15 mm. Figure 1 shows the annual SS value for MIROC-ESM-CHEM to be about 0.3 and thus it still ranks the fourth highest in terms of SS despite having relatively high values of MSE and low values of the correlation coefficient.

The seasonal analysis (Figure 4) continues to have FGOALS-g2 as one of the most accurate models with it falling the closest to the reference point, especially in DJF and MAM. FGOALS-g2 does not strongly stand out with respect to the other models for the different seasons, with several GCMs being about the same distance from the reference point. For JJA and SON the models that perform about the same as FGOALS-g2 include ACCESS1-0 and ACCESS1-3. Similar to the results for annual precipitation, all of the models fall below the

dashed SD line and many have consistently low values of the correlation coefficient. MIROC-ESM-CHEM is again an outlier seasonally falling close to the SD reference line. In general, model skill remains low because of the low values of SD and correlation coefficients.

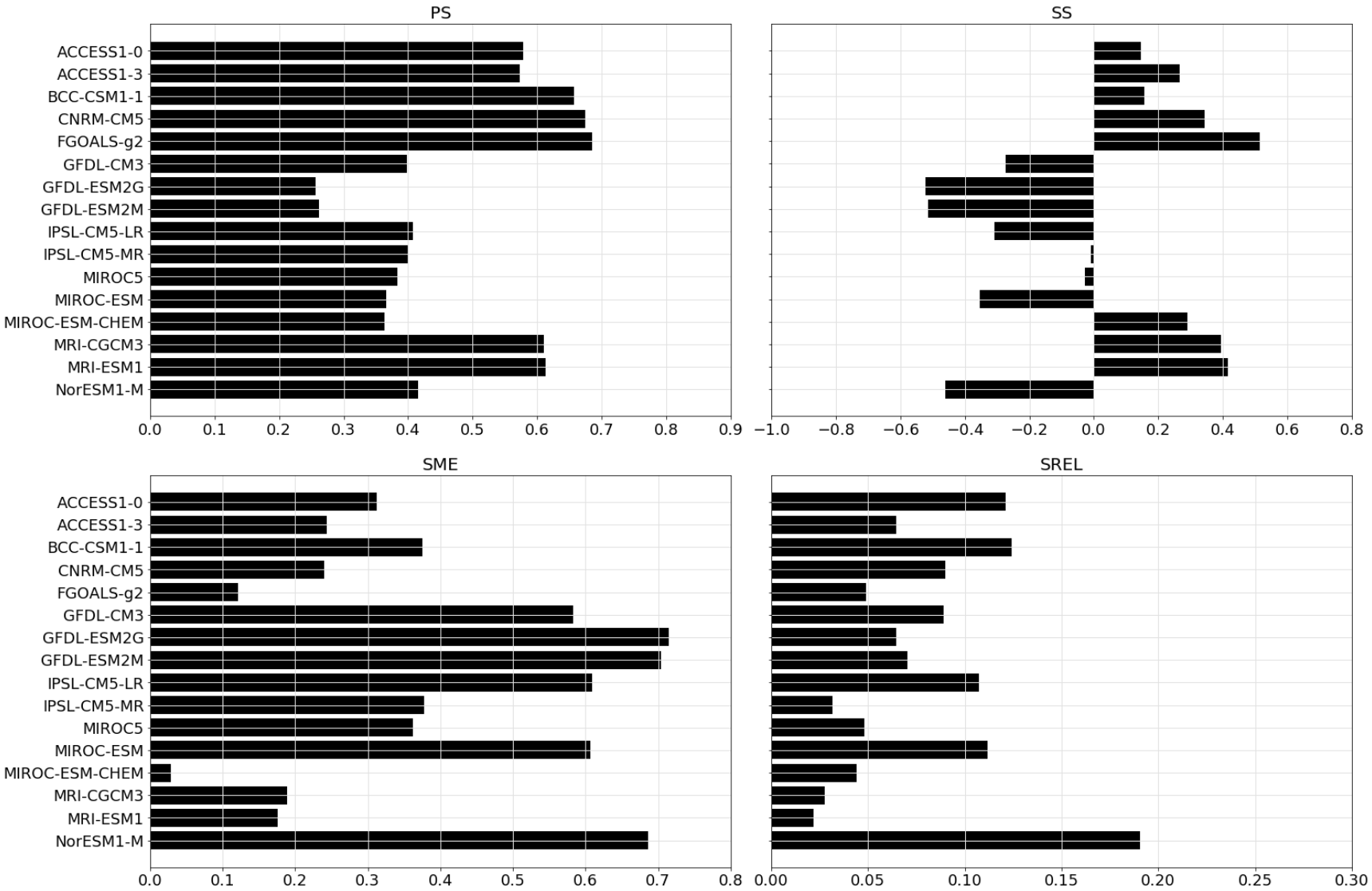

Figure 1: A set of bar graphs showing the values of SS (top right) and its different components: PS (top left), SME (bottom left) and SREL (bottom right) at the annual scale. The results are for model outputs at the 3-hour time scale.

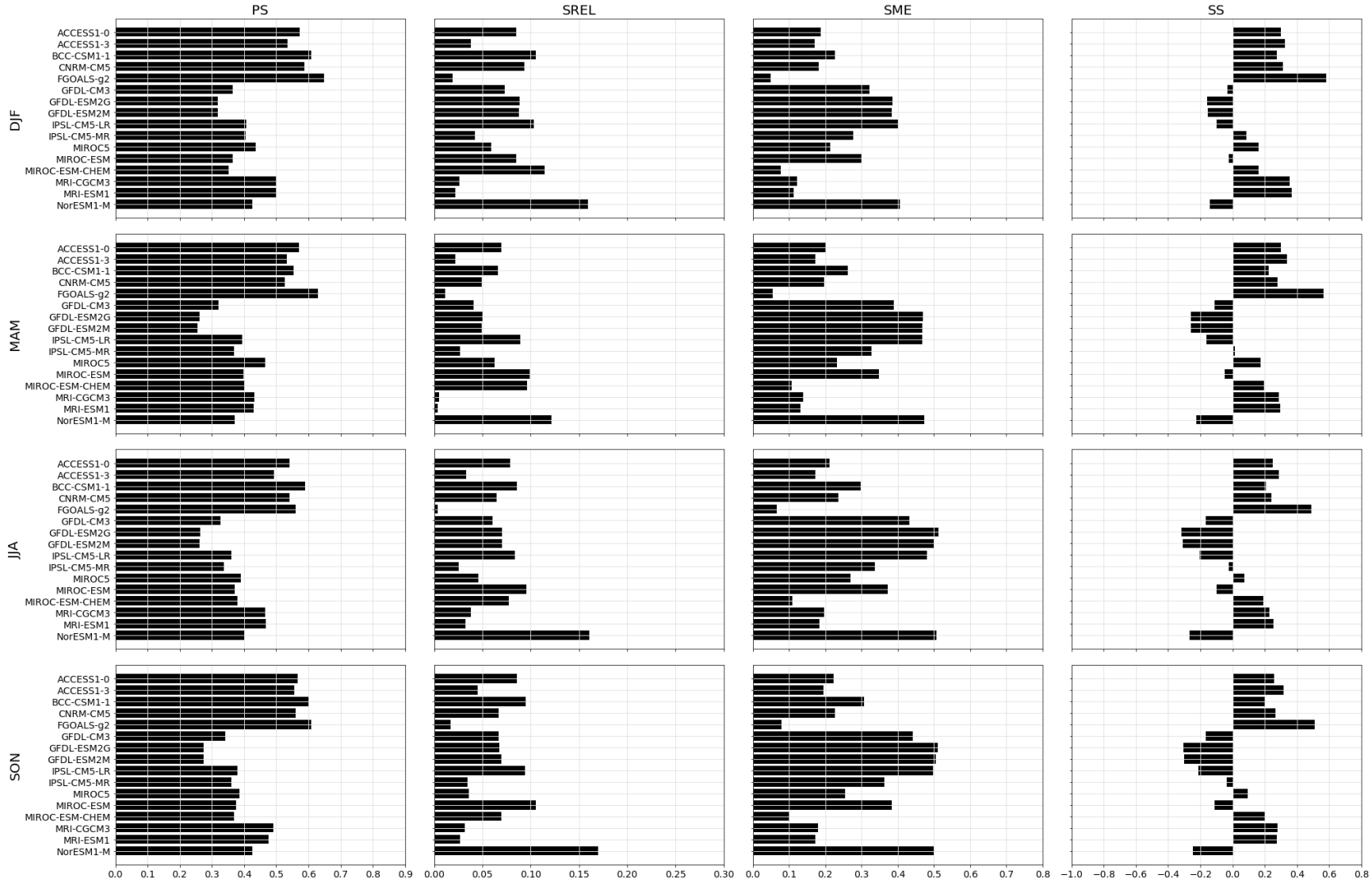

Figure 2: A set of bar graphs showing the values of SS (far right column) and its components: PS (first column) SREL (second column), and SME (third column). This was done for DJF (first row), MAM (second row), JJA (third row), and SON (bottom row). The results in this figure are for 3-hourly precipitation.

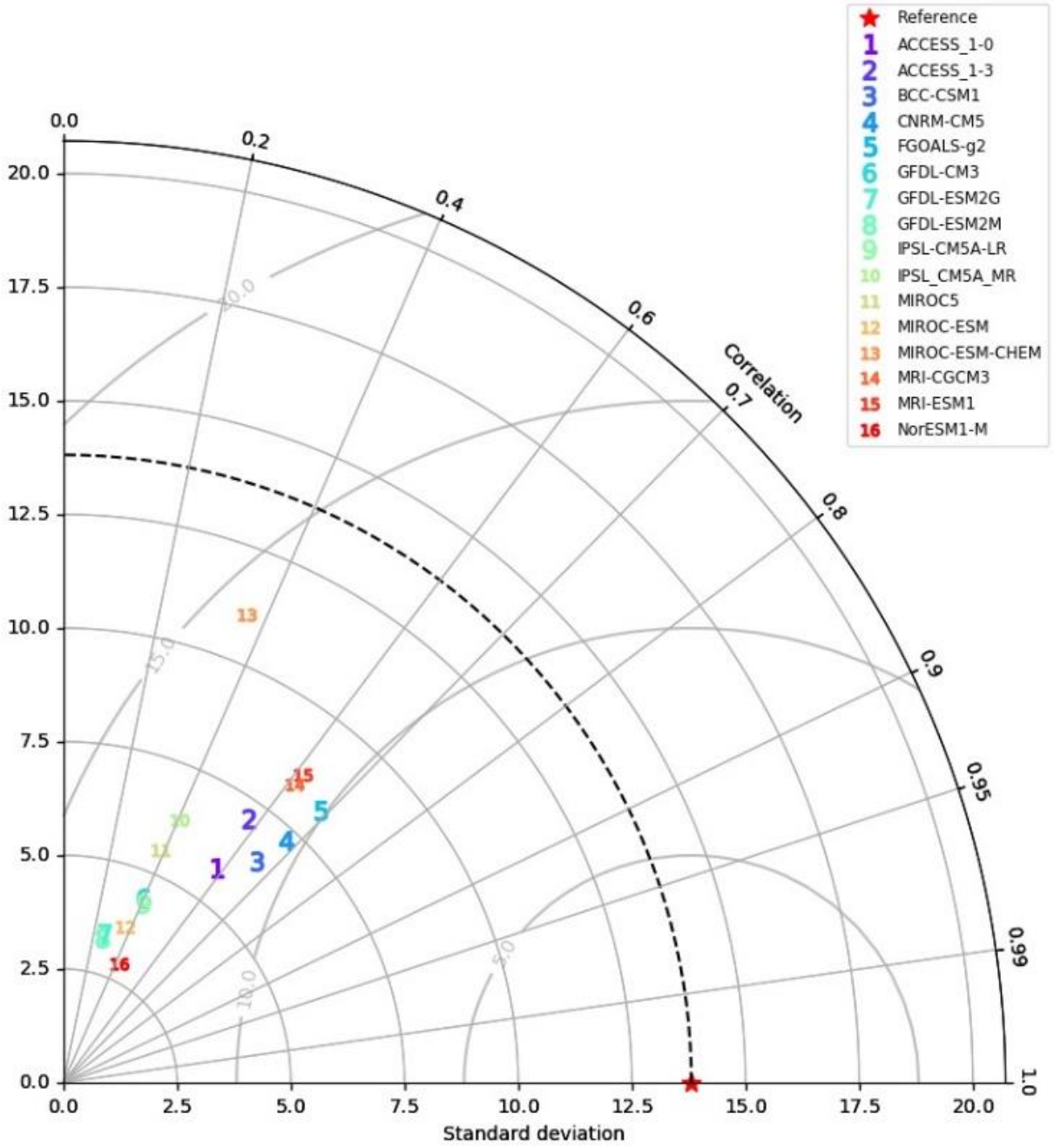

Figure 3: A Taylor diagram for 3-hourly annual precipitation. Colored numbers represent each of the 16 models considered here and a red star represents the observed precipitation. RMS difference is proportional to the distance from the reference point, SD is proportional to the radial distance from the origin, and the correlation coefficient is related to the azimuthal angle.

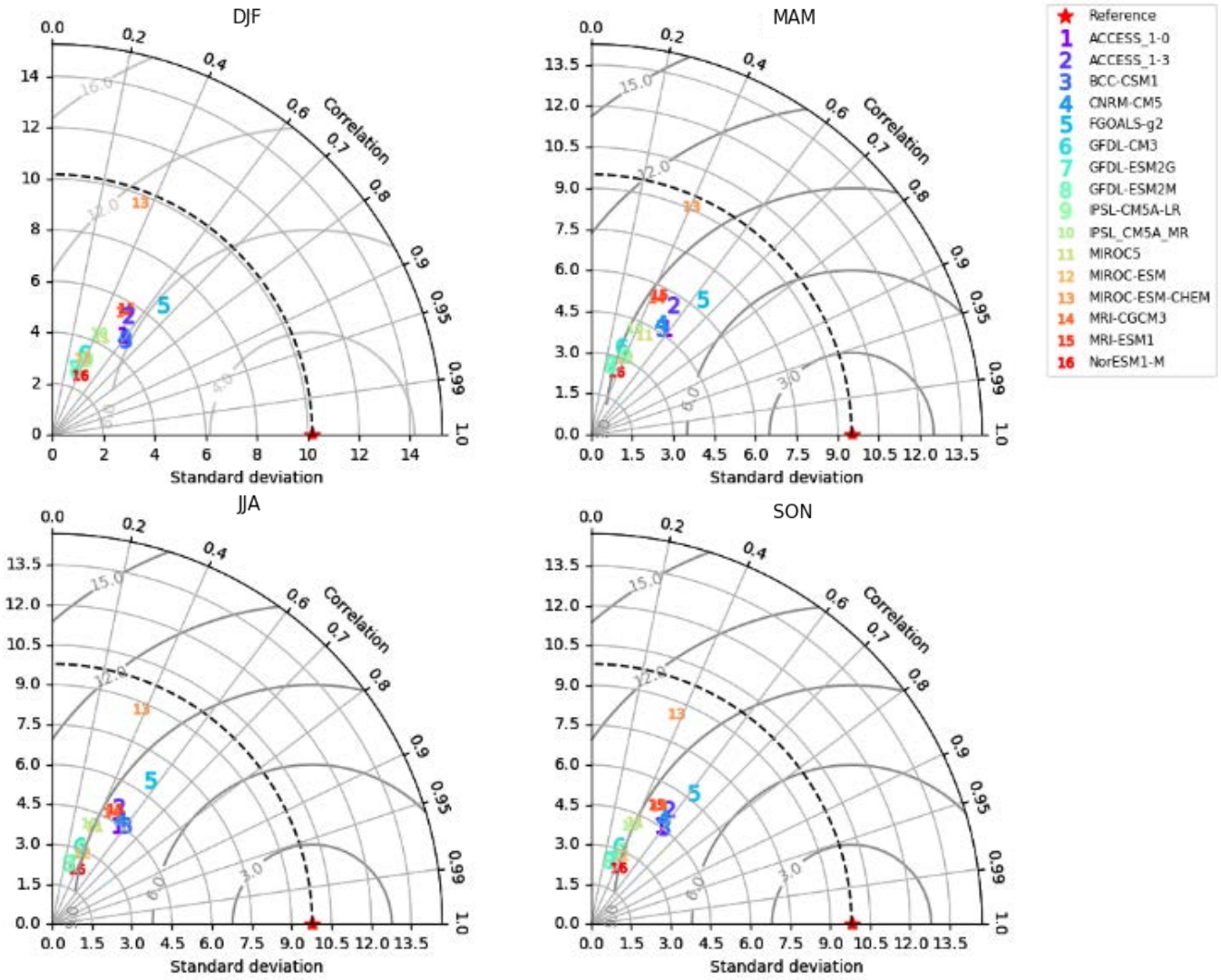

Figure 4: Same as Figure 3, but for DJF (upper left), MAM (upper right), JJA (lower left), SON (lower right)

3.1.2 Observation-Model Map Analysis

The map comparisons (Figures 5 and 6) show that most of the variability between models and observations is near the equator, largely between 30° N and 30° S, which is comparable to other analyses of global precipitation (Chadwick et. al. 2013; Long et. al. 2015). Models generally struggle at representing precipitation in the tropics due to problems with ocean-atmospheric coupling (Zhang et. al. 2015; Lin 2007). This typically results in a double ITCZ pattern which is fairly prominent in all of the best performing models in this analysis. FGOALS-g2 in particular shows a very well defined double ITCZ precipitation pattern (Figure 5). The pattern is clear for both annual and seasonal precipitation. Generally, the models tend to greatly underestimate precipitation, with the largest errors being in the tropics and better accuracy towards the poles.

Several models such as FGOALS-g2, MRI-CGCM3, and MRI-ESM1-1, greatly overestimate precipitation in the tropical Pacific and the El Niño Southern Oscillation (ENSO) region (Figure 5, Appendix E.1, and F.1). Other locations where the models tend to overestimate precipitation include Northern Africa, Australia, parts of Asia, and the western United States. However, specific areas of overestimation vary substantially by model and problematic areas for one model might not be for another.

Despite the errors in magnitude, most models still do an adequate job of matching the precipitation patterns. Maxima in annual precipitation are seen near the equator and extended over the Western Pacific Ocean and a minimum in precipitation is seen in the ENSO region. Almost every model consistently displays this feature. Another specific maximum can be seen in northern South America over the Amazon Rainforest. Models seem to underestimate the magnitude of this maximum, but it is still a prominent feature in most GCM outputs. Another

specific minimum in precipitation is in North Africa over the Sahara Desert, which is a location that some models tend to overestimate. One specific example of this is FGOALS-g2 which overestimates precipitation for this region (Figure 5).

Locations that experience the largest changes in precipitation throughout the year, which is shown in the seasonal analyses, are predominantly in the subtropics (about 30° N and 30° S). A maximum in precipitation is located just east of Asia over the Northern Pacific Ocean for annual precipitation, but this maximum weakens during certain times of the year. Precipitation is lower here during DJF and MAM and then increases in JJA and SON. This pattern is not well displayed in FGOALS-g2, but is more prominent in other models such as ACCESS1-0 and ACCESS1-3 (Figure 6 and Appendix B.1). Figure 6 shows the results for ACCESS1-0, which does a reasonable job of reproducing the precipitation patterns including some of the more specific seasonal changes seen in observations. However, this model struggles with the magnitude of precipitation significantly more than FGOALS-g2. ACCESS1-0 generally greatly underestimates precipitation, with only a few specific areas of slight overestimation.

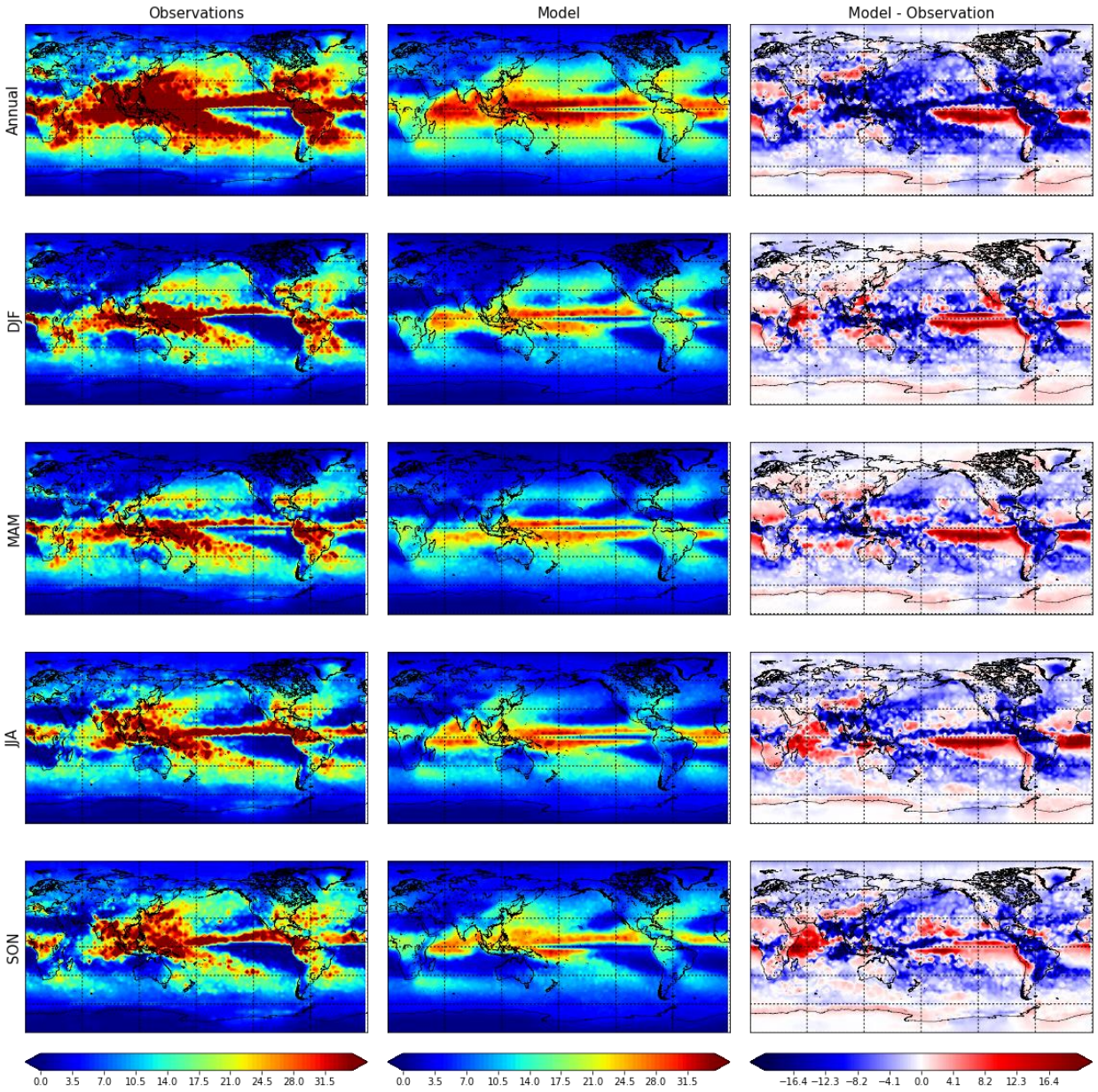

Figure 5: Maximum median 3-hourly precipitation (mm) for 1985-2005 for observations (left column), FGOALS-g2 (middle column), and the difference between them (right column). The results shown are for annual (first row), DJF (second row), MAM (third row), JJA (fourth row), and SON (bottom row) precipitation. The observations have been regridded to the GCM resolution (left column).

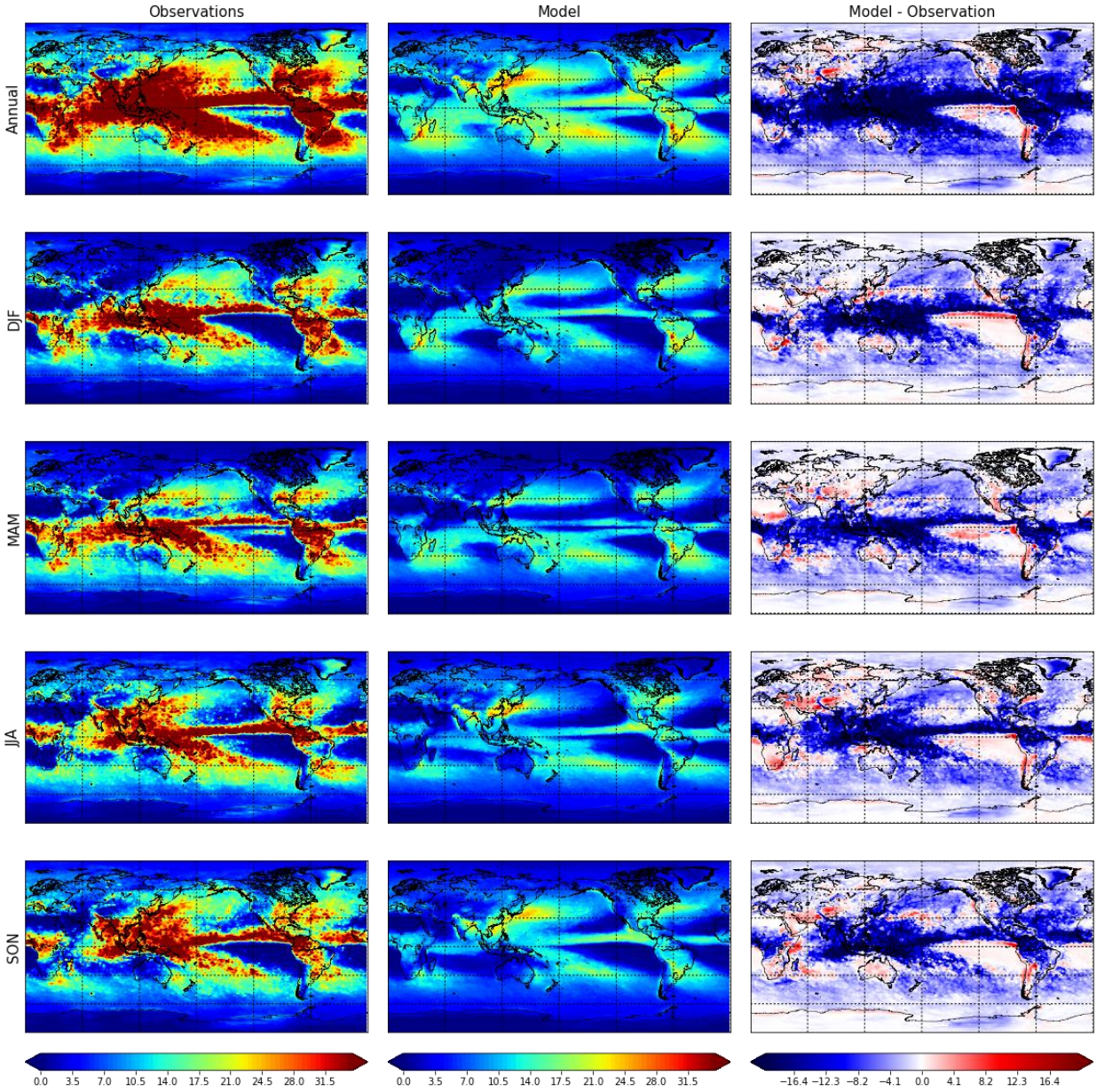

Figure 6: Same as Figure 5, but for ACCESS1-0.

3.1.3 Intermodel Variability

To further compare model accuracy and understand variability among models, composite meridional plots were created by averaging extreme precipitation horizontally for each model to get a single value at each latitude (Figure 7). The results for every model were then plotted together on one graph as dark grey lines and the range seen in the models is shaded in grey. Along with the meridional output for each model, observations and the mean of the models are also plotted in blue and red, respectively.

There is a great amount of variability among models at almost every latitude. For all the plots, variability is the greatest near the tropics with large peaks in variability just north and south of the equator. An additional maximum in variability is located in the mid-latitude regions. However, it is important to note that this additional maximum is largely due to one outlier (MIROC-ESM-CHEM) among all the models and when it is excluded, there is significantly less variability among models in the mid-latitudes both annually and seasonally. The least amount of variability is seen at the poles.

Model variability is the greatest for annual precipitation with a range of about 20 mm at its highest peak in the tropics (Figure 7). Seasonally, the greatest variability is seen during SON and SON at about 15 mm. The greatest variability for individual seasons also shifts locations throughout the year, but there are two clear peaks in precipitation just north and south of the equator, which also exhibits the greatest amount of variability. Variability is significantly greater in the northern hemisphere than the southern hemisphere in SON, slightly greater in the southern hemisphere in MAM, and the two peaks are about even in DJF and JJA. These peaks in variability range from about 10 to 15 mm.

Precipitation is largely underestimated by every model except for MIROC-ESM-CHEM, which again is a large outlier among the models and greatly overestimates precipitation in the

upper latitudes and up through to the poles. The mean of the model outputs was also included to help give a representation of all the models examined in this study, falling below the observed precipitation annually and for all four seasons at every latitude, with the differences between the two that are more pronounced annually versus seasonally. Annually, the largest difference between the two is about 25 mm, while seasonally the largest difference between the two is about 20 mm in JJA and SON. These large differences are both seen in the tropics at about 15° N. In both cases, this is a significant underestimation in precipitation and again highlights the significant problem these models have with accurately representing precipitation at the sub-daily scale.

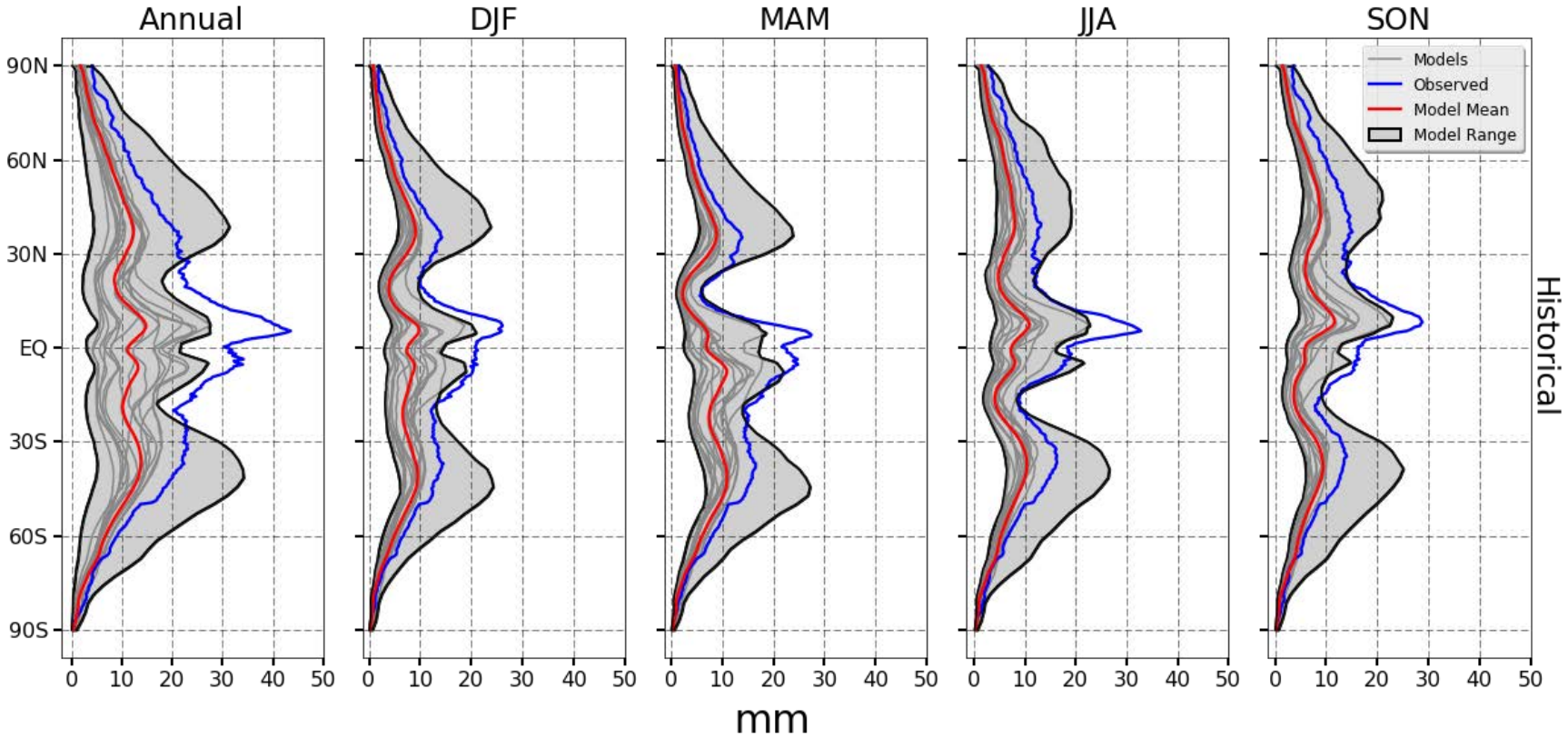

Figure 7: Meridional plots of the maximum median sub-daily precipitation (mm) for the models used in this study for the 1985-2005 reference period. Dark grey lines represent individual models and the shaded grey region is the range of values given by the models. The mean of all the models is also plotted (red) along with the observations (blue). This was done at the annual (Column 1) and seasonal scales: DJF (Column 2), MAM (Column 3), JJA (Column 4), and SON (Column 5).

3.2 Daily Scale

3.2.1 Skill Score Analysis

At the daily scale, the values of SS are significantly better both annually and seasonally compared to the results from the sub-daily analysis (Figures 8 and 9). Of the 16 models, all but two have a value of SS greater than 0 at the annual scale. Of these models, four of them have an SS value greater than 0.5, suggesting that they were able to reproduce the observations reasonably well.

FGOALS-g2 has the highest value of SS, but several other models have similar values including ACCESS1-0, ACCESS1-3, and CNRM-CM5. All four of these models have values of SS between 0.5 and 0.6. The two models that have negative SS values at the annual scale are still close to zero and are still greater than -0.1. From the seasonal analyses, it is clear model accuracy generally improves for individual seasons, and all models have SS values greater than zero for each season. SS values are consistently greater than 0.5 for most of the models across all four seasons, with the models that performed well annually continuing to show the best performance for individual seasons. FGOALS-g2 has the best SS for DJF and MAM while ACCESS1-0 has the best SS for JJA and SON. However, neither stands out far ahead of others models and several others perform about as well as ACCESS1-0 and FGOALS-g2.

Looking at the breakdown of the annual SS, PS is higher for all the models compared to the 3-hourly scale. Many models that performed poorly for the sub-daily analysis have improved greatly for the daily analysis, resulting in significantly higher PS and lower SREL and SME. For annual sub-daily precipitation, the smallest PS was about 0.25, which increases to ~0.4 at the daily scale. This is large leap in the PS and is a large reason why SS has also improved across the board. Models seem to have a higher SME compared to SREL, with BCC-CSM1-1 being an

exception. MRI-CGCM3 and MRI-ESM1 also have small SME values, but they still have SREL values that are fairly large compared to the other models that also end with high SS values. IPSL-CM5-MR has a near 0 SREL value, but a much higher SME, especially when compared to other models that perform well.

Seasonally, SREL and SME are both generally lower than SREL and SME values for annual precipitation in most cases. Models such as FGOALS-g2, ACCESS1-0, ACCESS1-3, and CNRM-CM5, the four models that have the highest SS values, have near 0 SREL, and SME has also decreased significantly for these models for each season. IPSL-CM5-MR, MRI-CGCM3, and MRI-ESM1 also have low SREL and SME seasonally.

Taylor diagrams were made as well for daily annual and seasonal precipitation (Figures 10 and 11). Annually, the model that falls the closest to the reference point is ACCESS1-0 with a correlation coefficient of about 0.75, SD of just over 24 mm, and an MSE of about 23 mm. FGOALS-g2 still performs well as the next closest model to the reference point. ACCESS1-3 and CNRM-CM5 also do a good job, with correlation coefficients greater than 0.6, MSE falling within the 30.0 mm contour line and SD between 24 and 30 mm. Unlike sub-daily precipitation, the models have a much larger spread with generally higher values of the correlation coefficient and SD values much closer to the reference line. All models for the daily analysis have correlation coefficients greater than 0.4, with most GCMs located above or just below the 0.6 line. SD values are less than the reference SD except for MRI-CGCM3 (which falls on the reference line), MRI-ESM1-1, and BCC-CSM1-1 (which both have SD values greater than the reference point).

The seasonal analysis continues to have ACCESS1-0 being the closest to the reference point for all four seasons, with FGOALS-g2 being close behind it for DJF and MAM. JJA and

SON both have several models clustered at about the same distance from the reference point just behind ACCESS1-0, including ACCESS1-3, MRI-CGCM3, MRI-ESM1, FGOALS-g2, and CNRM-CM5. These models also do well for DJF and MAM. Models have slightly more variability in accuracy for DJF and MAM and are slightly more clustered for JJA and SON. For all four seasons, the models continue to have values of the correlation coefficient greater than 0.4 (with several being greater than 0.6 and near 0.7) and all models except for BCC-CSM1-1 also fall between the 16.0 and 24.0 mm MSE contours.

The SD for MRI-ESM1-1 is greater than the observations for the annual analyses, but is smaller than the SD for all four seasons. MRI-ESM1-1 and MRI-CGCM3 are on or near the reference line for DJF and MAM, but are much smaller than the reference point for JJA and SON. BCC-CSM1-1, however, lies further away from all the other models across the four.

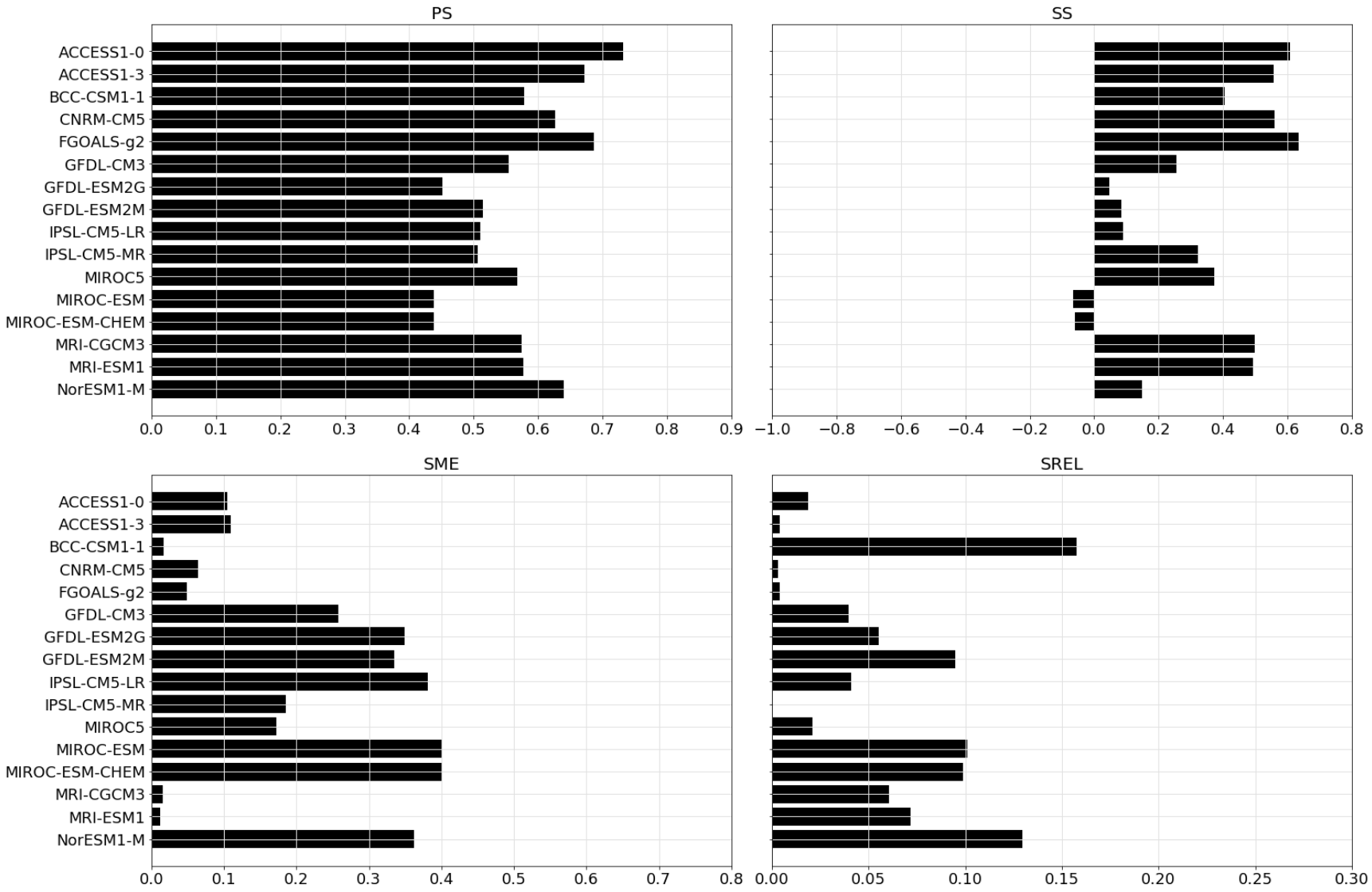

Figure 8: Same as Figure 1, but for annual daily precipitation.

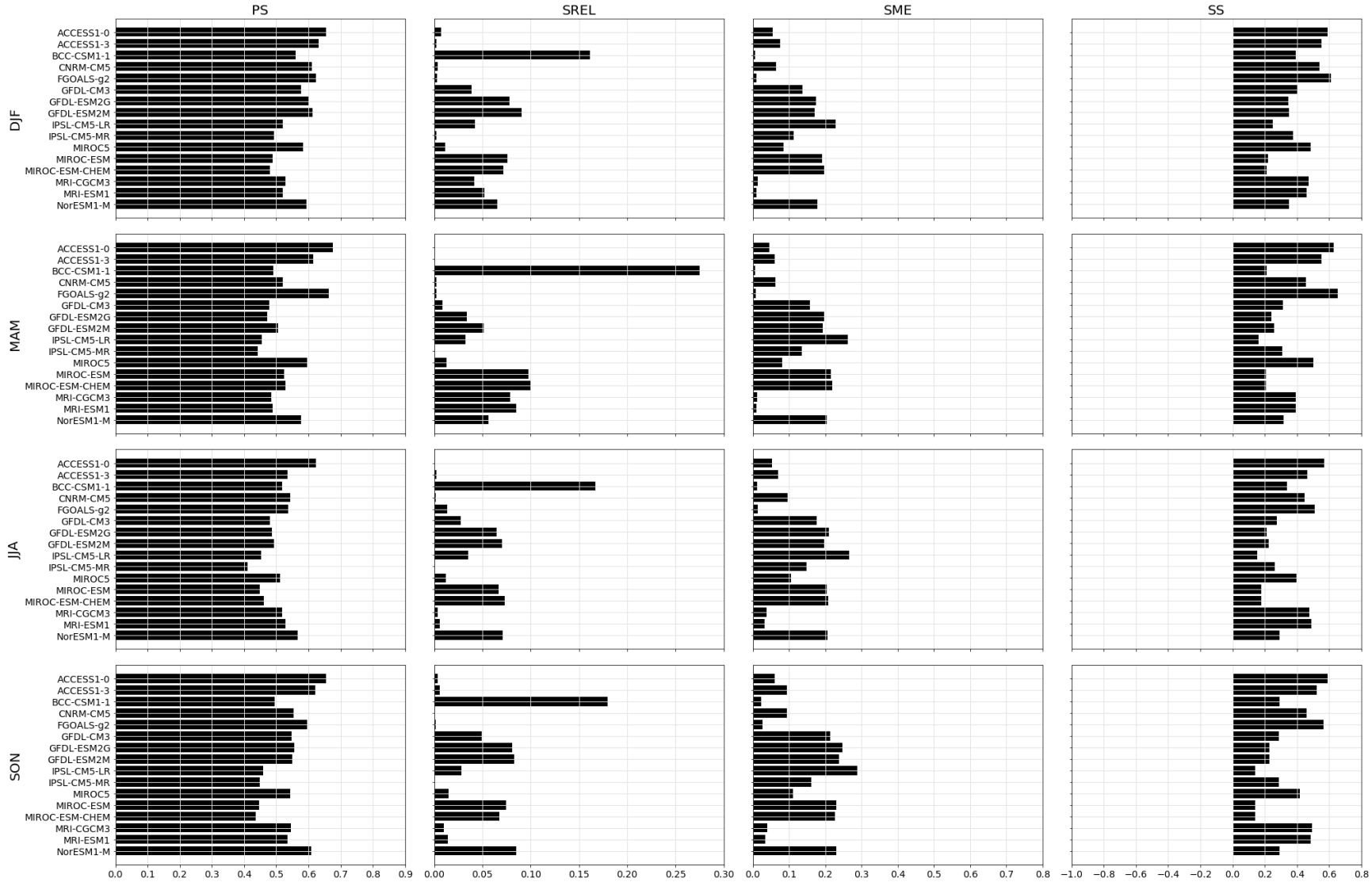

Figure 9: Same as Figure 2, but for seasonal daily precipitation.

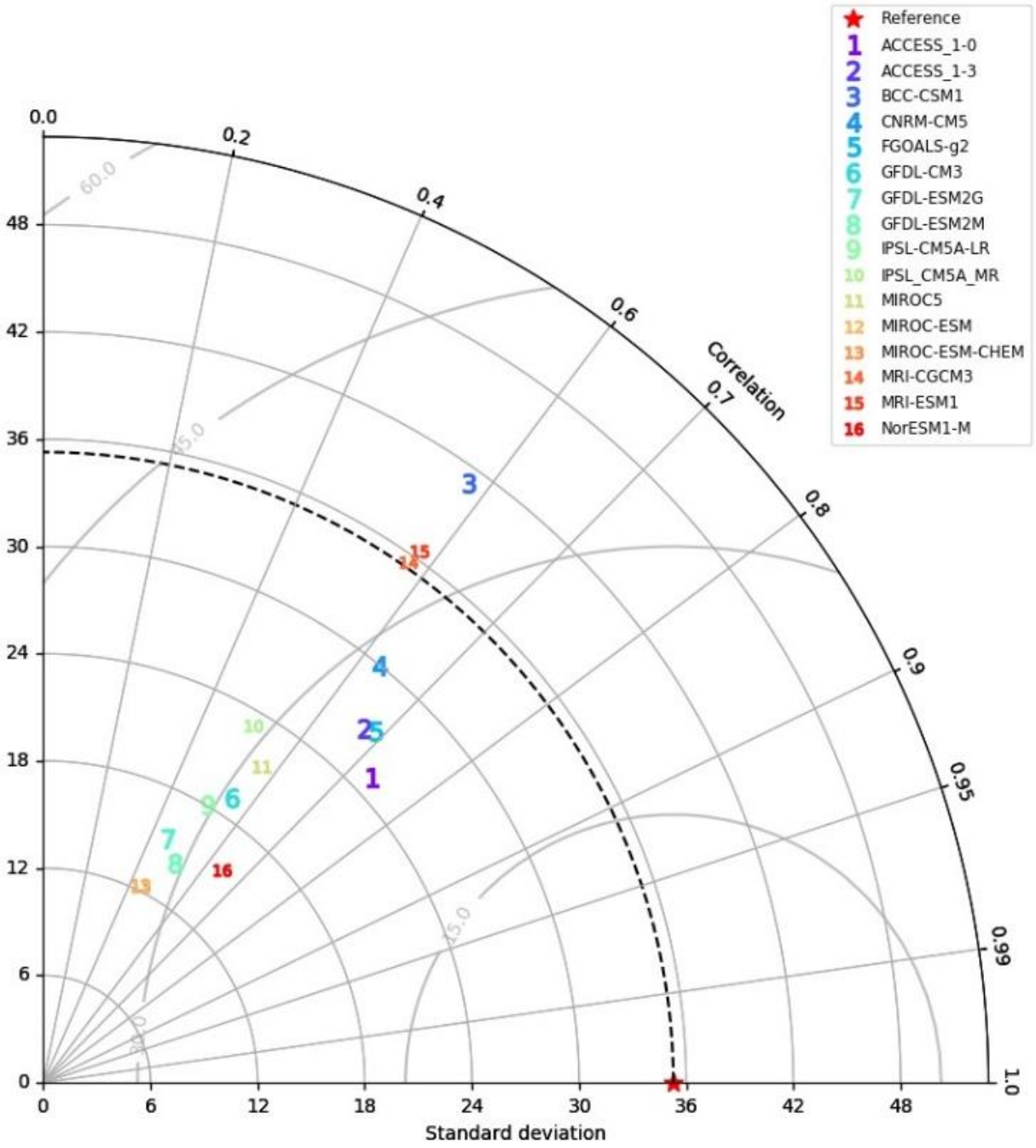

Figure 10: Same as Figure 3 but for daily annual precipitation.

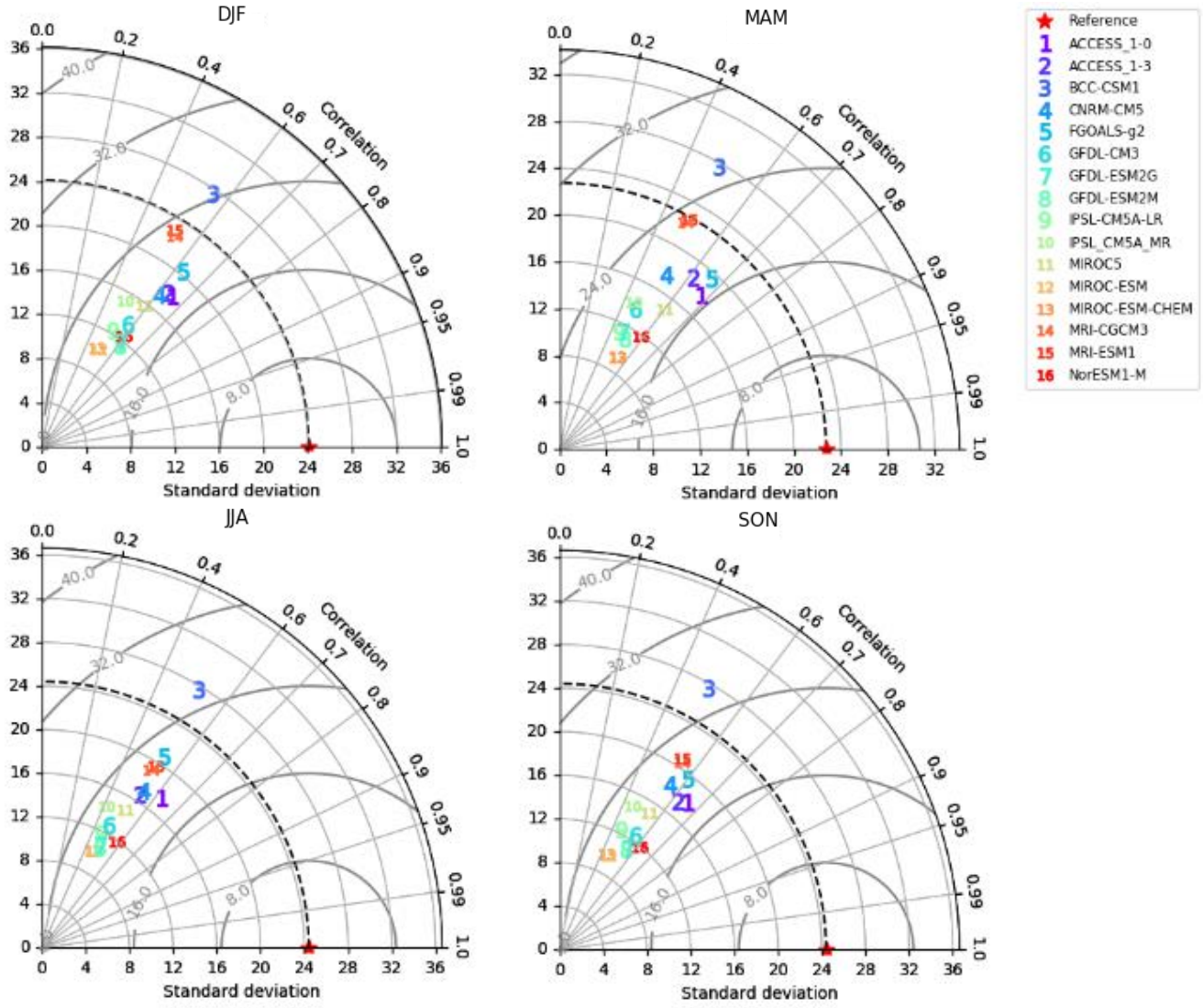

Figure 11: Same as Figure 4, but for daily seasonal precipitation.

3.2.2 Observation-Model Map Analysis

Like the SS analysis indicated, models do a reasonable job at reproducing observations in both location and magnitude at the daily scale (Figure 12). The pattern for daily precipitation is similar to the sub-daily one, with precipitation being the largest near the equator in the tropics and also the smallest in the ENSO region.

According to this analysis, models have the greatest problems with precipitation in the tropics. In general, model accuracy improves towards the poles with little to no errors in some areas and accuracy that is about the same for annual precipitation and individual seasons. Locations characterized by the greatest errors vary slightly by season, but the magnitude of the error is about the same annually and seasonally. Models tend to underestimate precipitation throughout most of the tropics and overestimate near the ENSO region and typically drier regions such as locations over Africa and Australia. Precipitation overestimation and underestimation still vary between models, but the areas listed are common problem locations for a majority of the models in the study. For example, FGOALS-g2 underestimates precipitation in the western United States (Figure 12); a few of the other best performing models (e.g., MRI-CGCM3 and MRI-ESM1-1; Appendix E.5 and F.5) also have large underestimation in this area, while models such as ACCESS1-0 and ACCESS1-3 (Appendix A.4 and B.4) appear to more accurately represent precipitation for this location.

Models also do a good job of representing the precipitation pattern shown in the observations. As previously described, the general pattern has the heaviest precipitation in the tropics near the equator with a minimum in precipitation near the ENSO region. There is also high precipitation in the west Pacific and Atlantic Oceans as far as 30° N and 30° S of the equator and there is an additional maximum in precipitation over the Indian Ocean. Heavy

precipitation shifts in location by season resulting in it being distributed more equally between hemispheres in the tropics in JJA and SON and a maximum in precipitation just north of the equator and east of Asia. In DJF and MAM, on the other hand, heavy precipitation decreases in this location. Models such as FGOALS-g2, ACCESS1-0, ACCESS1-3, CNRM-CM5, MRI-CGCM3, MRI-ESM1 all match the general pattern annually and also have this shift in precipitation with seasons (Figure 12, Appendix A.4, B.4, D.5, E.5, and F.5).

From the analysis of both sub-daily and daily precipitation, it is evident there are several models that do a reasonable job representing precipitation, but there are still significant differences in specific details and precipitation intensity. Of the 16 GCMs analyzed, FGOALS-g2 consistently performs the best or better than most models and, therefore, will be the focus of most of Chapter 4. However, because FGOALS-g2 does not perform significantly better than other models and there are several that perform just as well and even better in some cases for both sub-daily and daily precipitation, several other models will be discussed in the second part of this study as well. These models will be used to look further into specific locations that are projected to have significant changes in precipitation and understand the magnitude of the changes. With that said, it is worth remembering that there is no guarantee that a good performance during the historical period ensures a good performance in the futures as well.

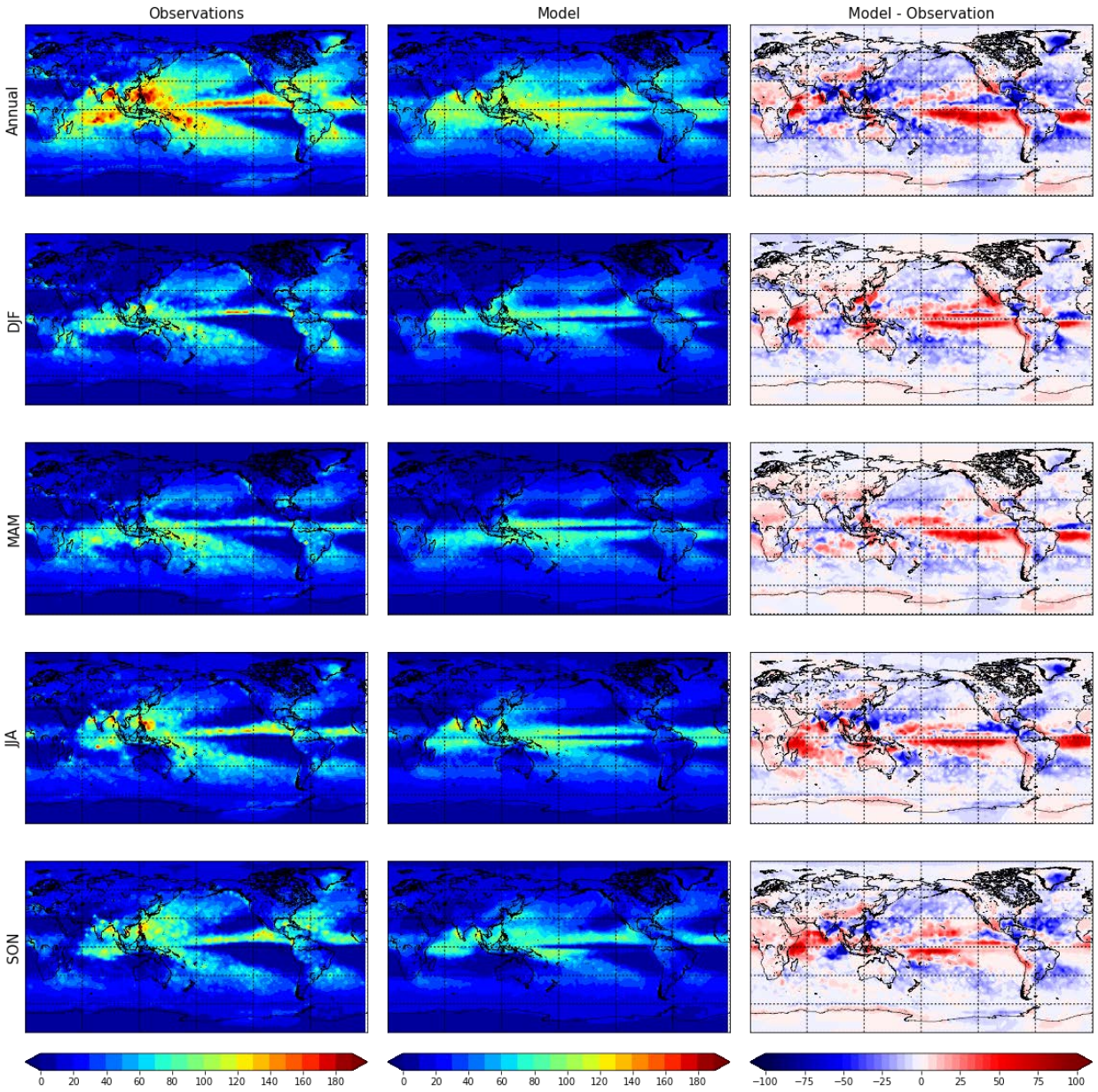

Figure 12: Same as Figure 5, but for daily precipitation and FGOALS-g2.

3.2.3 Intermodel Variability

The daily plots have a significantly different amount of variability than what is seen at the sub-daily scale. MIROC-ESM-CHEM, which was a strong outlier for sub-daily precipitation, performs significantly better for daily precipitation, resulting in much less variability among models, particularly towards the poles and in the mid-latitudes where I previously saw a large amount of variability due to this outlier (Figure 13). Again, the greatest variability among models is in the tropics and there are two peaks in variability just north and south of the equator, but it is difficult to differentiate the two peaks for daily precipitation annually.

Variability is the greatest at the annual scale with a range of 75 mm at its highest peak in the tropics and variability at higher latitudes has decreased significantly. Seasonally, variability is also high in the tropics for daily precipitation with a range of 50 mm at its highest peak, which is seen in MAM in the tropics. In the seasonal analysis, MAM has the greatest amount of variability in the tropics and DJF has the least amount of variability in the tropics.

Similar to annual precipitation, there are generally two peaks in variability that fall just north and south of the equator at the seasonal scale, but depending on the season the peaks shift and merge. In DJF and MAM, variability is larger in the southern hemisphere, with the peak in the northern hemisphere almost being lost in it. In JJA and SON, the larger peak shifts to the northern hemisphere, and the southern peak has almost completely disappeared in SON.

The mean of the models and the observations were again included in these plots (Figure 13). Models tend to still underestimate precipitation at the daily scale, but it is evident there is great improvement by comparing the observations and the mean of the GCMs; this is particularly true at the seasonal scale. Annually, the greatest difference between observations and the mean of the GCMs is about 30 mm at about 15° N. Seasonally, the greatest difference is about 50 mm

at 15° N in JJA and the closest agreement between observations and models is during DJF with a difference of about 50 mm at 15° N.

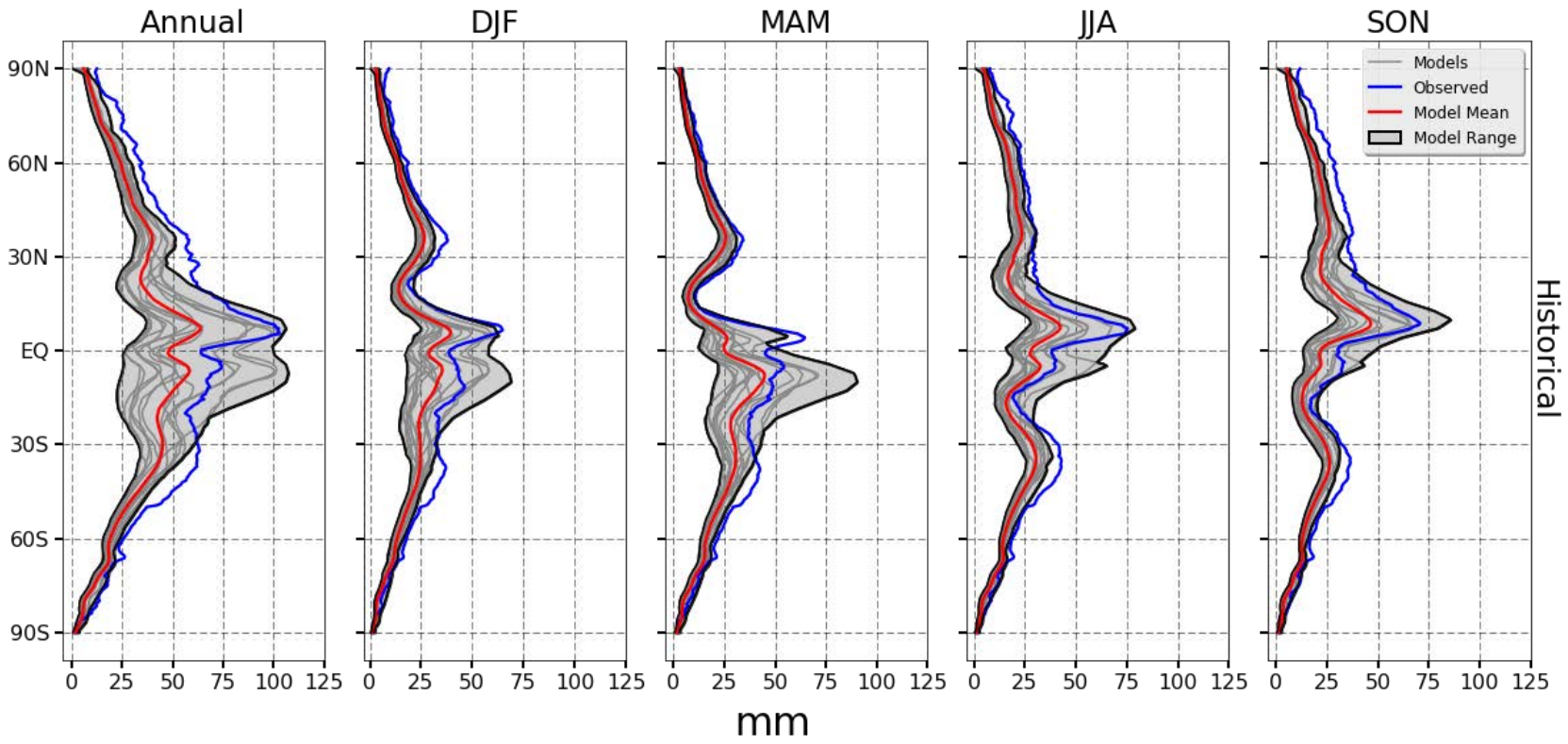

Figure 13: The same as Figure 7, but for daily precipitation.

CHAPTER 4: RESULTS

This analysis primarily focuses on the models that performed the best for sub-daily and daily precipitation based on the results in the previous chapter: ACCESS1-0, ACCESS1-3, FGOALS-g2, CNRM-CM5, MRI-CGCM3, and MRI-ESM1. Selected figures from these models are used as examples, while Appendices A-F provide the complete set of figures. Outputs from other models not listed are still evaluated, and general tendencies among all models are discussed in the following sections, but specific figures for these models are not provided.

4.1 Sub-daily Precipitation Results

When examining the different RCP outputs, the results are similar to other studies on global precipitation with precipitation largely increasing and a "wet-get-wetter and the dry-get-drier" pattern (Trenberth 2011; Langenbrunner et. al. 2015). The least amount of change is seen for RCP 2.6 in the 2026-2045 time period, which has lower greenhouse gas concentrations (Figure 14). Higher greenhouse gas concentrations, on the other hand, result in a greater magnitude of changes in precipitation. Changes (both increasing and decreasing) are more significant towards the end of the century, which relates back to greenhouse gas concentration trends in the RCPs. Generally, there are mostly increases in precipitation with some specific areas where decreases are more dominant, primarily in locations that already experience heavy droughts, such as the western United States and parts of Africa. The greatest increases and decreases fall within the tropics between 30° N and 30° S for all the models, but the magnitude of the change and specific locations with the greatest change vary by model. Based on this analysis, it is evident that increases in precipitation will be of a higher magnitude than the decreases. Increases (decreases) are projected to be greater (smaller) than 10 mm for most of the models analyzed.

Looking at annual precipitation, most of the models have an area of large increases in precipitation close to the equator. Models tend to show either no change or a decrease in precipitation directly on the equator in the eastern Pacific Ocean, with decreases also extending south into the ENSO region for several of the models including ACCESS1-3 and ACCESS1-0 (Figure 14 and Appendix A.2). In general, the areas where decreases in precipitation are prominent are comparable to locations other studies have shown to be likely areas of decreases (e.g., Liu 2013; Carrao 2017); this includes locations like Australia, Central America, and the western United States. ACCESS1-3, for example, exhibits decreases in several of these locations (Figure 14), but specific locations of decreasing precipitation vary by model and in the case of ACCESS1-3 output, increases in precipitation throughout the tropics are also a prominent feature.

Seasonal changes vary greatly by model. In general, extreme precipitation in the northern hemisphere changes more in JJA and SON and precipitation in the southern hemisphere changes more in DJF and MAM. The magnitude of the seasonal changes is smaller than the annual changes in precipitation. Similar to the annual precipitation, the greatest changes are seen in the tropics between about 30° N and 30° S and these observed changes are mostly increases across the globe, but there are some areas where precipitation decreases. For instance, in the northern hemisphere there are primarily decreases in the western United States and in the southern hemisphere, most of the decreases in precipitation are seen over Australia and the ENSO region. However, as with the results for annual precipitation, results vary by model.

The meridional plots give us a good insight into general changes that we can expect to see at each latitude. The heaviest precipitation is located just north and south of the equator with a slight decrease in precipitation right at the equator. These precipitation maxima shift slightly by

season (Figure 15). In SON, the precipitation peak in the northern hemisphere is larger than the one in the southern hemisphere, in DJF and JJA the two peaks are closer in magnitude with the northern hemisphere peak still being slightly greater, and in MAM the southern peak has a greater magnitude than the northern one.

Both seasonally and annually, the magnitude of the change is much smaller near the poles and much larger near the equator and, similar to the results seen in the global maps, changes in precipitation are larger towards the end of the century. However, a few models exhibit small decreases in precipitation. For example, FGOALS-g2 shows precipitation decreasing right at the equator towards the end of the century, but also shows increases in precipitation at almost every other latitude (Figure 15).

Other models such as ACCESS1-0 and ACCESS1-3 (Appendix A.3 and B.3) also have decreases in precipitation, but these changes are small and vary by season. Similar to what was mentioned before, the models project an increase in precipitation through the end of the century, and the most significant changes are expected to be in the tropics. Most of the models confirm the large increases in precipitation near the equator and decreases near the ENSO region. Other areas with decreases in precipitation still include Australia, west of Australia over the Indian Ocean, Central America, and the western United States (Figure 14). The changes also vary by model.

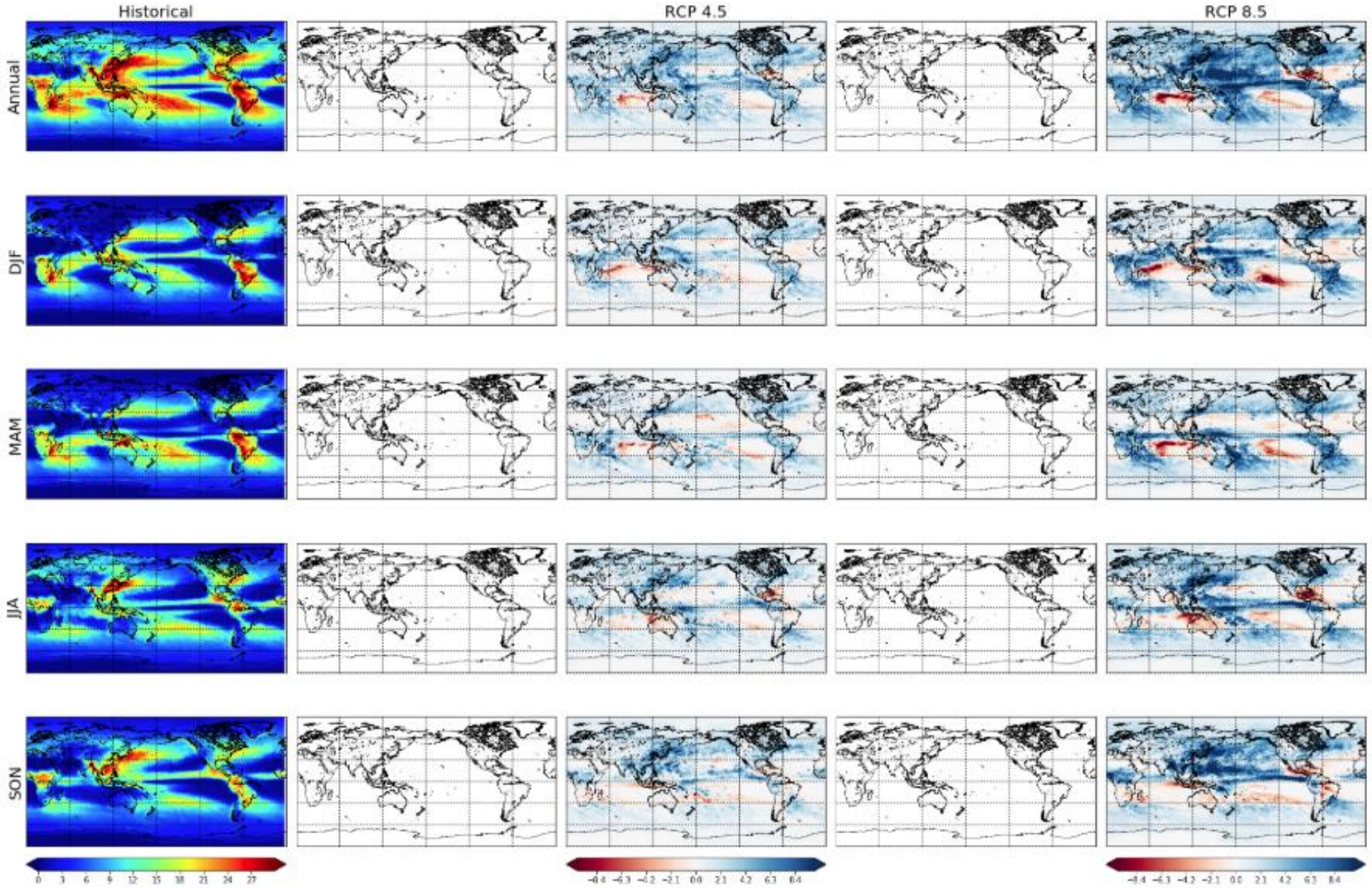

Figure 14: Median maximum 3-hourly precipitation (mm) for ACCESS1-3. The results for the RCPs 4.5 and 8.5 (Columns 3 and 5 represent the differences between the projected changes (2081-2100) and the historical period (1985-2005; Column1). The columns for RCPs 2.6 and 6.0 (columns 2 and 4) are empty because this GCM does not have outputs for those RCPs. Results are for annual precipitation (Row 1), DJF (Row 2), MAM (Row 3), JJA (Row 4), and SON (Row 5).

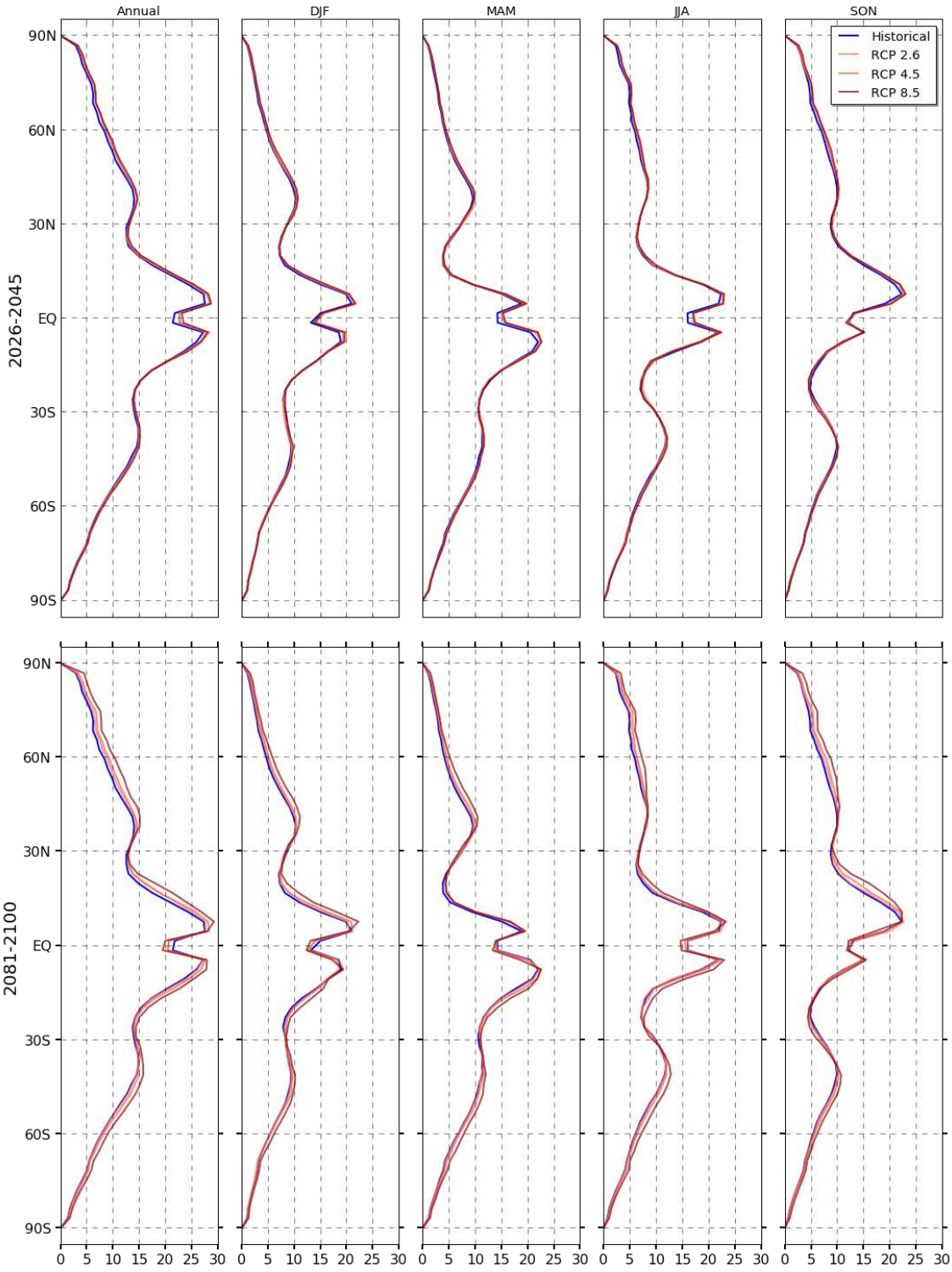

Figure 15: Zonally averaged median maximum sub-daily precipitation (mm) for FGOALS-g2. Results for RCPs were found the same way as described in Figure 14 and then averaged by latitude. These results are for 2026-2045 (Top Row) and 2081-2100 (Bottom Row) at the annual scale (Column 1), and seasonal scale: DJF (Column 2), MAM (Column 3), JJA (Column 4), and SON (Column 5).

4.2 Daily Precipitation Results

Similar to results for the 3-hourly precipitation, there is a clear relation between greenhouse gas concentrations and precipitation. The greatest changes that occur between the historical reference period and projections are shown in the RCP 8.5 output for each model. There are also greater changes towards the end of the century with the greatest changes occurring in the 2081-2100 time period (Figure 16 and Appendix C.4).

The greatest changes in magnitude are in the tropics, generally between 30° N and 30° S. Models show a general agreement that the greatest increases will be near the equator and the greatest decreases will be near the ENSO region, with other specific locations of increases and decreases that vary by model. For example, models ACCESS1-0 and ACCESS1-3 (Appendix A.6 and B.6) show significant decreases in annual precipitation over the Indian Ocean and Australia, while other models do not have any decreases in these areas and some models even display no decreases in precipitation, with increases being dominant across the globe. The magnitude of change for FGOALS-g2 at the daily scale is much larger than what is seen at the sub-daily one, with the greatest increase and decrease in precipitation having a magnitude greater than 25 mm for RCP 8.5 in the 2081-2100 time period (Figure 16). Looking back at sub-daily precipitation for FGOALS-g2 for this same RCP and time period, the greatest increase and decrease in precipitation have a magnitude of 10 mm (Appendix C.2). Based on these results, we would expect daily precipitation to have a larger change than sub-daily precipitation.

Seasonally, models generally show the greatest increases at or near the equator with the greatest decreases over the ENSO region. Models indicate precipitation will increase more in the northern hemisphere's tropics during JJA and SON, but precipitation is slightly more evenly spread for DJF and MAM. However, this is not the case for all models. For example, FGOAL-g2 does not show this shift in precipitation increases and instead has precipitation increasing in DJF

and MAM (Figure 16). Areas of large decreases vary greatly among models, but as previously stated, the ENSO region remains an area where models consistently show decreases in precipitation and other areas some models exhibit decreases include Australia, over the Indian Ocean, the western United States, and Central America. The magnitude of change is smaller at the seasonal scale than the annual scale.

The meridional plots give further insight into how precipitation is projected to change by latitude (Figure 17). Compared to the historical reference period for each model, there is a clear increase in precipitation at about every latitude, with the greatest increase seen in the tropics and less of a change (and in some cases no change) near the poles. FGOALS-g2 is one of the only models that shows a decrease in precipitation and this is right along the equator (Figure 17). This is not surprising considering the global maps also showed a strong decrease in precipitation along the equator, while increases in precipitation are dominant everywhere else for FGOALS-g2.

Seasonally, there are several models that indicate a shift in maximum precipitation with the maximum north of the equator being larger in SON, the maximum south of the equator being larger in MAM, and both peaks tending to be about even in DJF and JJA. The shift in precipitation can be seen in several models including FGOALS-g2, MRI-ESM1-1 and MRI-CGCM3 (Figure 17, Appendix F.8, and E.8). This is due to the shift in the ITCZ with seasons. However, due to the double ITCZ pattern that is typically seen in the tropics, precipitation between the equator and 15° S is likely misrepresented and overestimated on these plots as well as the global plots. This is also a problem seen in sub-daily precipitation and could be the source of the shift in those plots as well.

As previously stated, model projections show an increase in precipitation at almost every latitude compared to the model's historical reference period. Projections show the precipitation pattern annually and seasonally are about the same for the historical reference period compared to the projections. Figure 17 also confirms the role greenhouse gas concentrations play on the changes with RCP 2.6 showing the smallest change, RCP 8.5 showing the greatest change, and the greatest changes in precipitation occurring towards the end of the century.

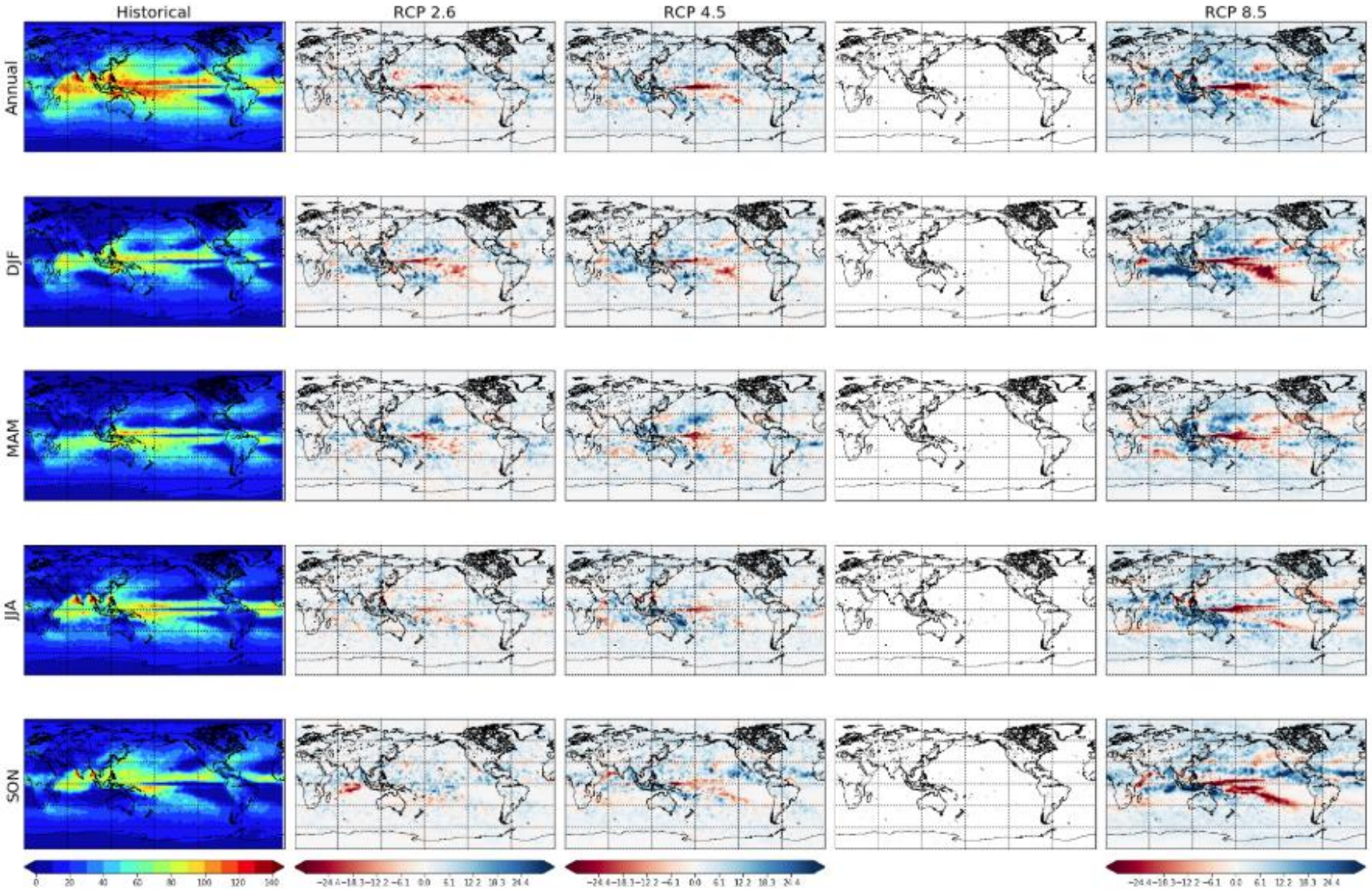

Figure 16: Same as Figure 14, but for FGOALS-g2 output for RCPs 2.6 (Column 2), 4.5 (Column 3), and 8.5 (Column5) and is for daily precipitation. RCP 6.0 is unavailable for this model, so one column (Column 4) is left empty.

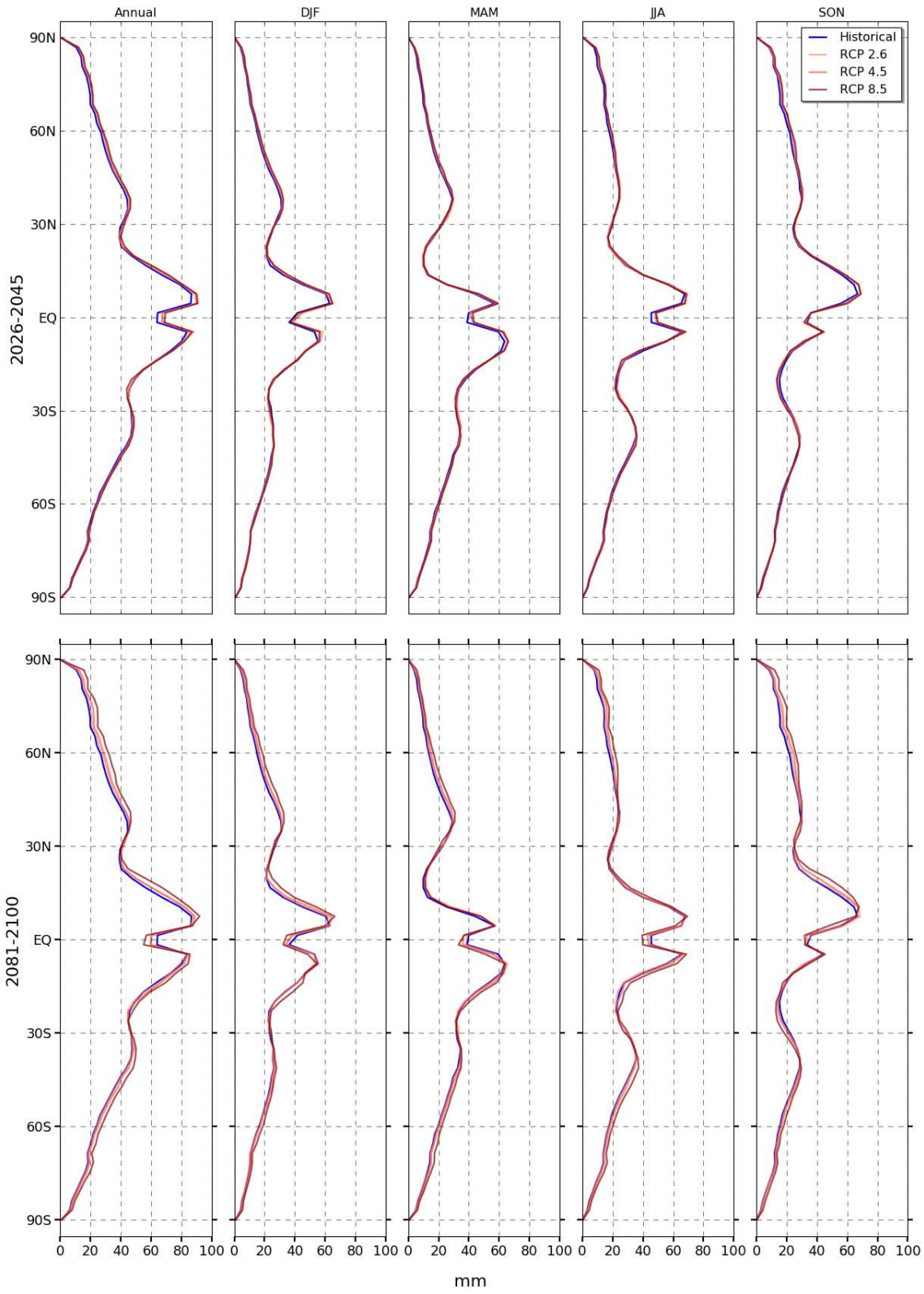

Figure 17: Same as Figure 15, but for FGOALS-g2 and daily precipitation.

CHAPTER 5: SUMMARY AND CONCLUSIONS

5.1 Summary

The goal of this work was to evaluate projected changes in precipitation at both the daily and sub-daily time scales. The first step was evaluating model accuracy with respect to the observations over the historical past. With a better understanding of model performance, the next goal was to examine the results for the best performing models and determine potential changes in extreme precipitation through the end of the century. In addition, I also wanted to understand whether daily or sub-daily precipitation would change more through the end of the century.

From the skill score model evaluation, it is evident that accuracy is greater for daily than 3-hourly precipitation. Biases are consistently lower and correlation values are consistently higher for daily precipitation. FGOALS-g2 performs relatively well for sub-daily precipitation both annually and seasonally and tends to stand out compared to the performance of other models. However, for daily precipitation, accuracy greatly improves, and thus multiple models perform well, including FGOALS-g2, but other models such as ACCESS1-0, ACCESS1-3, and CNRM-CM5 have high skill as well.

Comparing global plots of sub-daily and daily precipitation to observations confirms the results from the decomposition of the skill score, with models that have higher accuracy for daily precipitation, and also reveals where the greatest errors are. Generally, models are more accurate closer to the poles and the largest errors are in the tropics between 30° N and 30° S. For most models, underestimation of precipitation is the largest problem, as also highlighted by the values of the unconditional bias. There are few areas of overestimation particularly near the ENSO region, which is likely due to a double ITCZ pattern that is seen in many of the models. MIROC-ESM-CHEM is the only model that struggles more with overestimation and has few areas where

precipitation is underestimated. The overestimation for this model is more significant for sub-daily precipitation over daily precipitation, but for daily precipitation, it is still a significant problem in the tropics.

Variability among models also produces errors that need to be considered. The largest amount of variability is in the tropics, with models showing more agreement towards the poles. It is also evident variability among models is generally larger for sub-daily precipitation. However, the variability for daily precipitation is not negligible and also needs to be considered when examining the results. The results from all the models were averaged and plotted on these plots as well as the average observations, and when comparing the two, it is evident most of the models largely underestimate precipitation at both time scales.

Compared to the historical runs for each model, there is a general increase in precipitation with few areas of decreasing precipitation that vary by model. In general, most models show a large increase in precipitation in the tropics, and one particular region that consistently shows decreases is the ENSO region. More specific locations associated with the greatest increases and decreases vary by season depending on the model. Largely, models show a more significant increase in precipitation just north of the equator in JJA and SON and less significant changes in DJF and MAM. These patterns are true for both sub-daily and daily precipitation. Looking at the specific magnitude of changes in precipitation indicates daily precipitation will change more than sub-daily precipitation, which is true for both increases and decreases in precipitation.

In these models there is also a clear connection between precipitation and greenhouse gas concentrations. The greatest precipitation changes are seen in the outputs for RCP 8.5, the RCP with the greatest greenhouse gas concentrations, and is shown to have an impact on both

increases and decreases in precipitation for sub-daily and daily precipitation. There is also a connection between time and precipitation changes, with changes of a higher magnitude for the time period 2081-2100.

When averaged by latitude, there will be a general global increase in precipitation. The global maps show that the increases will be more widespread than the decreases, and this confirms that globally precipitation will increase more than it will decrease. Precipitation will increase the most in the tropics, with smaller changes closer to the poles. Comparing these plots for sub-daily and daily precipitation indicates that the magnitude of the change will be larger for daily precipitation than sub-daily, confirming what is seen in the global maps.

5.2 Conclusions

In recent decades, precipitation has changed greatly. In some areas precipitation has increased in frequency and intensity causing more significant flooding, and other areas have experienced more intense and longer droughts resulting in a lack of water security. It is also evident that this trend will continue through the end of the century as greenhouse gas concentrations increase and climate continues to change rapidly.

This study has confirmed many of the changes past works have shown and explores a research area, global changes in sub-daily precipitation compared to daily precipitation, which has not been explored in great detail. Precipitation is projected to increase in some locations while it will decrease in others, and the largest changes will be in the tropics between 30° N and 30° S, particularly over the oceans. Both sub-daily and daily precipitation will be impacted by these climate changes. However, based on this analysis there is still a lot of uncertainty on what exactly will happen. Model accuracy has improved in recent years, and I expect the new

generation of models to mitigate some of these issues and create higher confidence in projected precipitation.

Further research is necessary to improve our understanding of projected precipitation changes. Variability among models is still high and accuracy is generally low, especially at sub-daily timescales. For these reasons further research into improving sub-daily precipitation accuracy, and model accuracy in general, is important moving forward. Future work could try to examine the reasons for the differences in performance among the different models. Moreover, analyses at the regional scale could provide more details about the performance of the models for different land regions. Finally, while my emphasis has been on the median of the maxima, other quantities could have been considered, including expanding the work on extremes (e.g., computing statistics related to the frequency of precipitation exceeding high thresholds) or focusing on overall precipitation amounts accumulated over a given season or year. These additional analyses would complement the results in this thesis, providing a perspective on different aspects of precipitation and its changes. With more work, we can gain a better understanding of future trends in precipitation and implement best management practices.

REFERENCES

Abramson, D., I. Redlener (2012), Hurricane Sandy: Lessons Learned, Again. *Disaster Medicine and Public Health Preparedness,* ***6*****(4)**, 328-329, doi:10.1001/dmp.2012.76.

Adler, R., G. Gu, M. Sapiano, J. Wang, G. Huffman, Global Precipitation: Means, Variations, And Trends During the Satellite Era (1979-2014). *Surveys in Geophysics*, **38(4)**, 679-699.

Alexander, L., (2015), Global Observed Long-Term Changes in Temperature and Precipitation Extremes: A Review of Progress and Limitations in IPCC Assessments and Beyond. *Weather and Climate Extremes*, **11**, 4-16.

Anderegg, W. (2010), Moving Beyond Scientific Agreement. *Climatic Change*, **101**, 3-4, 331-337, doi:10.1007/s10584-010-9925-3.

Beck, H., E. Wood, M. Pan, C. Fisher, D. Miralles, A. van Dijk, T. McVicar, and R. Adler, (2018), MSWEP V2 Global 3-hourly 0.1° Precipitation: Methodology and Quantitative Assessment. *Bull. Amer. Meteor. Soc.,* doi:10.1175/BAMS-D-17-0138.1.

Bradley, A., J. Demargne, K. Franz, Attributes of Forecast Quality, *Handbook of Hydrometeorological Ensemble Forecasting*, 1-44.

Carbone, E., M. Wright (2015), Hurricane Sandy Recovery Science: A Model for Disaster Research, *Disaster Medicine and Public Health Preparedness*. **10(3)**, 304-5.

Carrao, H., G. Naumann, and P. Barbosa, (2017), Global Projections of Drought Hazard in a Warming Climate: A prime for Disaster Risk Management, *Climate Dynamics*. **50(6)**, 2137-2155.

Chadwick, R., I. Boutle, and G. Martin, (2013), Spatial Patterns of Precipitation Change in CMIP5: Why the Rich do not get Richer in the Tropics. *J. Climate*, **26**, 3803–3822, doi:https://doi.org/10.1175/JCLI-D-12-00543.1.

Chiang, F., O. Maxdiyasni, A. AghaKouchak, (2018), Amplified Warming of Droughts in Southern United States in Observations and Model Simulations. *Science Advances*, **4(8)**. doi:10.1126/sciadv.aat2380.

Chou, C., C. Chen, P. Tan, and K. T. Chen, (2012), Mechanisms for Global Warming Impacts on Precipitation Frequency and Intensity. *J. of Climate*, **25**, 3291-3306.

Dai, A., (2013). Increasing Drought Under Global Warming in Observations and Models. *Nature Climate Change*, **3(1)**, 52–58 https://doi.org/10.1038/nclimate1633.

Dobler, C., S. Hagemann, R. L. Wilby, and J. Stötter, (2012): Quantifying Different Sources of

Uncertainty in Hydrological Projections in an Alpine Watershed. *Hydrol. Earth Syst. Sci.*, **16**, 4343–4360, doi:https://doi.org/10.5194/hess-16-4343-2012.

Doocy, S. A. Daniels, S. Murray, and T. Kirsch, (2013), The Human Impact of Floods: A Historical Review of Events 1980-2009 and Systematic Literature Review. *PLOS Currents Disasters*, doi: 10.1371/currents.dis.f4deb457904936b07c09daa98ee8171a.

Fischer, E., U. Beyerle, R. Knutti, (2013), Robust Spatially Aggregated Projections of Climate Extremes, *Nature Climate Change*, **3**, 1033-1038, doi:10.1038/NCLIMATE2051.

Greve, P., et al. (2014), Global Assessment of Trends in Wetting and Drying Over Land. *Nature Geoscience*, 716-721 ,doi: 10.1038/NGEO2247.

Groisman, P. Y., R. W. Knight, and T. R. Karl, (2012): Changes in Intense Precipitation Over the Central United States. *Journal of Hydrometeorology*, **13**, 47-66, doi:10.1175/JHM-D-11-039.1.

Hashino T, Bradley AA, Schwartz SS, (2007) Evaluation of Bias-Correction Methods for Ensemble Streamflow Volume Forecasts. *Hydrol Earth Syst Sci*, **11(2)**, 939–950. doi: 10.5194/hess-11-939-2007.

Hawkins, E. R. Sutton, (2010), The Potential to Narrow Uncertainty in Projections of Regional Precipitation Change. *Clim. Dyn.*, **37(1)**, 407-418.

Huang, P., S.-P. Xie, K. Hu, G. Huang, and R. Huang, 2013: Patterns of the Seasonal Response of Tropical Rainfall to Global Warming. *Nat. Geosci.*, **6**, 357–361.

IPCC, (2014), Climate Change 2014: Synthesis Report. Contribution of Working Groups I, II and III to the Fifth Assessment Report of the Intergovernmental Panel on Climate Change [Core Writing Team, R.K. Pachauri and L.A. Meyer (eds.)]. IPCC, Geneva, Switzerland, 151 pp.

Jankovix, V. and D. Schultz, (2016), Atmosfear: Communicating the Effects of Climate Change on Extreme Weather. *Weather, Climate, and Society,* 27-37.

Jenkins, K., (2013), Extreme Weather and Climate Change Cost Assessments. *J Climatol. Weather Forecasting*, **1(1)**, doi: 10.4172/2332-2594.1000e104.

Kao, S. and A. Ganguly, (2011), Intensity, Duration and Frequency of Precipitation Extremes Under 21st-Century Warming Scenarios. *J. of Geophys. Res.*, **116**, D16119, doi 10.1029/2010JD015529.

Kent, C., R. Chadwick, D. Rowell, (2015), Understanding Uncertainties in Future Projections of Seasonal Tropical Precipitation. *J. of Climate*, **28**, 4390-4413.

Kharin, V., V., F. W. Zwiers, X. Zhang, and G. C. Hegerl, (2007), Changes in Temperature and Precipitation Extremes in the IPCC Ensemble of Global Coupled Model Simulations, *J.Clim.*, **20(8)**, 1419–1444.

Langenbrunner, B., J. Neelin, (2015), Patterns of Precipitation Change and Climatological Uncertainty Among CMIP5 Models, With a Focus on the Midlatitude Pacific Storm Track. *J. of Climate*, **28**, 7857-7872.

Lehmann, J., D. Coumou, K. Frieler, (2015), Increased Record-Breaking Precipitation Events Under Global Warming. *Climate Change*, **132(4)**, 501-515.

Lin, J. (2007), The Double-ITCZ Problem in IPCC AR4 Coupled GCMs: Ocean-Atmosphere Feedback Analysis. *J. of Clim.,* **20**, 4497-4525.

Liu, C., R. Allan, (2013), Observed and Simulated Precipitation Responses in Wet and Dry Regions 1850-2100. *Environ. Res. Lett.*, **8(3)**, doi:10.1088/1748-9326/8/3/034002.

Long, S., S. Xie, W. Liu, (2015), Uncertainty in Tropical Rainfall Projections: Atmospheric Circulation Effect and the Ocean Coupling. *J. of Clim.*, **29**, 2671-2687.

Mann, ME., et al., (2017), Influence of Anthropogenic Climate Change on Planetary Wave Resonance and Extreme Weather Events, *Sci Rep*, **7(46822)**.

Murphy, A. H. and Winkler, R. L., (1987), A General Framework for Forecast Verification. *Mon. Wea. Rev.*, **115**, 1330–1338.

O'Gorman, P. A., and T. Schneider, (2009), The Physical Basis for Increases in Precipitation Extremes in Simulations of 21st-Century Climate Change. *Proc. Natl. Acad. Sci.*, **106(35),** 14,773–14,777, doi:10.1073/pnas.0907610106.

Ornes, S., (2018), Core Concept: How Does Climate Change Influence Extreme Weather? Impact Attribution Research Seeks Answers. *Proceedings of the National Academy of Sciences*, **115(33)**, 8232-8235.

Rajsekhar, D., and S. Gorelick, (2017), Increasing Drought in Jordan: Climate Change and Cascading Syrian Land-use Impacts on Reducing Transboundary Flow. *Science*, **3(8)**, doi:10.1126/sciadv.1700581.

Rice, D., (2015), California Drought Cost is 2.7 Billion in 2015, *USA Today.*

Scoccimarro, E., et. al., (2015), Projected Changes in Intense Precipitation over Europe at the Daily and Subdaily Time Scales. *J. of Climate*, **28**, 6193-6203.

Seager, R. et al., (2015), Causes of the 2011-14 California Drought. *J. of Climate*, **28(18)**, 6997-7024

Sheffield, J., Wood, E. F., & Roderick, M. L., (2012). Little Change in Global Drought Over the Past 60 years. *Nature*, **491**(7424), 435–438.

Sillmann, J., V. Kharin, F. Zwiers, X. Zhang, D. Bronaugh, (2013), Climate Extreme Indices in the CMIP5 Multimodel Ensemble: Part 2. Future climate Projections. *J. Geophys. Res.,* **118**, 2473-2493, doi:10.1002/jgrd.50188.

Swain, D., (2015), A Tale of Two California Droughts: Lessons Amidst Record Warmth and Dryness in a Region of Complex Physical and Human Geography. *Geophysical Research Letters*, **42(22)**, 9999-10,003.

Taylor, K., (2001), Summarizing Multiple Aspects of Model Performance in a Single Diagram. *J. of Geophysical Research: Atmospheres*, **106(D7)**, 7183-7192.

Taylor, K., R. Stouffer, G. Meehl, (2012), An Overview of CMIP5 and the Experiment Design. *BAMS*, 485-498.

Trenberth, K., A. Dai, R. Rasmussen, and D. Parsons, (2005), The Changing Character of Precipitation. *BAMS*, 1205-1217, doi: 10.1 175/BAMS-84-9-1205.

Trenberth, K. E., (2011): Changes in Precipitation with Climate Change. *Climate Research*, **47**, 123-138, doi:10.3354/cr00953.

Wang, L., X. Yuan, Z. Xie, P. Wu, and Y. Li, (2016), Increasing Flash Droughts over China During the Recent Global Warming Hiatus. *Scientific Reports*, **6**, doi:10.1038/srep30571.

Westra, S., L. Alexander, F. Zwiers, (2012), Global Increasing Trends in Annual Maximum Daily precipitation. *J. of Clim.,* **26**, 3904-2918.

Xie, S.-P., C. Deser, G. A. Vecchi, L. Ma, H. Teng, and A. T.Wittenberg, (2010), Global Warming Pattern Formation: Sea Surface Temperature and Rainfall. *J. Climate*, **23**, 966–986.

Zhang, W., G. Villarini, E. Scoccimarro, G. Vecchi, (2017), Stronger Influences of Increased CO_2 on Subdaily Precipitation Extremes than at the Daily Scale. *Geophys. Res. Letters*, **44**, 7464-7471, doi:10.1002/2017GL074024.

Zhang, X., L. Hailong, M. Zhang, (2015), Double ITCZ in Coupled Ocean-Atmosphere Models: From CMIP4 to CMIP5. *Geophysical Research Letters*, **42(20)**, 8651-8659.

Zhu, Y., (2012), Variations of the Summer Somali and Australia Cross-Equatorial Flows and the Implications for the Asian Summer Monsoon. *Adv. Atmos. Sci.*, **29**, 509–518, doi:https://doi.org/10.1007/s00376-011-1120-6.

APPENDIX

A. ACCESS1-0

A.1 Median Maximum Sub-Daily Precipitation (2026-2045)

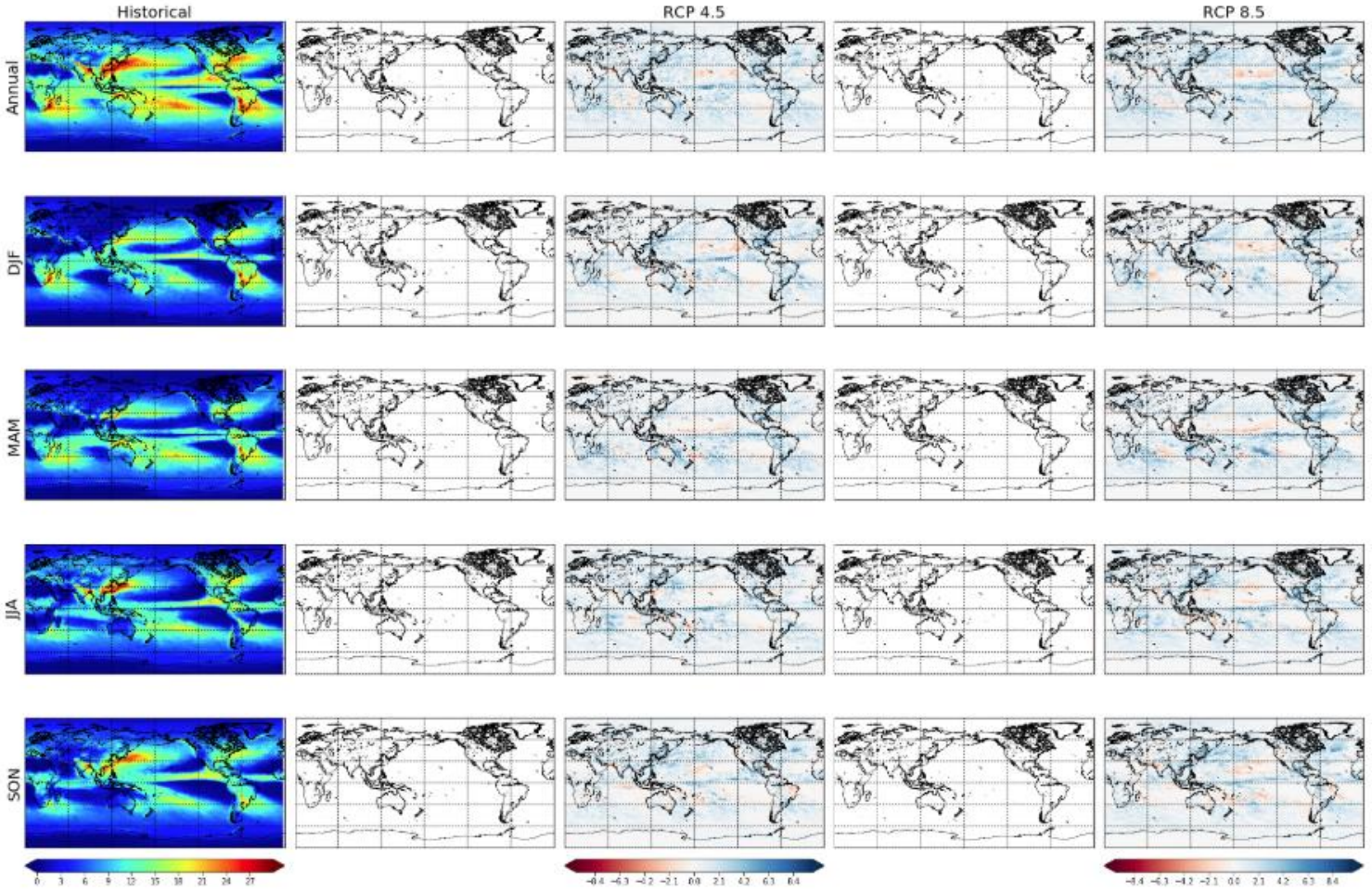

A.2 Median Maximum Sub-Daily Precipitation (2081-2100)

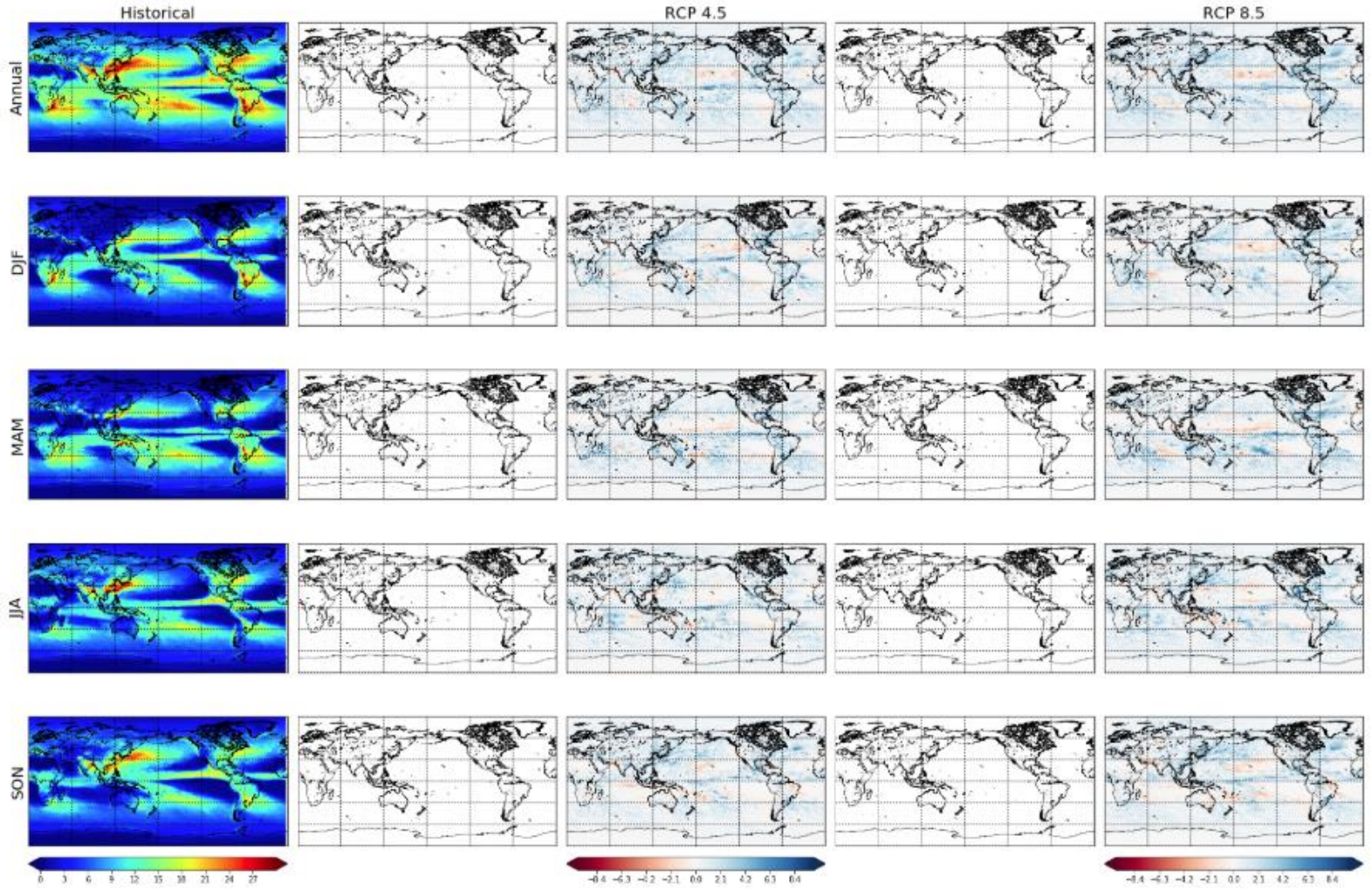

A.3 Average Median Maximum Sub-Daily Precipitation

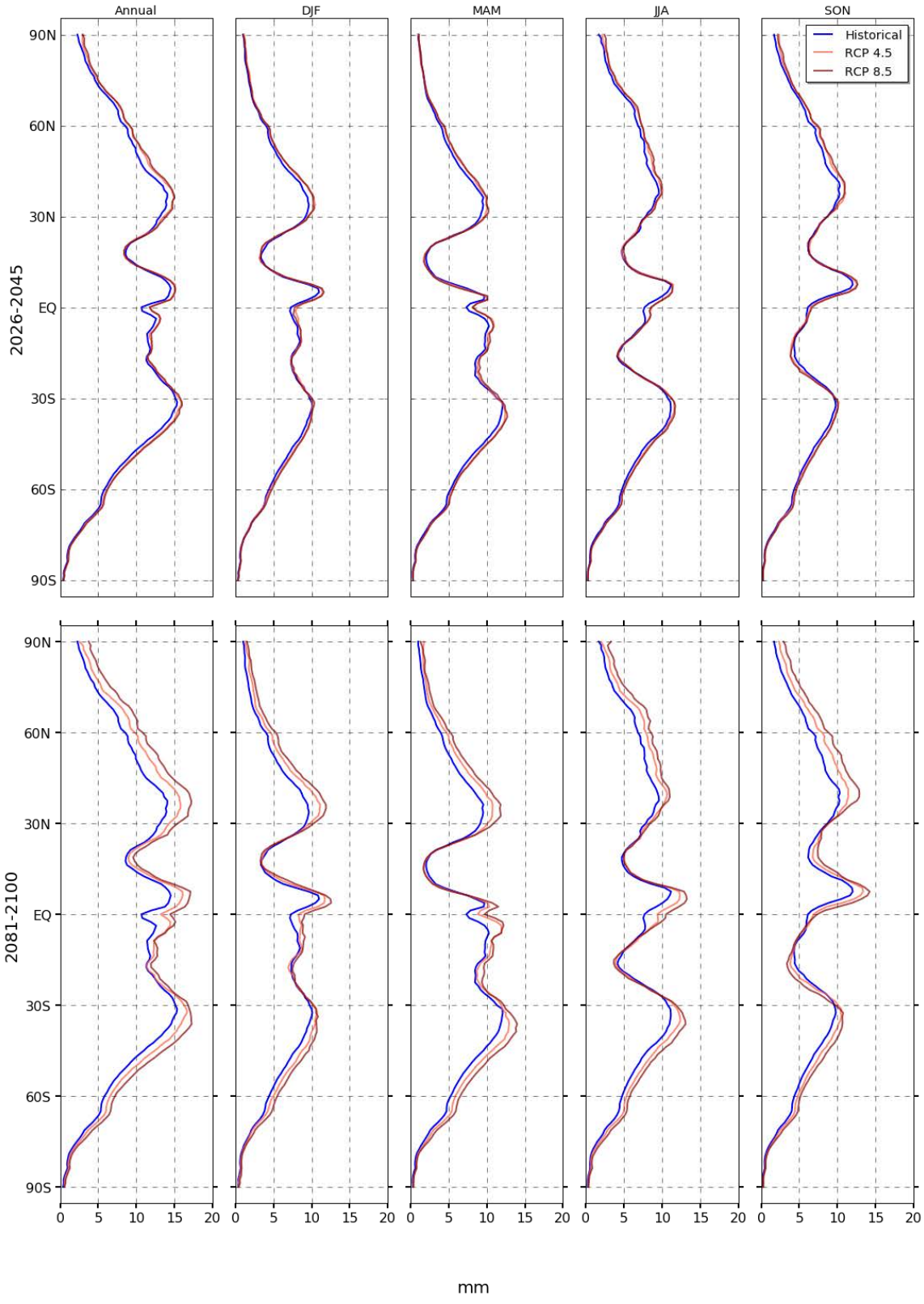

A.4 Median Maximum Daily Precipitation Model-Observations

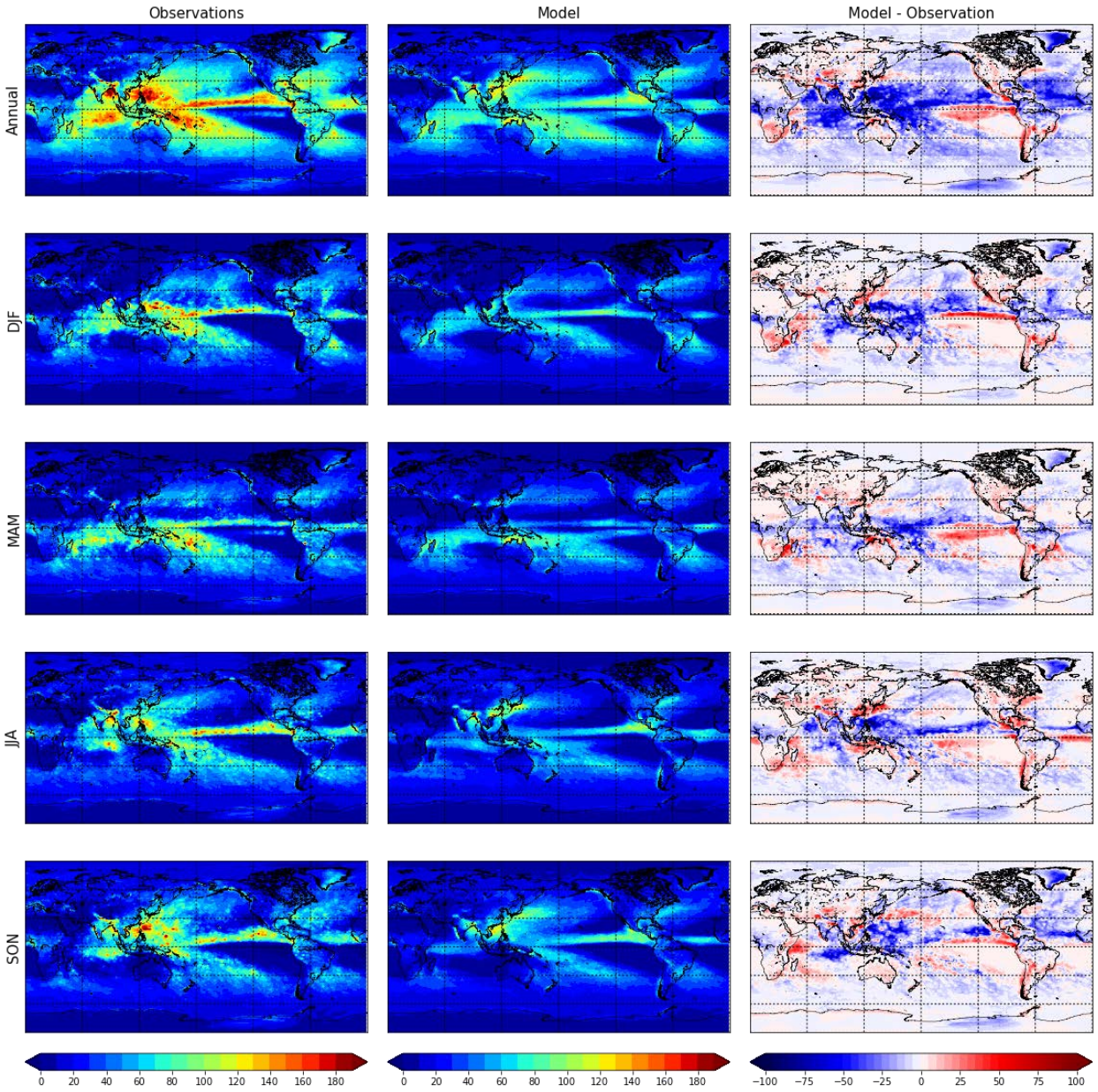

A.5 Median Maximum Daily Precipitation (2026-2045)

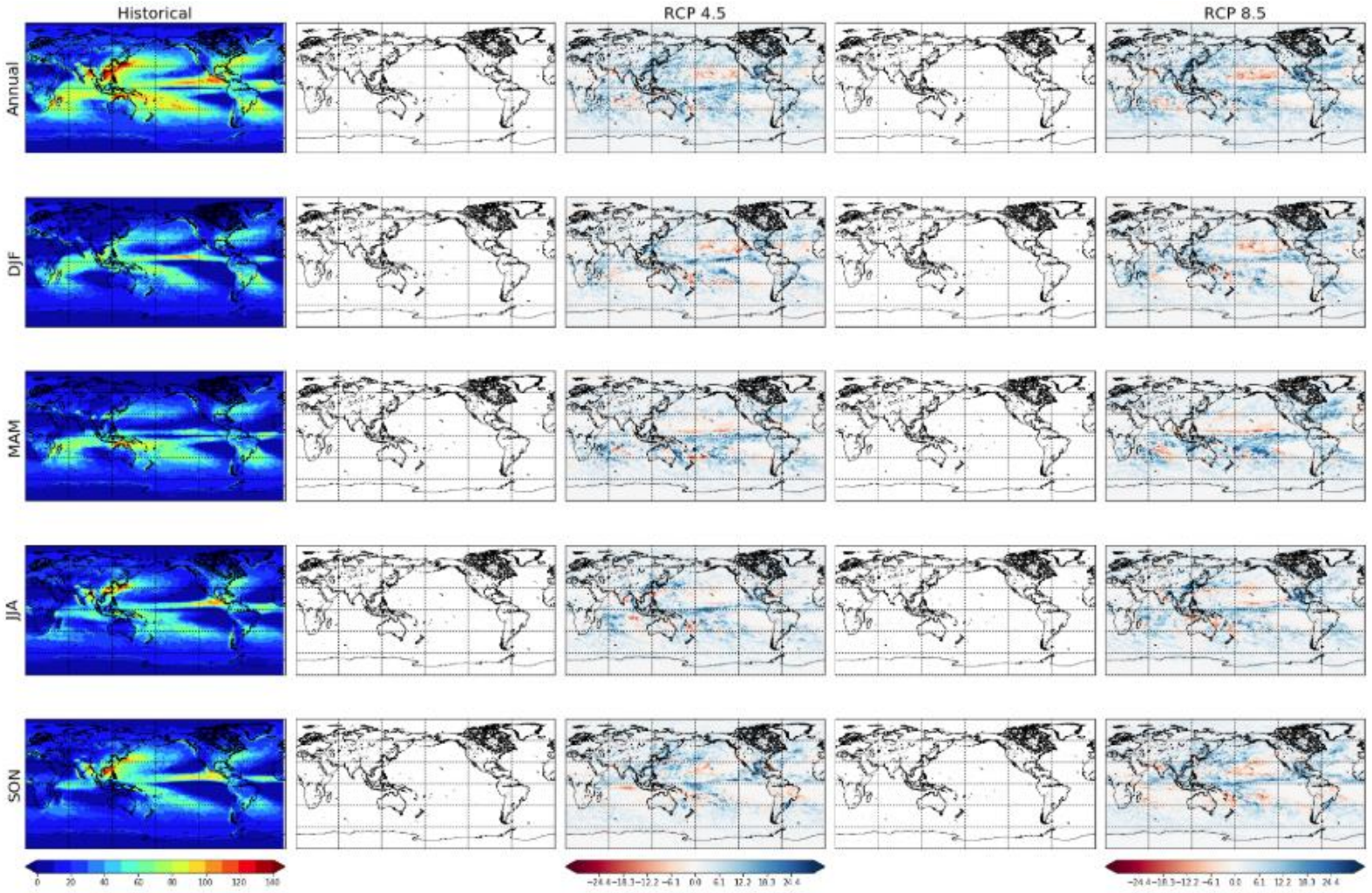

A.6 Median Maximum Daily Precipitation (2081-2100)

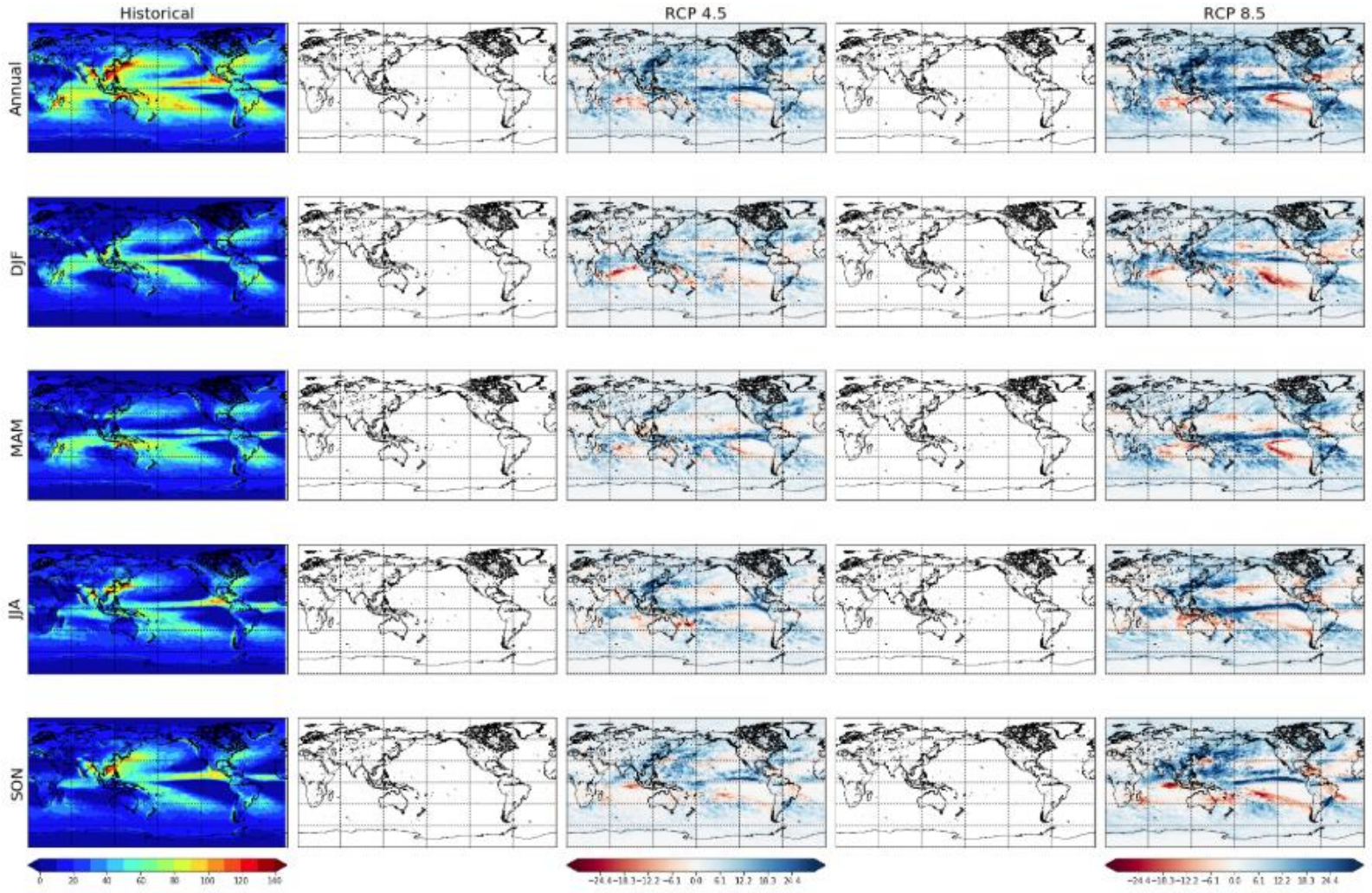

A.7 Average Median Maximum Daily Precipitation

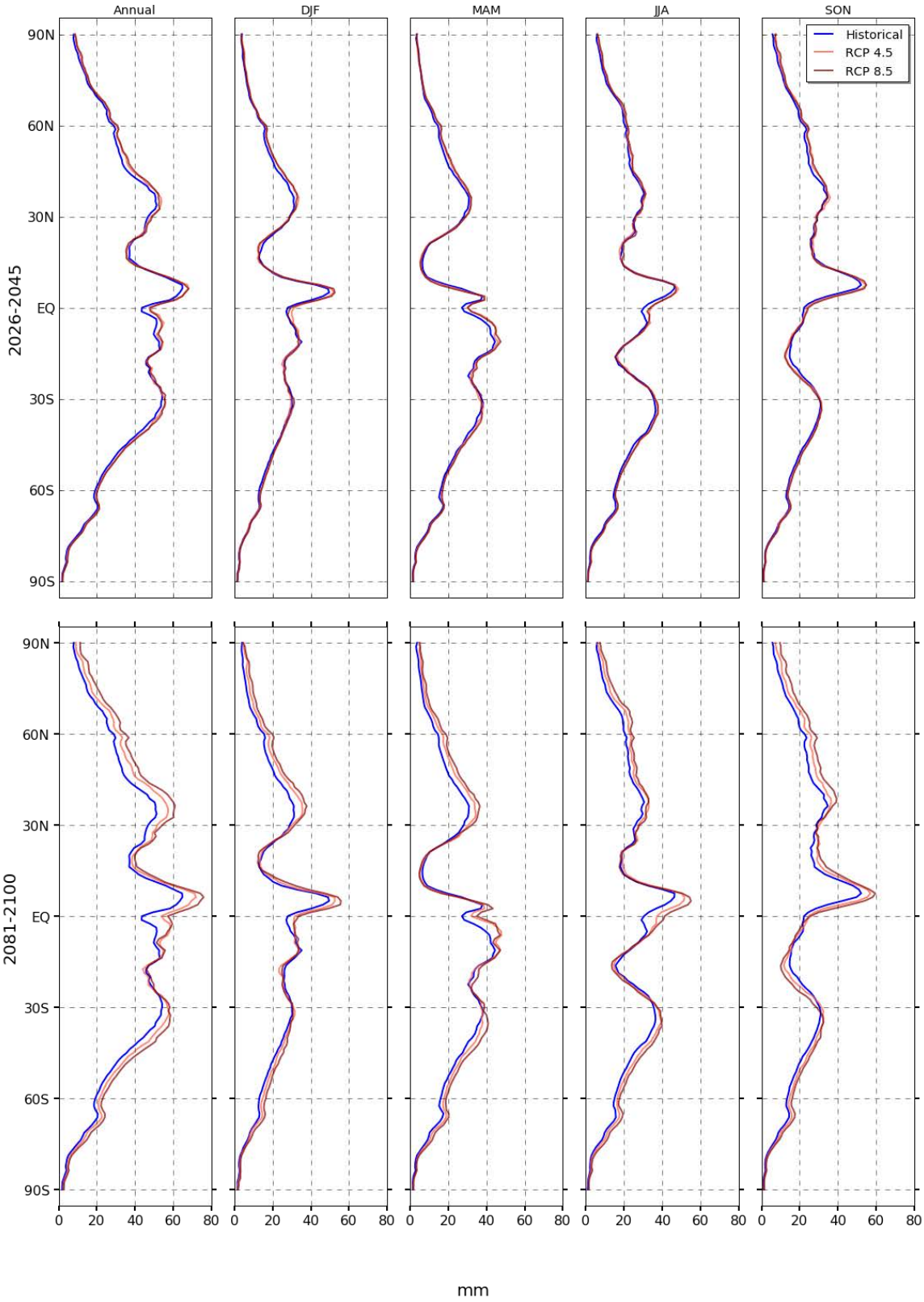

B. ACCESS1-3

B.1 Median Maximum Sub-Daily Precipitation Model-Observations

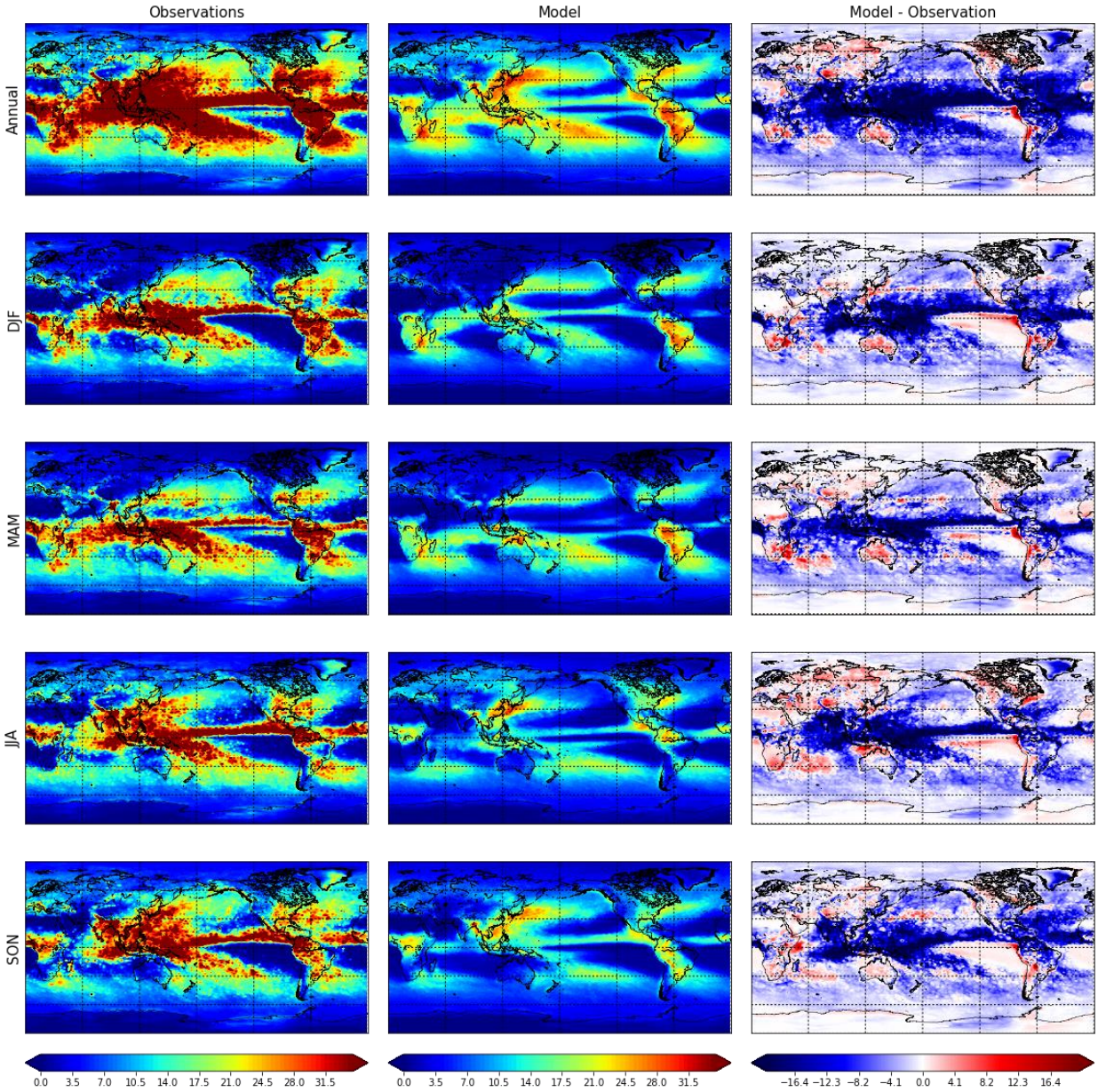

B.2 Median Maximum Sub-Daily Precipitation (2026-2045)

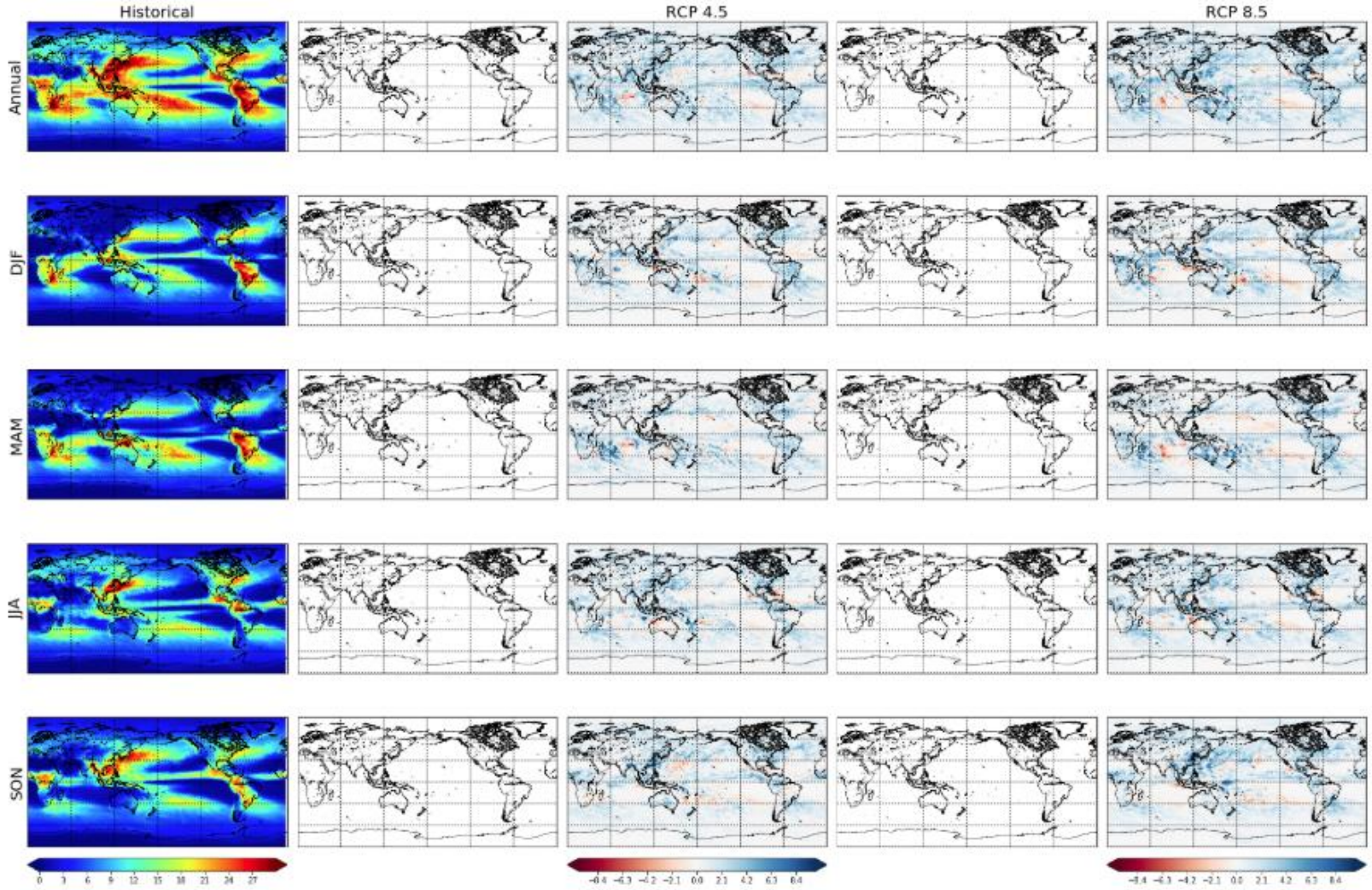

B.3 Average Median Maximum Sub-Daily Precipitation

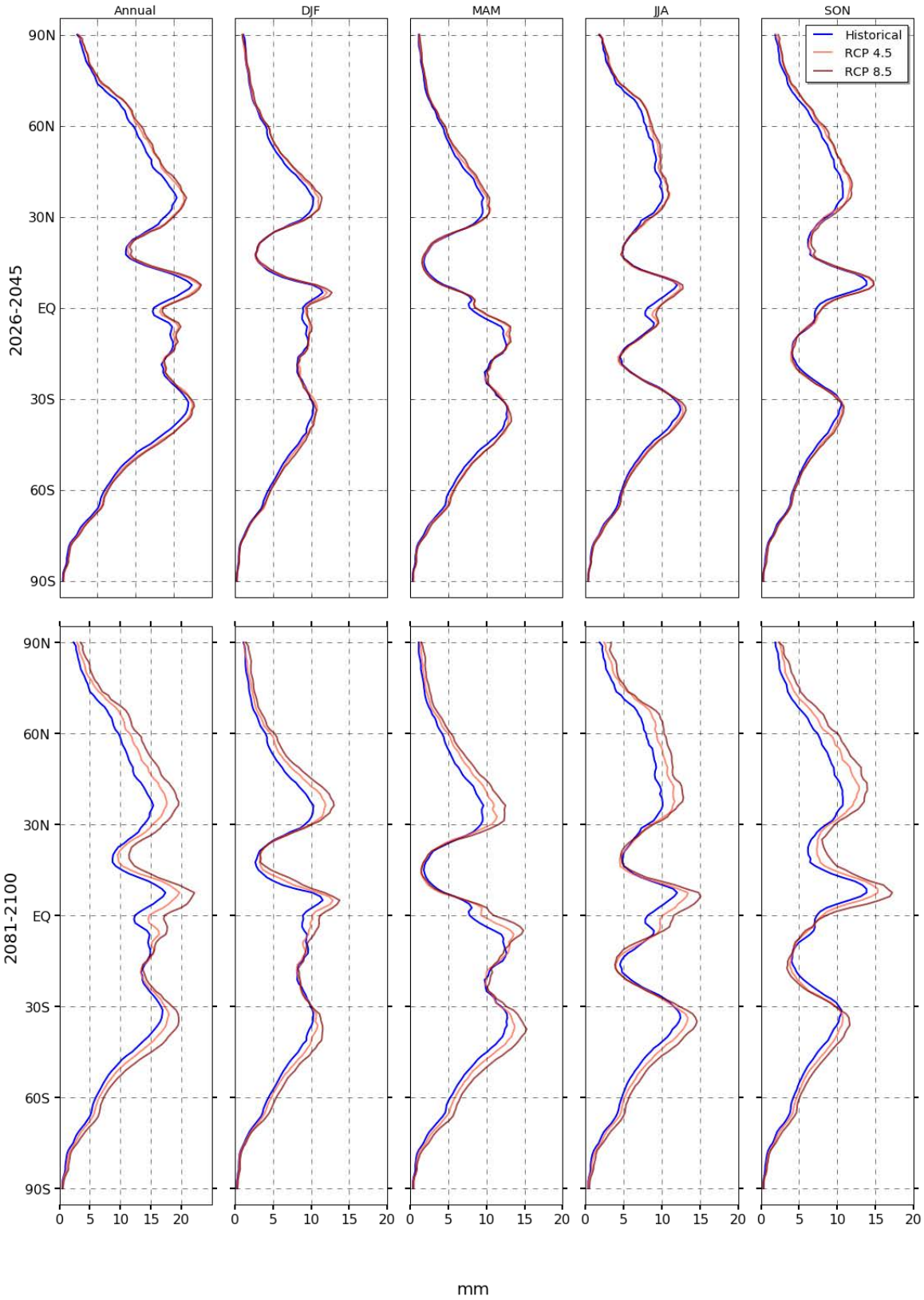

B.4 Median Maximum Daily Precipitation Model-Observations

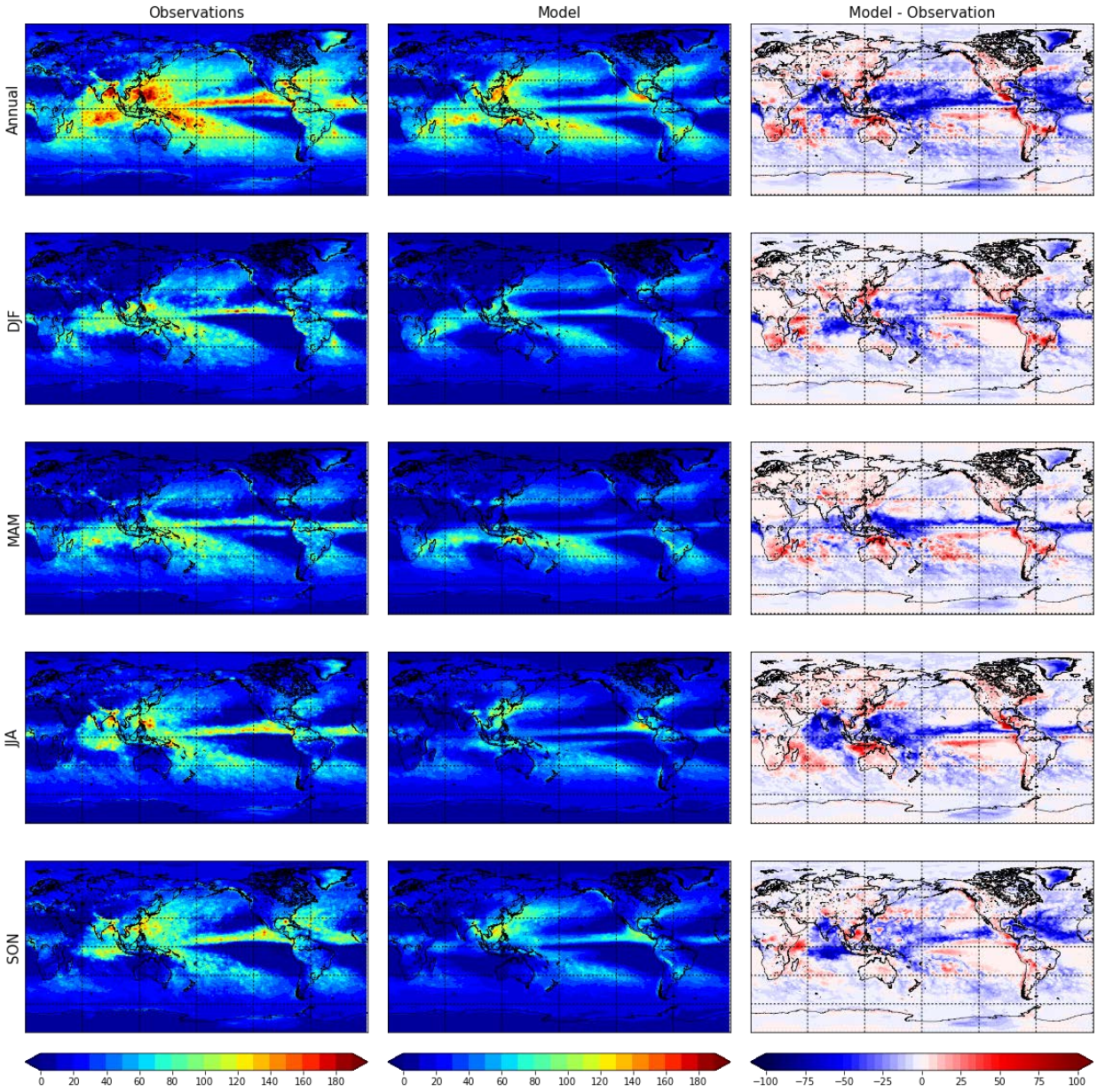

B.5 Median Maximum Daily Precipitation (2026-2045)

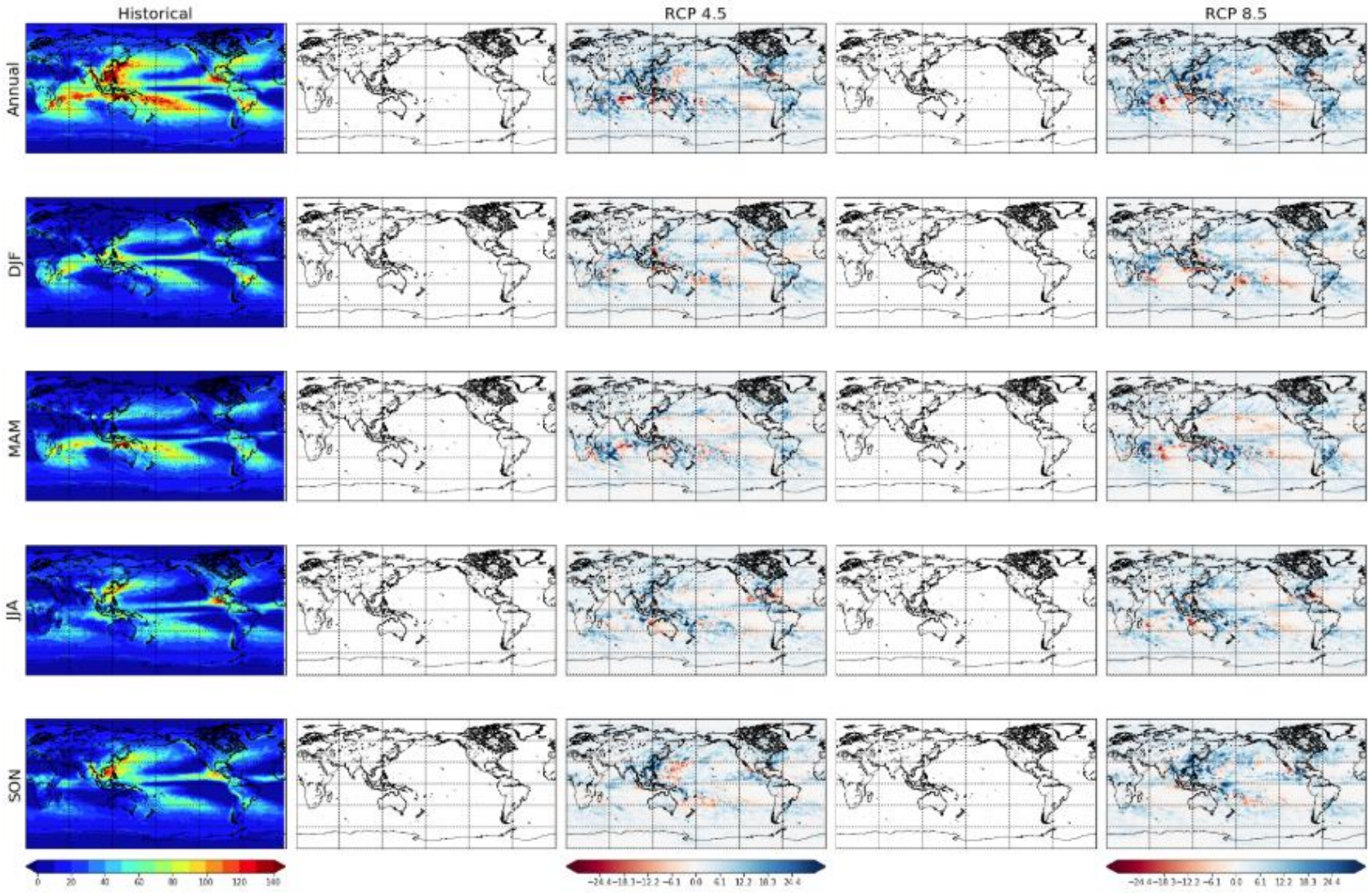

B.6 Median Maximum Daily Precipitation (2081-2100)

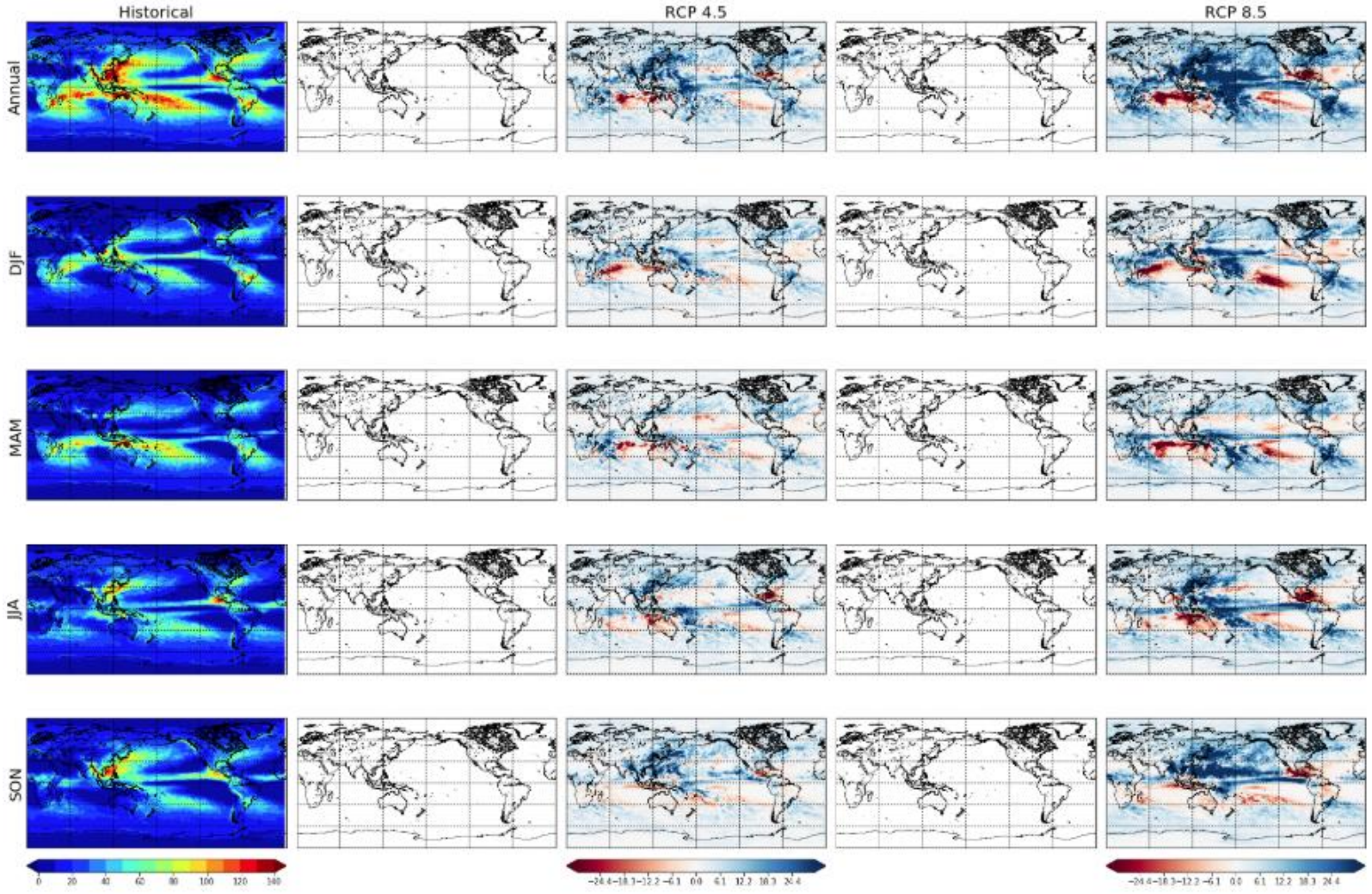

B.7 Average Median Maximum Daily Precipitation

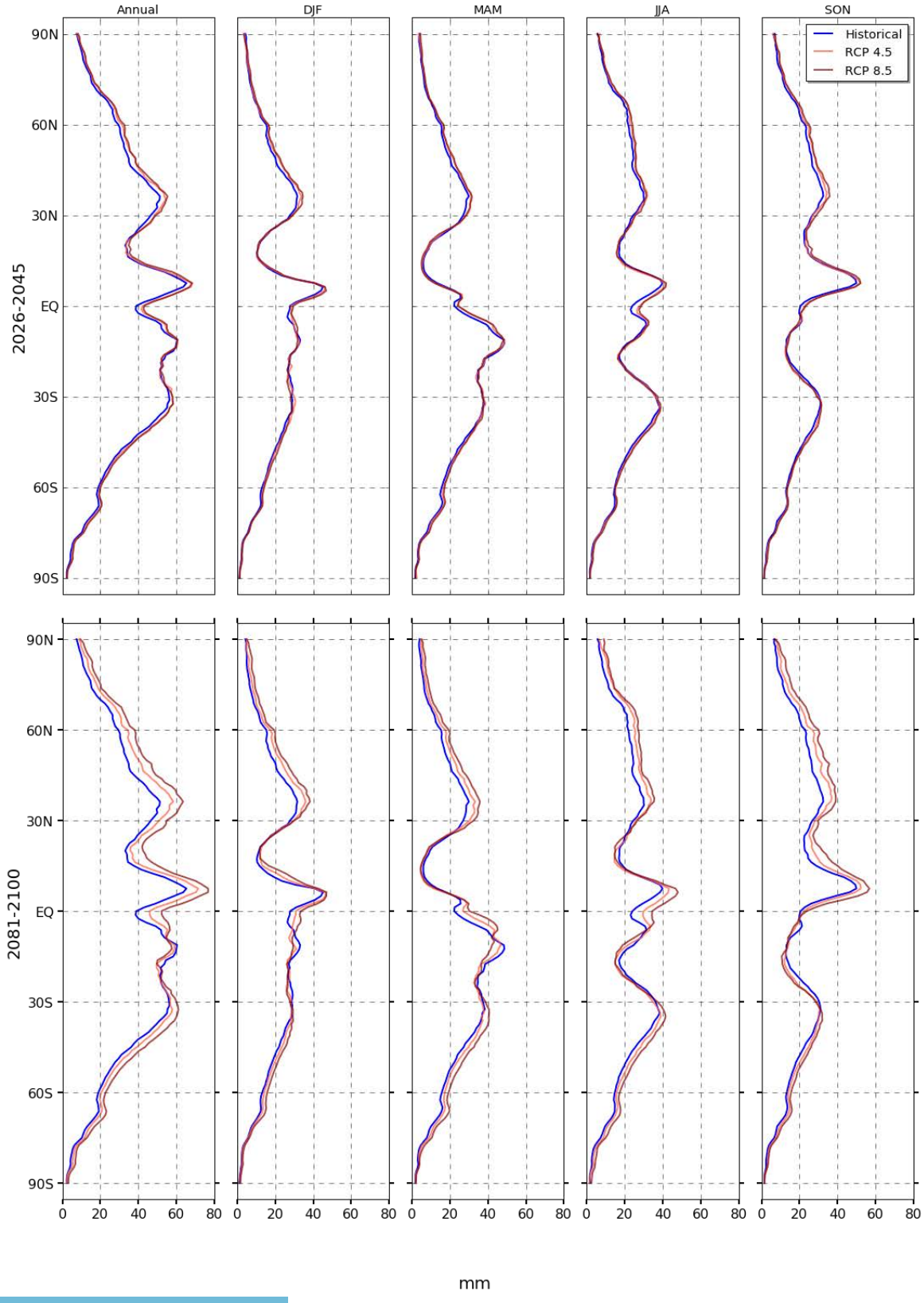

C. FGOALS-g2

C.1 Median Maximum Sub-Daily Precipitation (2026-2045)

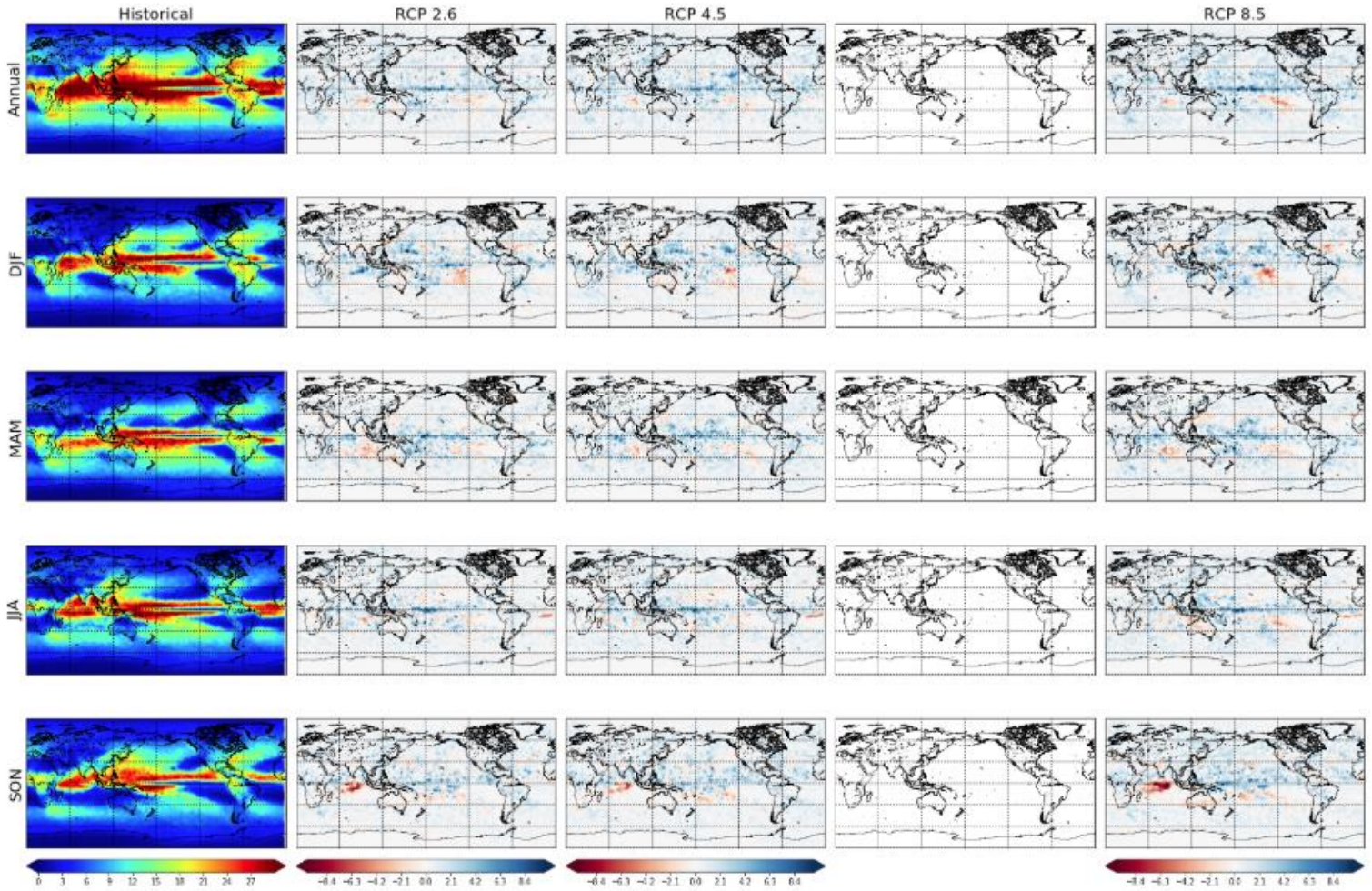

C.2 Median Maximum Sub-Daily Precipitation (2081-2100)

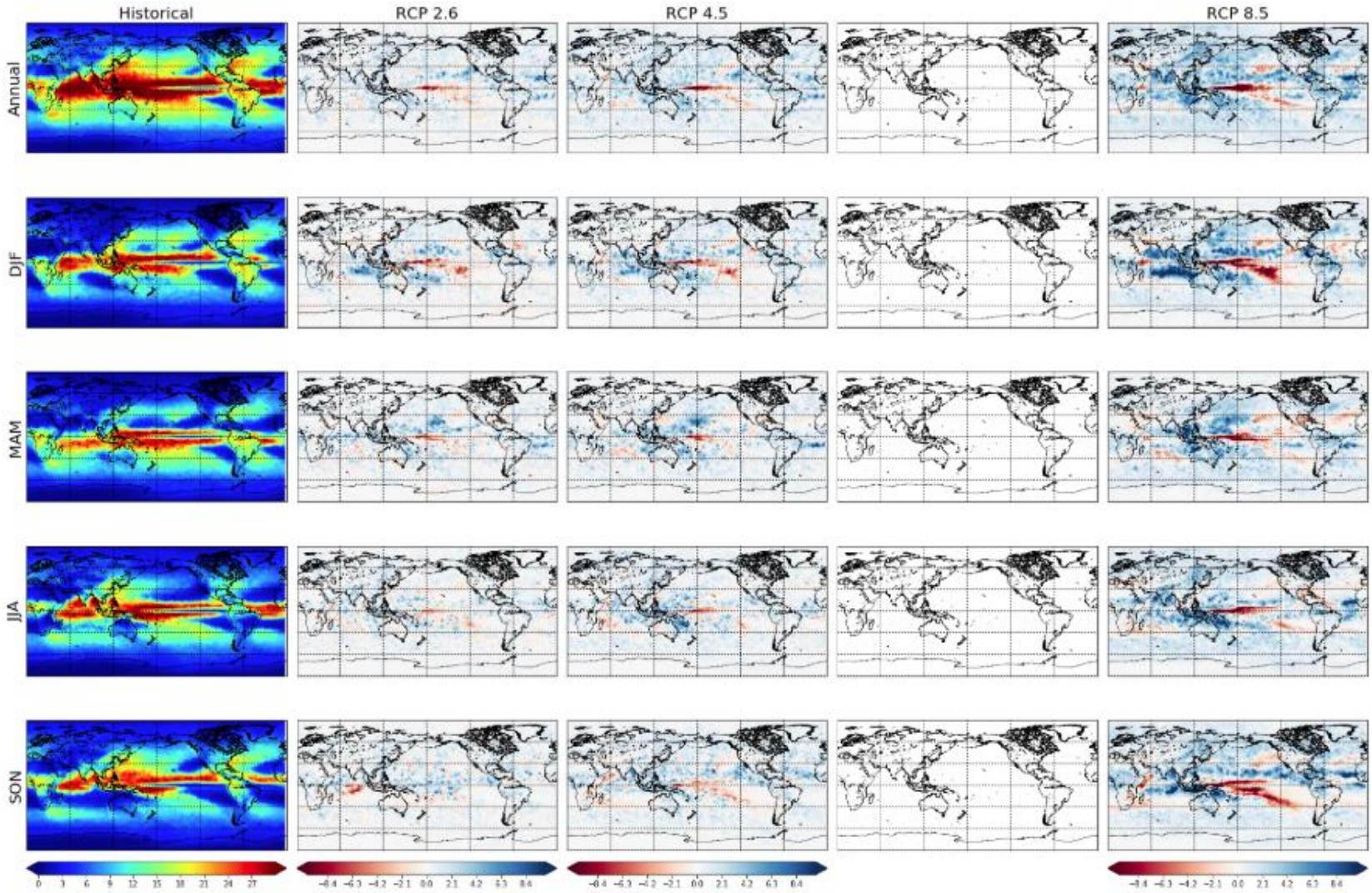

C.3 Average Median Maximum Sub-Daily Precipitation

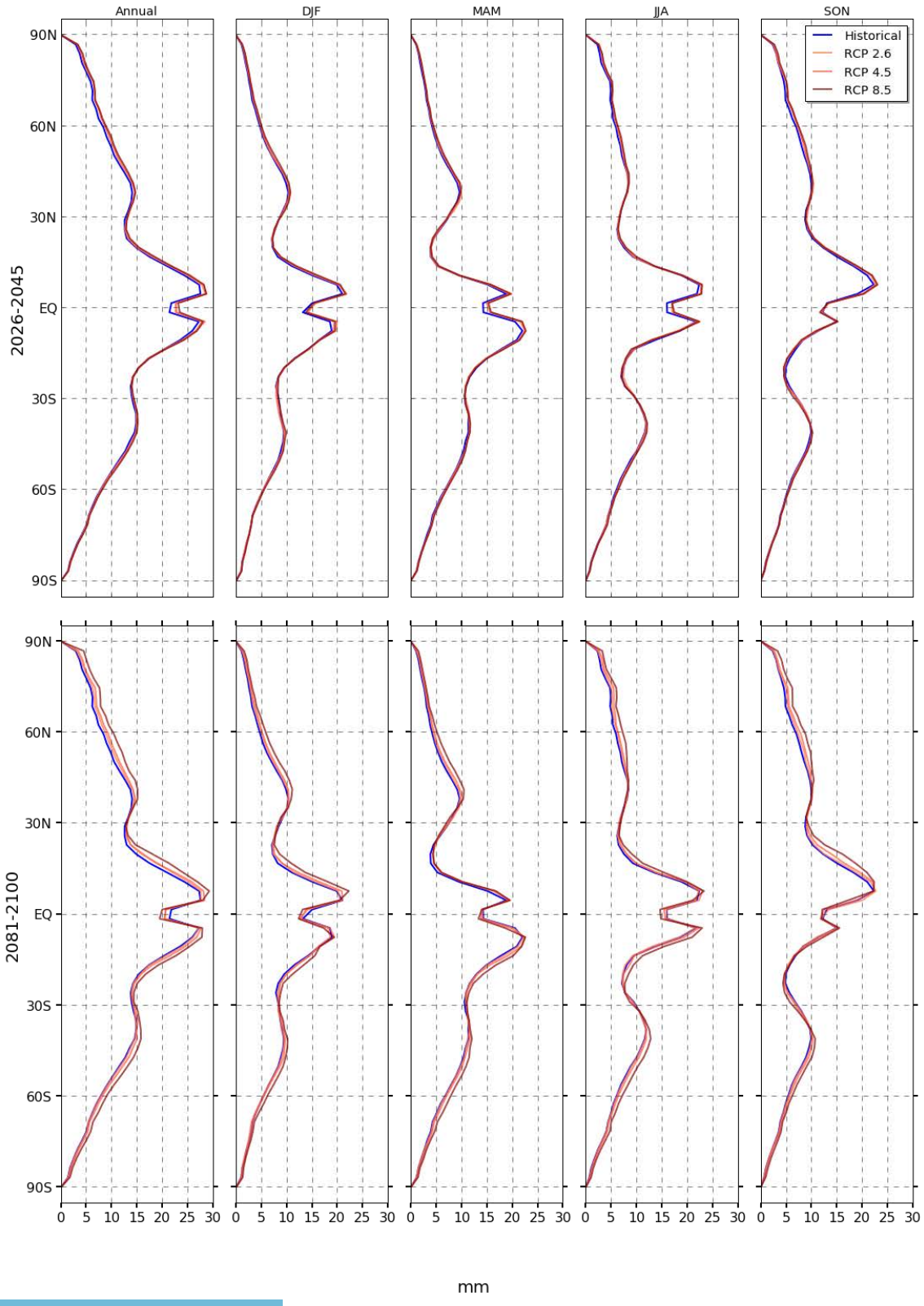

C.4 Median Maximum Daily Precipitation (2026-2045)

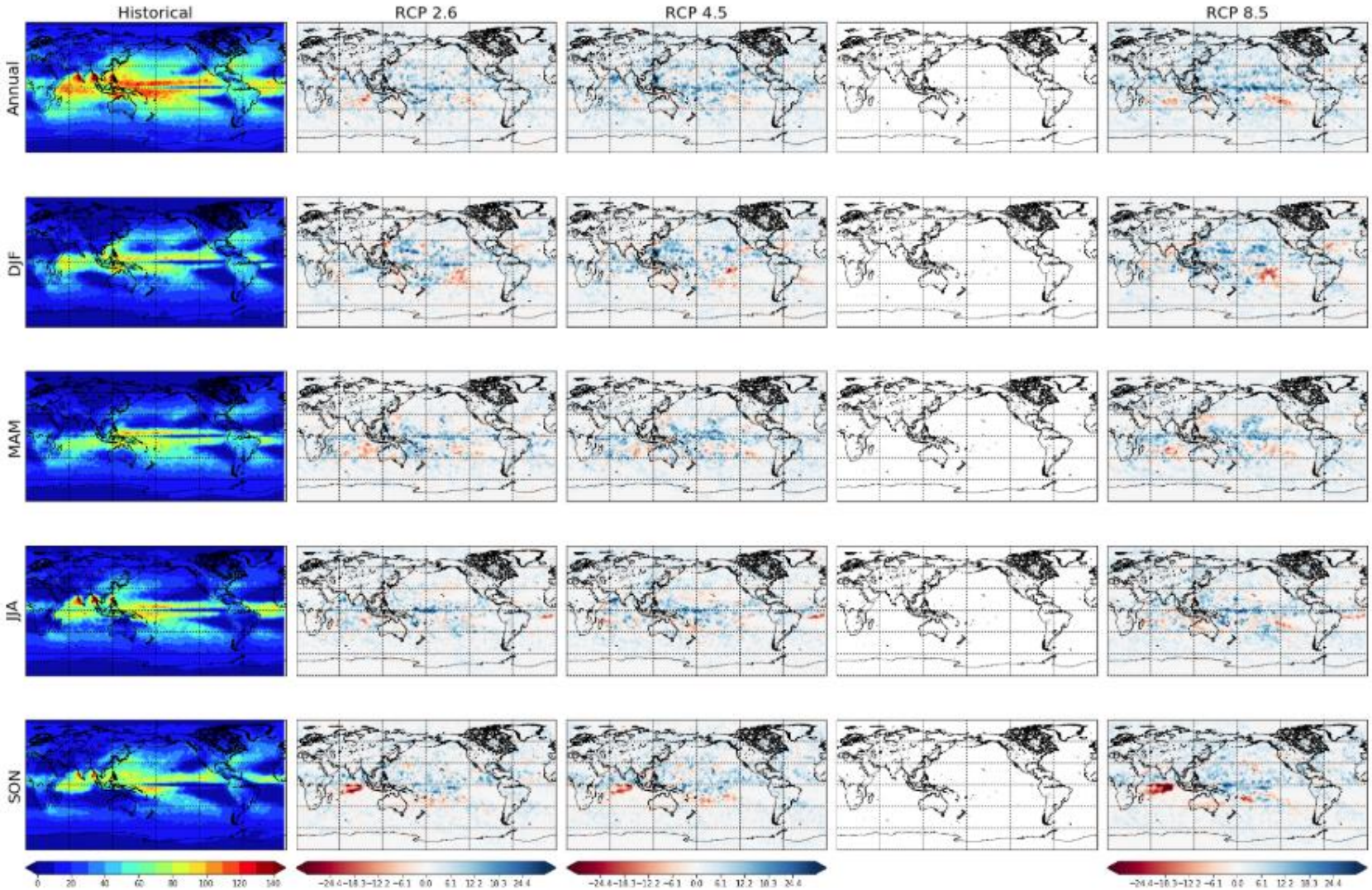

C.5 Average Median Maximum Daily Precipitation

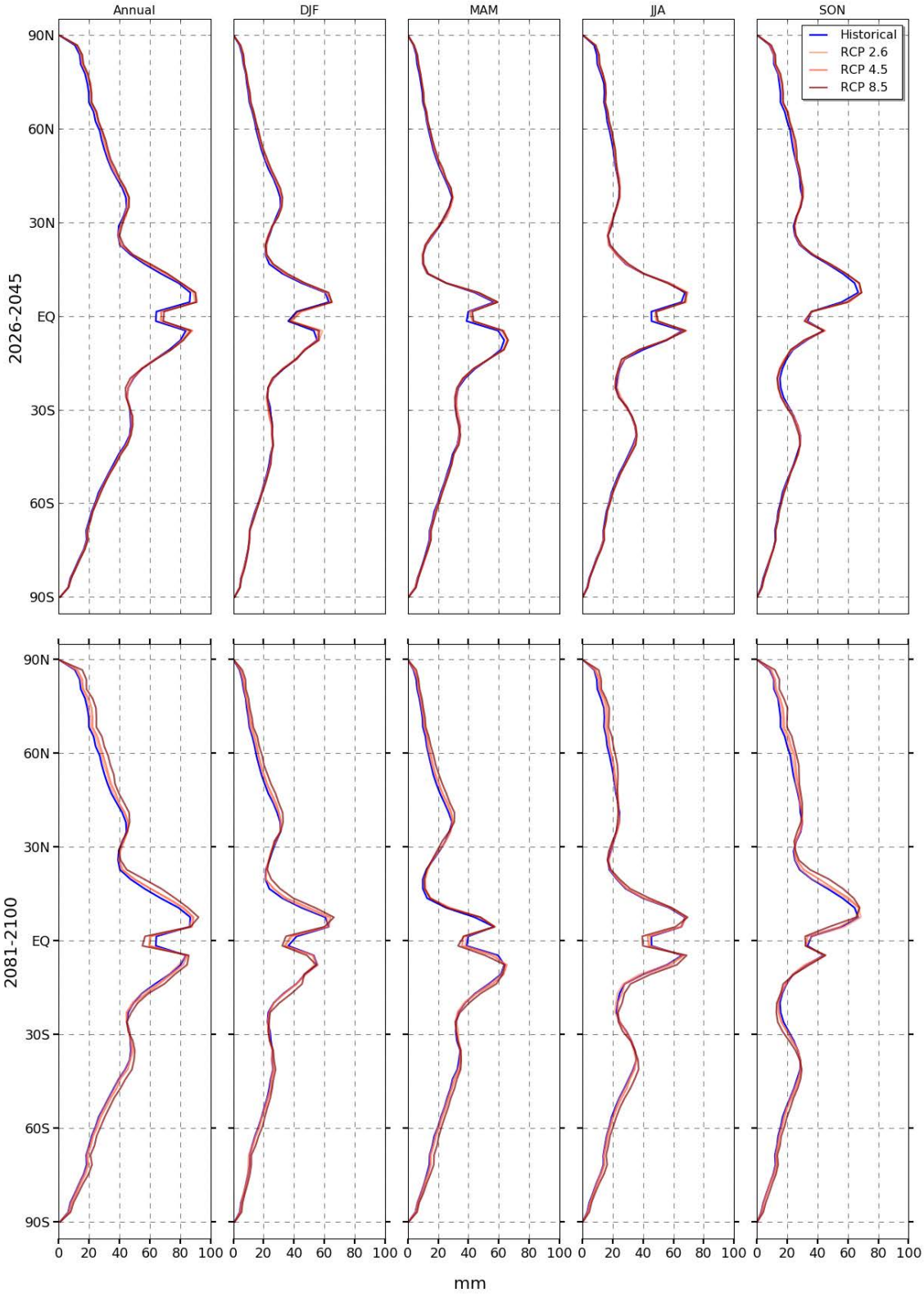

D. CNRM-CM5

D.1 Median Maximum Sub-Daily Precipitation Model-Observations

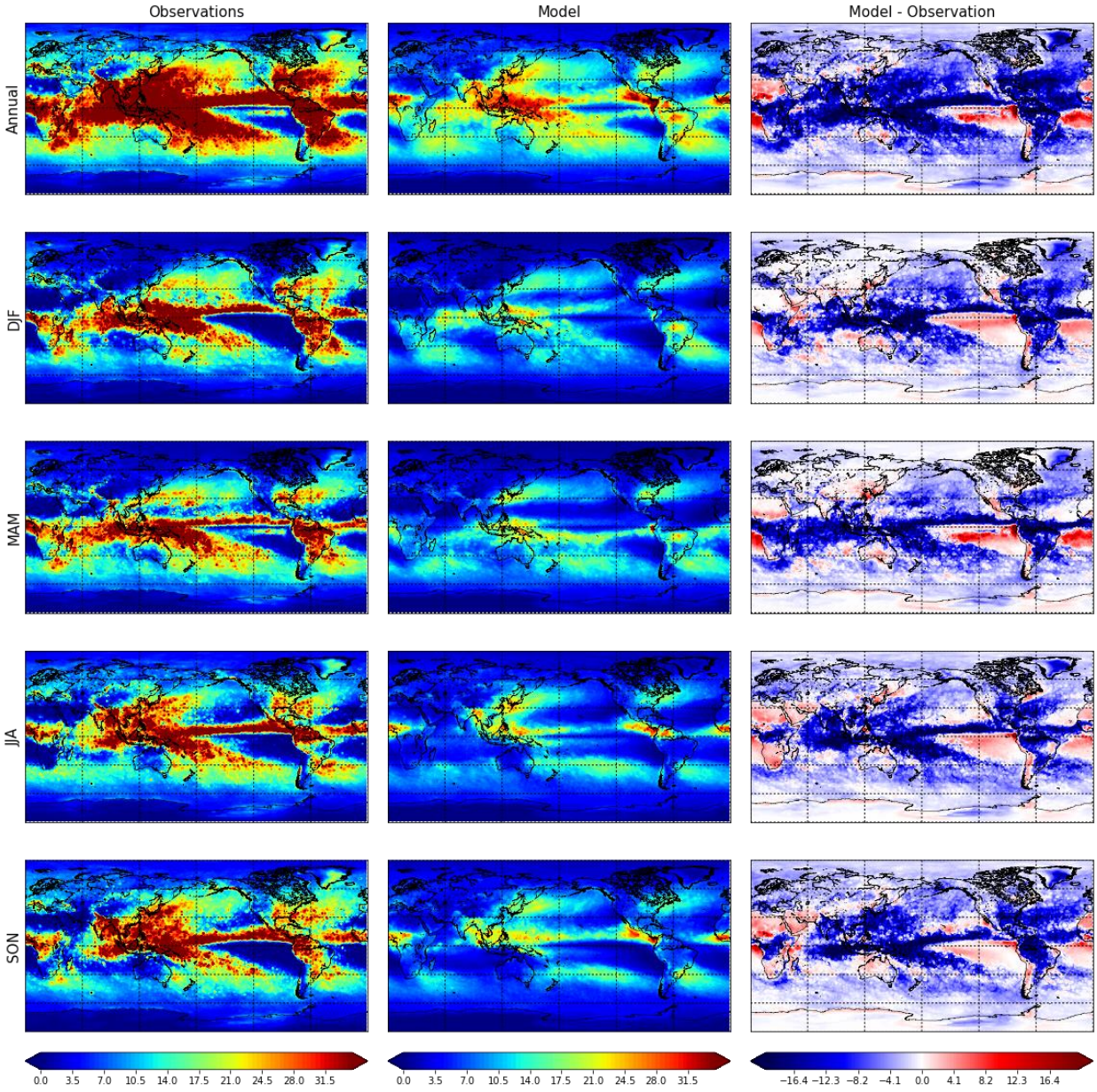

D.2 Median Maximum Sub-Daily Precipitation (2026-2045)

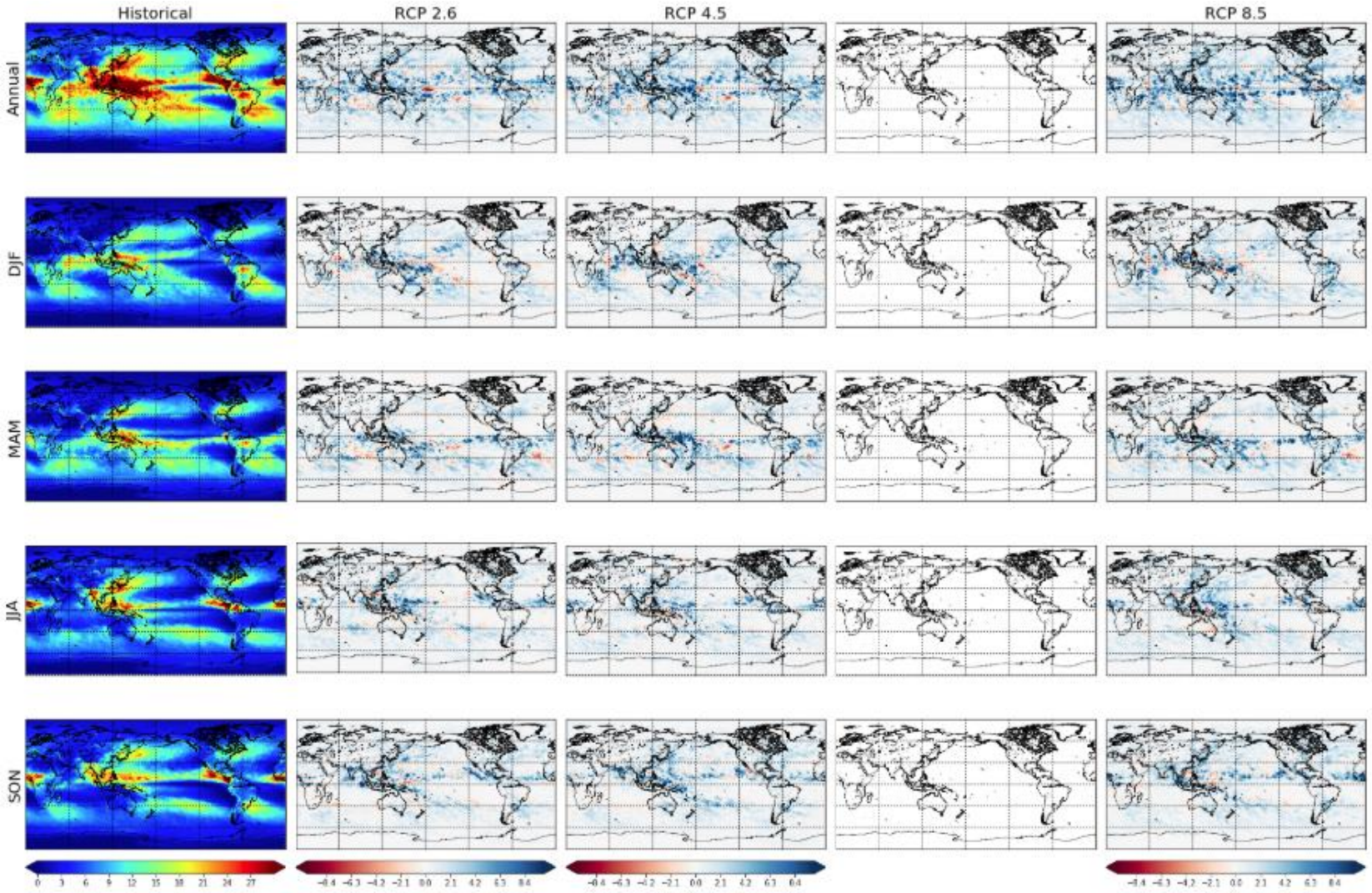

D.3 Median Maximum Sub-Daily Precipitation (2081-2100)

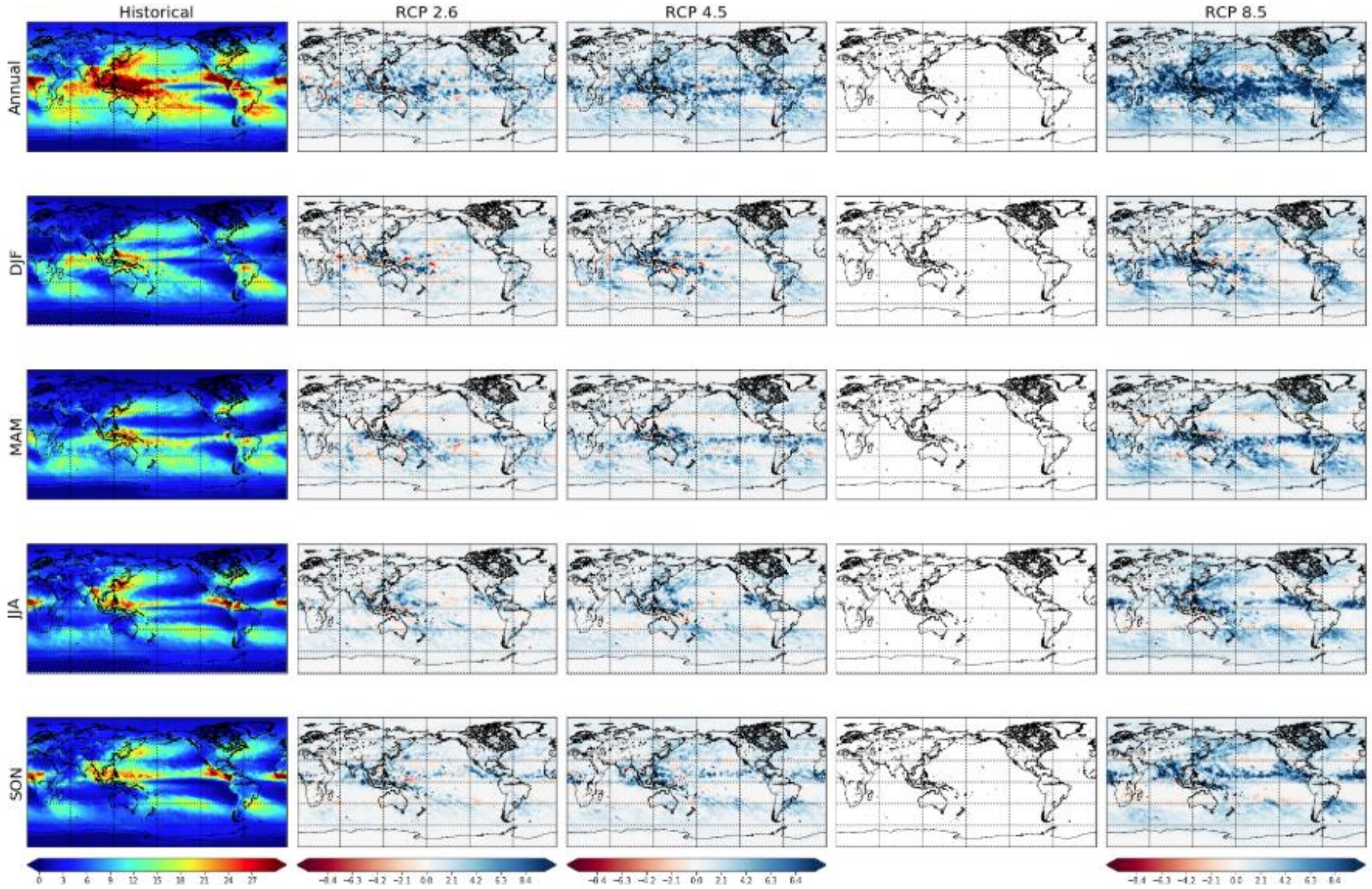

D.4 Average Median Maximum Sub-Daily Precipitation

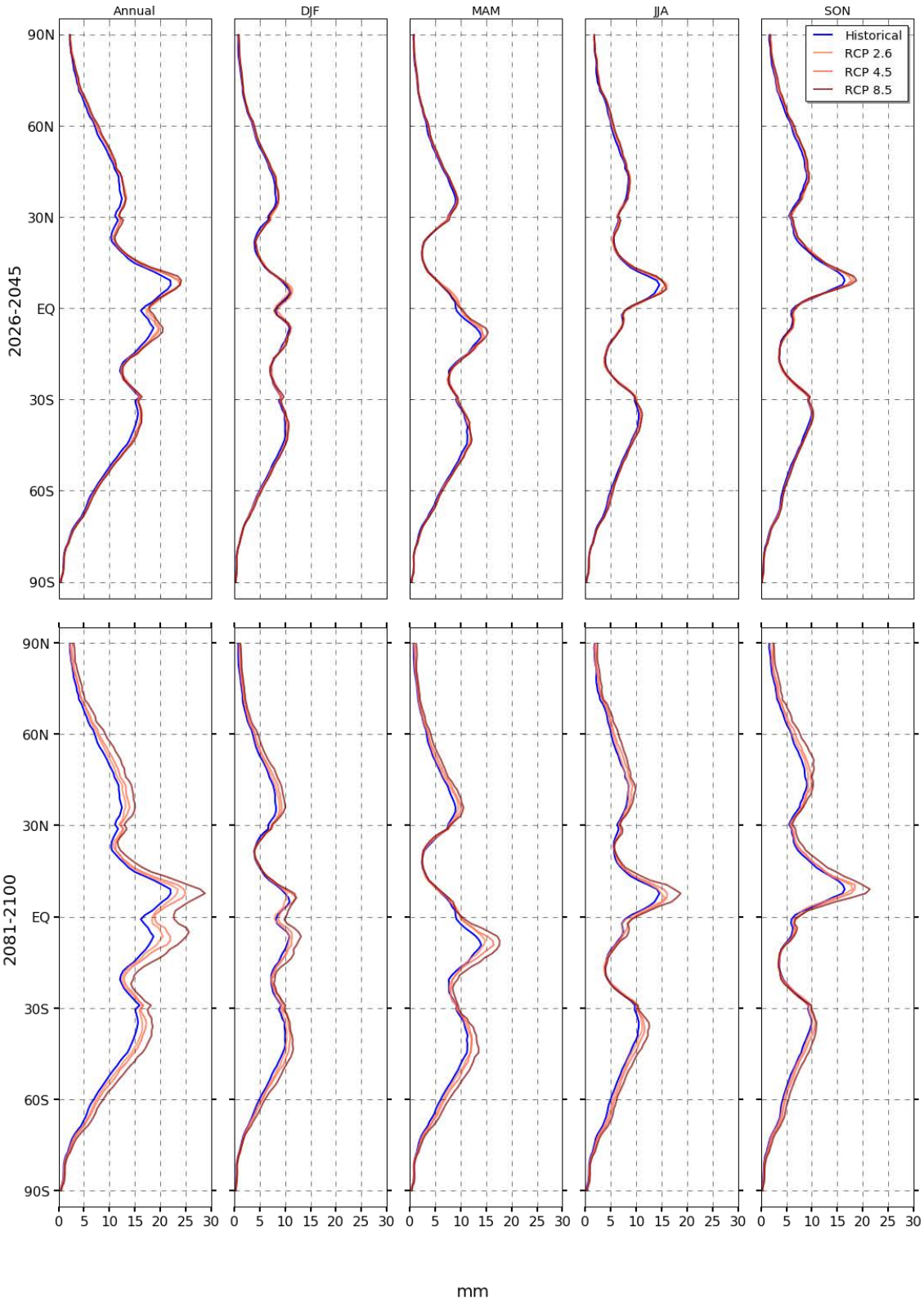

D.5 Median Maximum Daily Precipitation Model-Observations

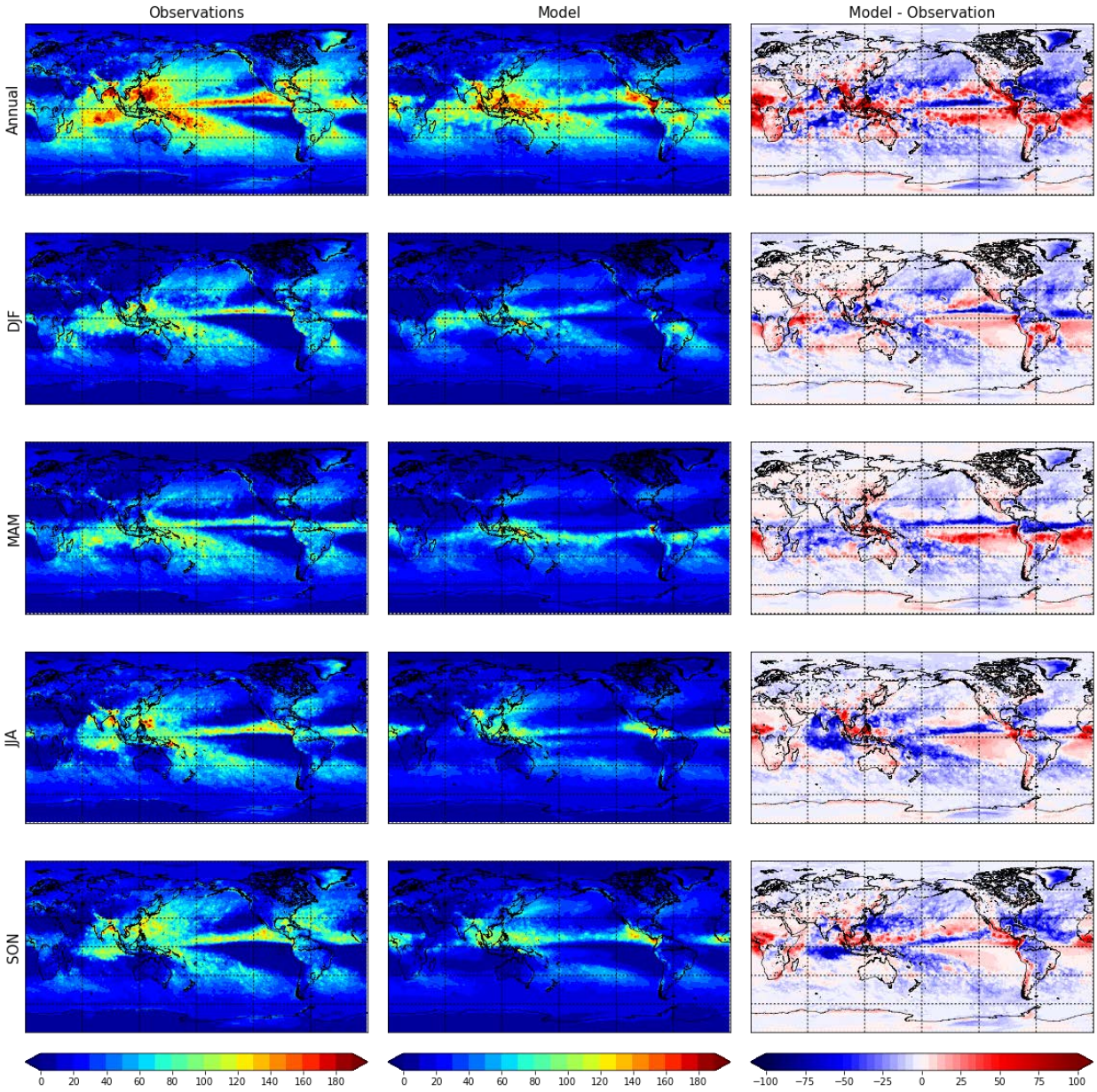

D.6 Median Maximum Daily Precipitation (2026-2045)

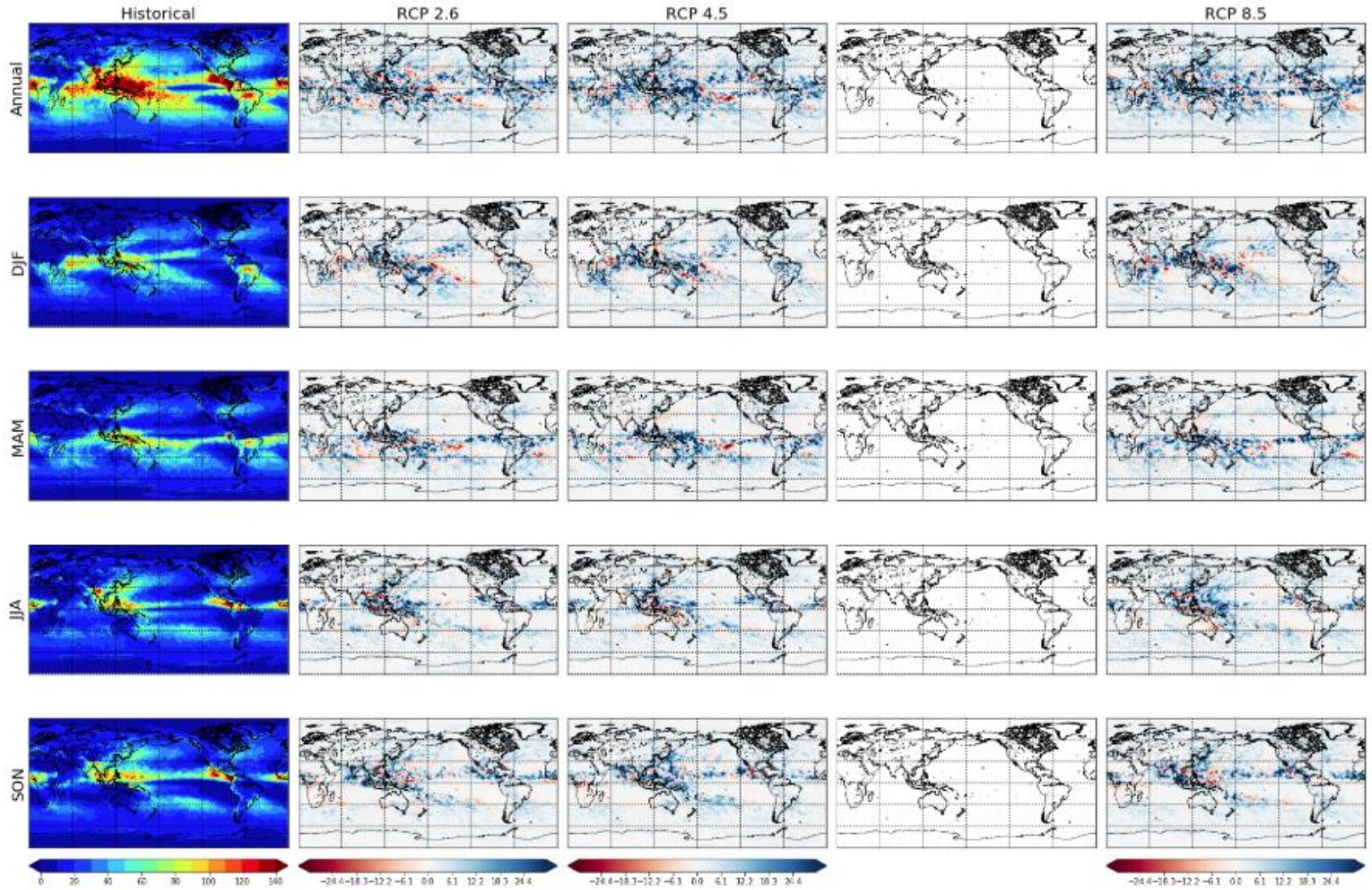

D.7 Median Maximum Daily Precipitation (2081-2100)

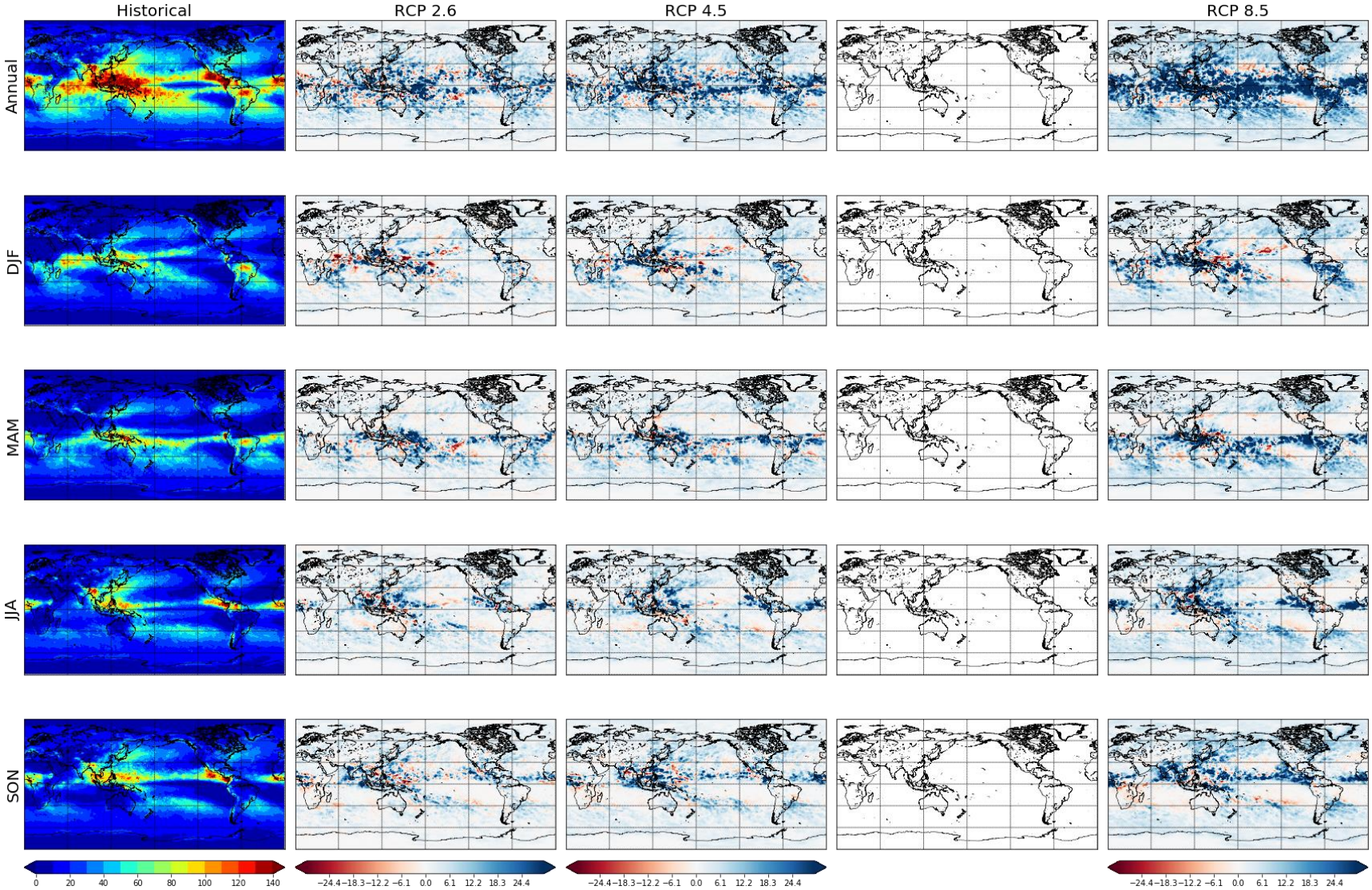

D.8 Average Median Maximum Daily Precipitation

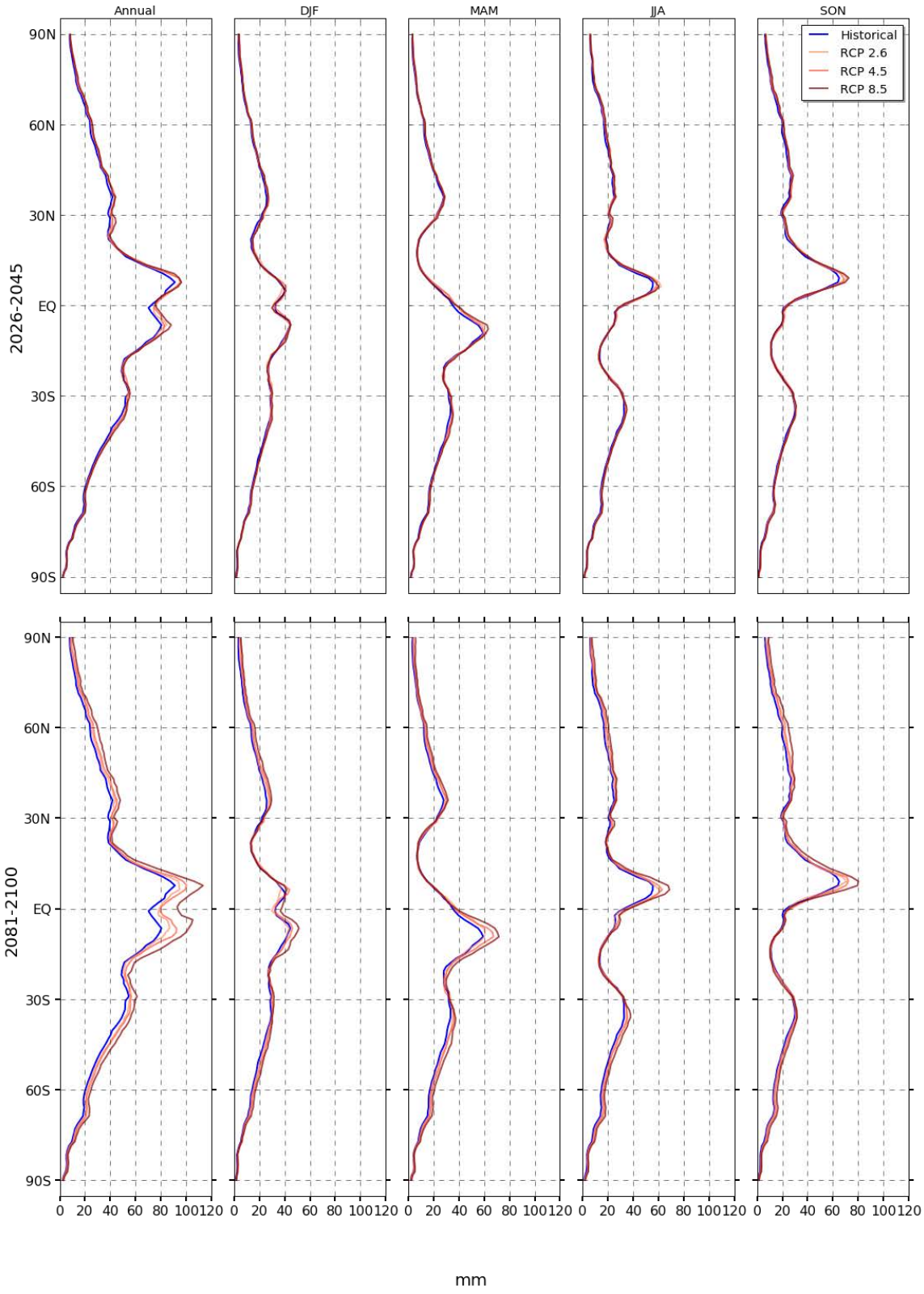

E. MRI-CGCM3

E.1 Median Maximum Sub-Daily Precipitation Model-Observations

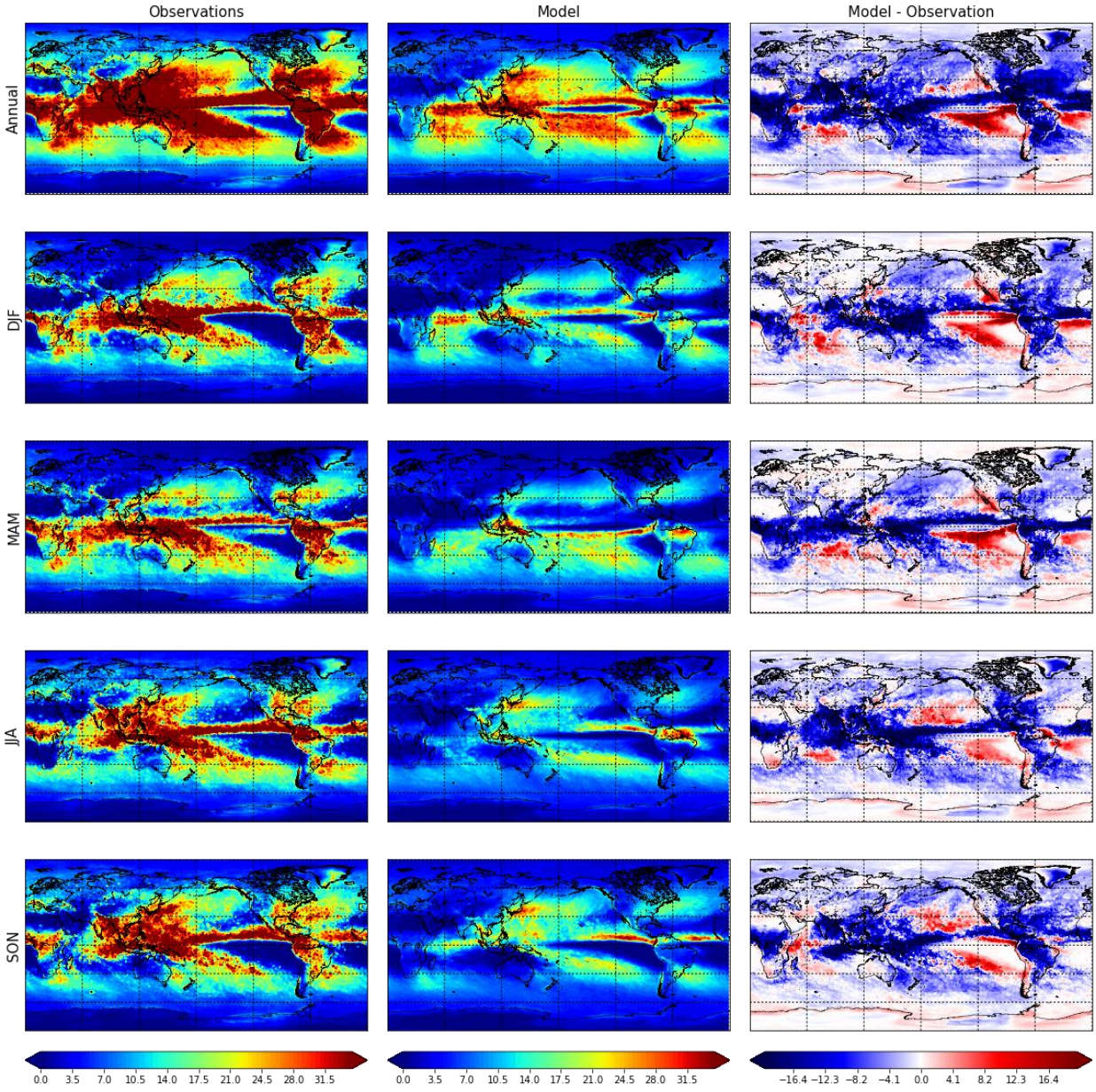

E.2 Median Maximum Sub-Daily Precipitation (2026-2045)

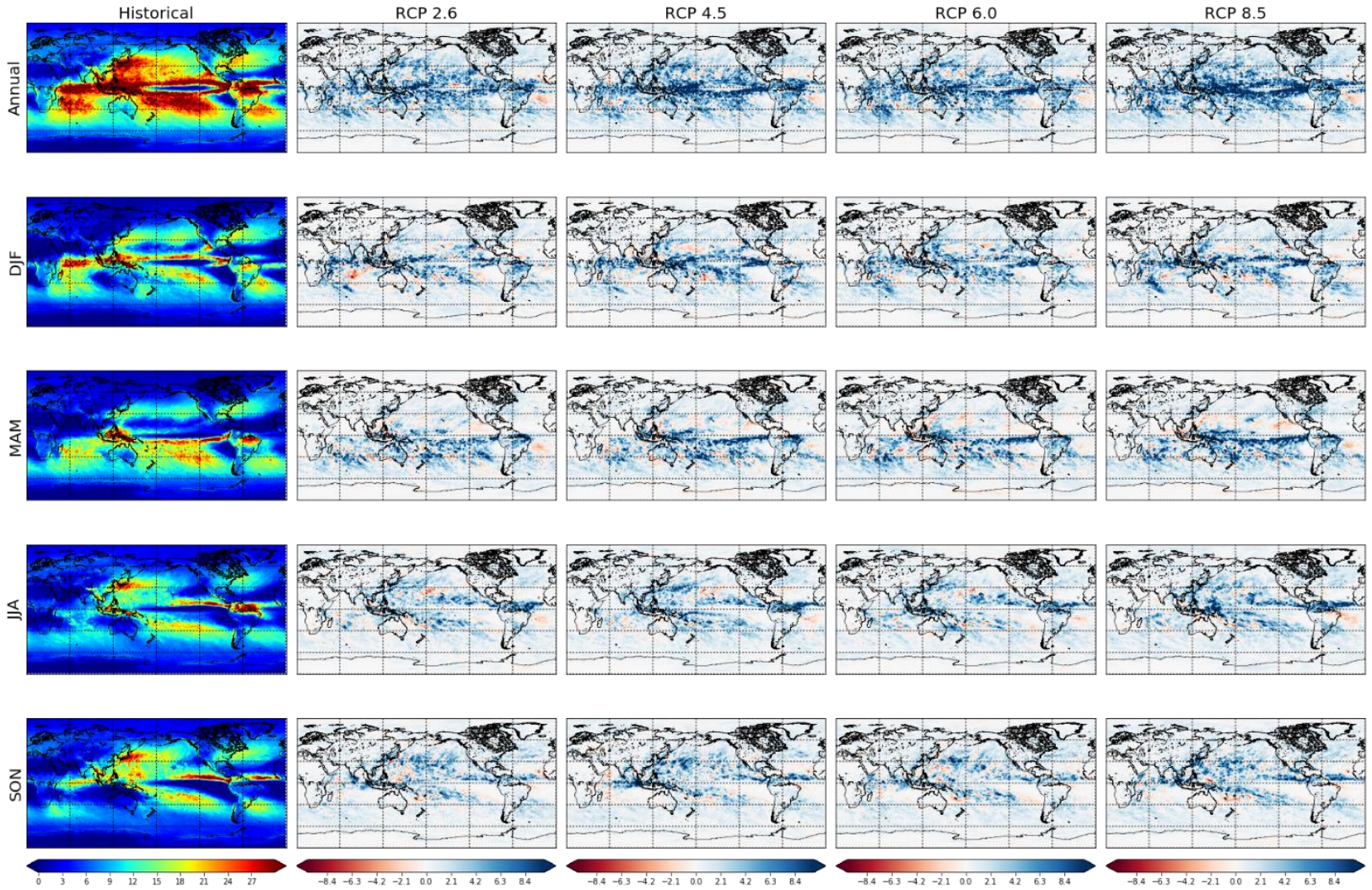

E.3 Median Maximum Sub-Daily Precipitation (2081-2100)

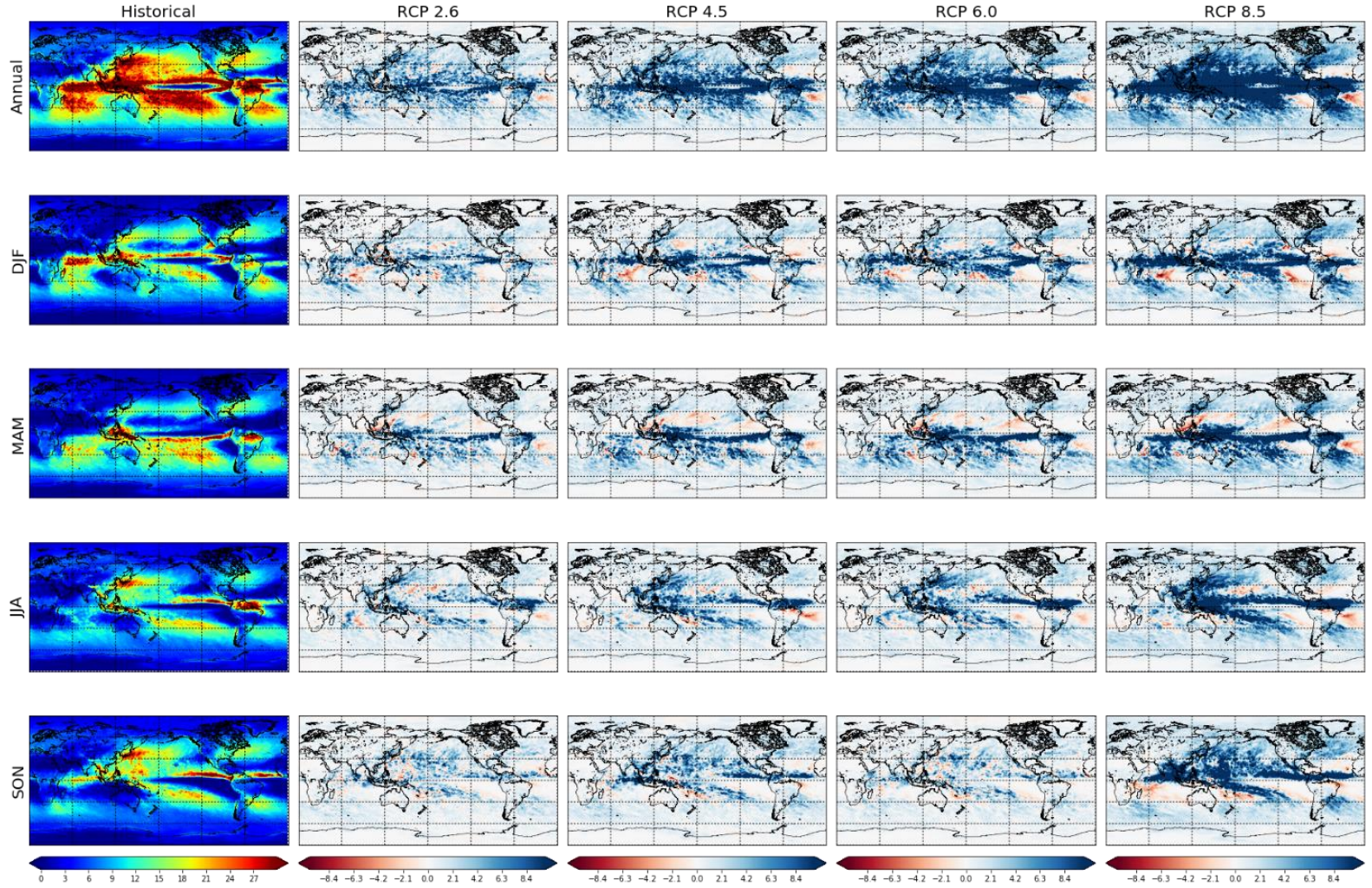

E.4 Average Median Maximum Sub-Daily Precipitation

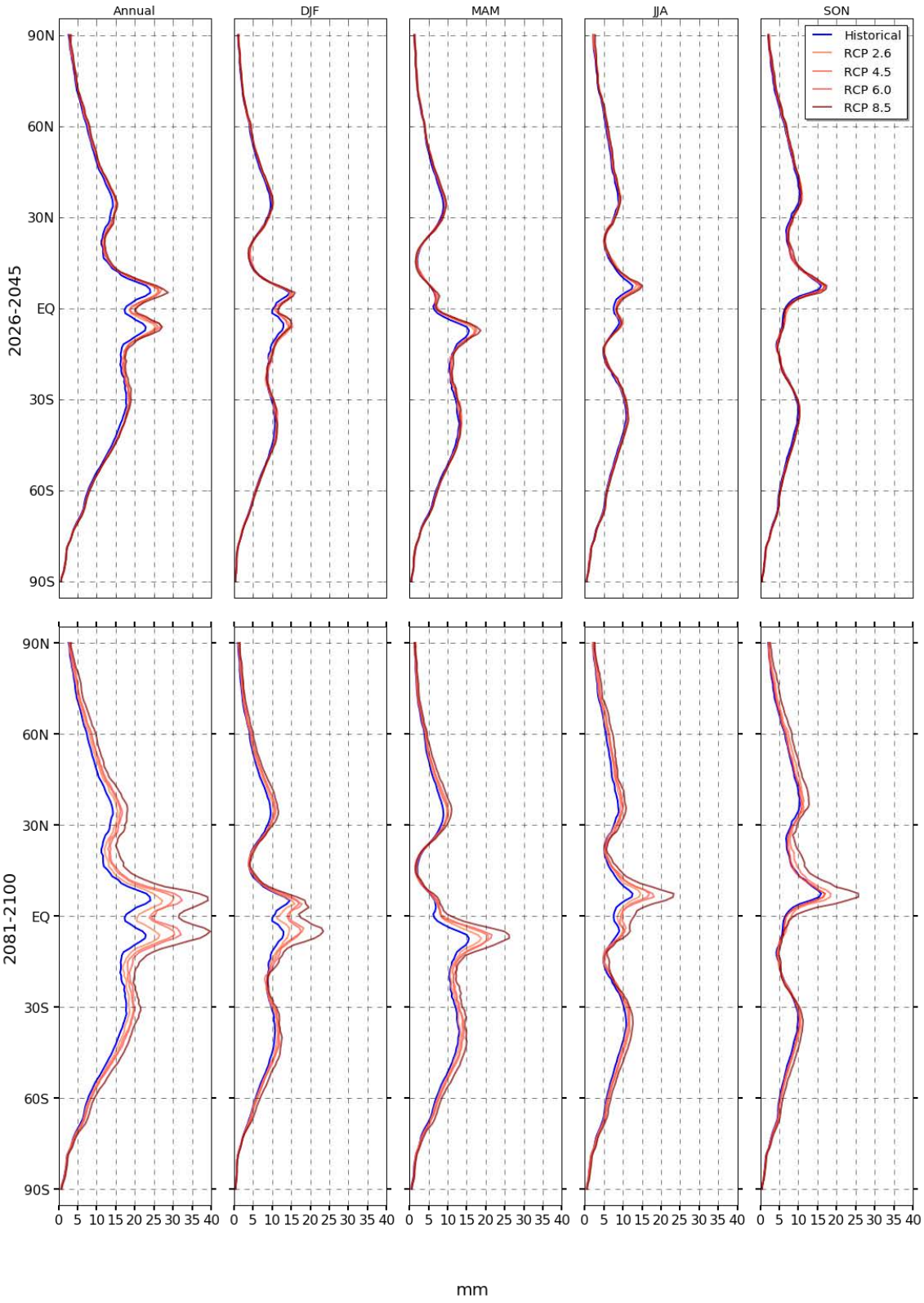

E.5 Median Maximum Daily Precipitation Model-Observations

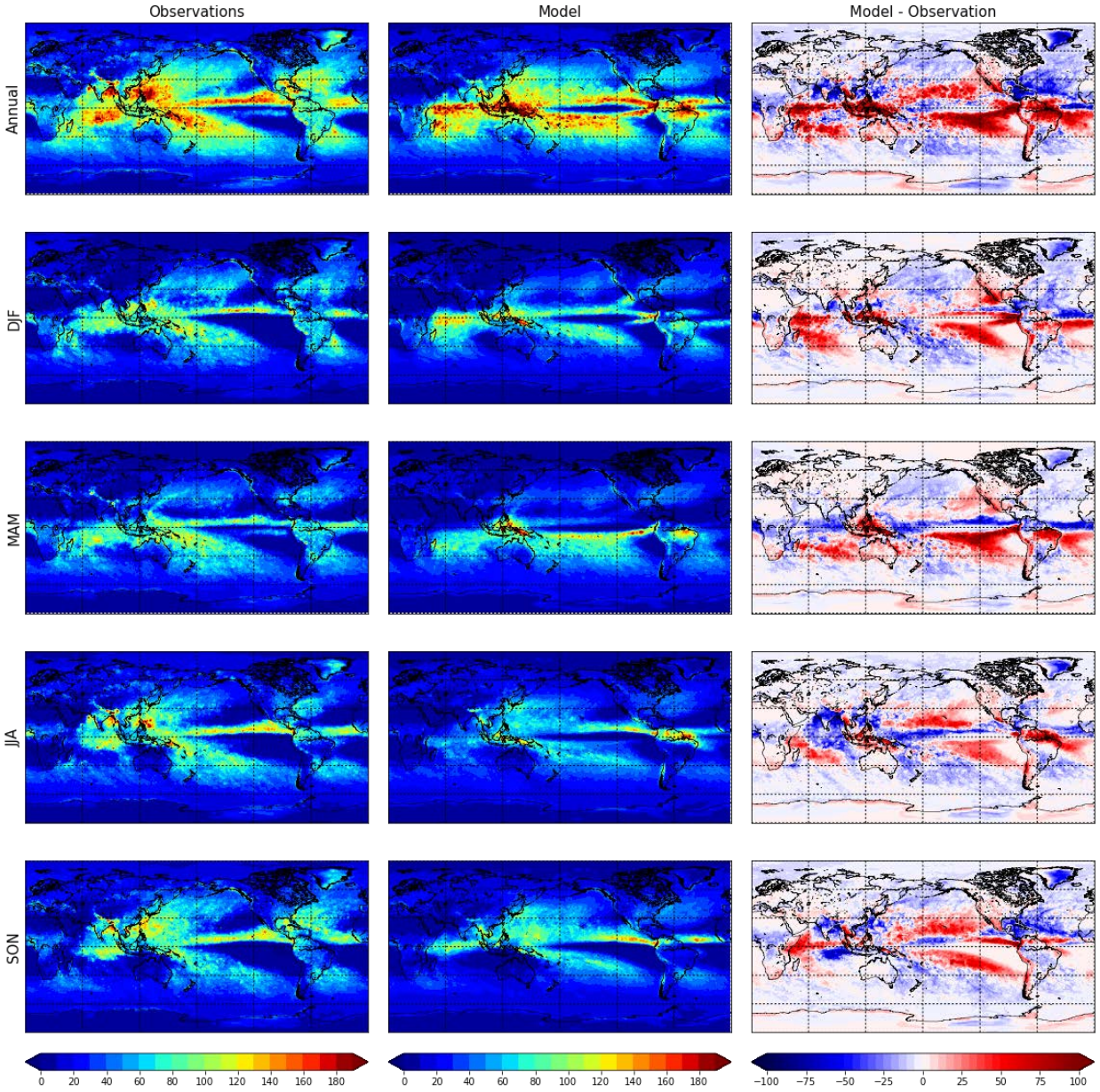

E.6 Median Maximum Daily Precipitation (2026-2045)

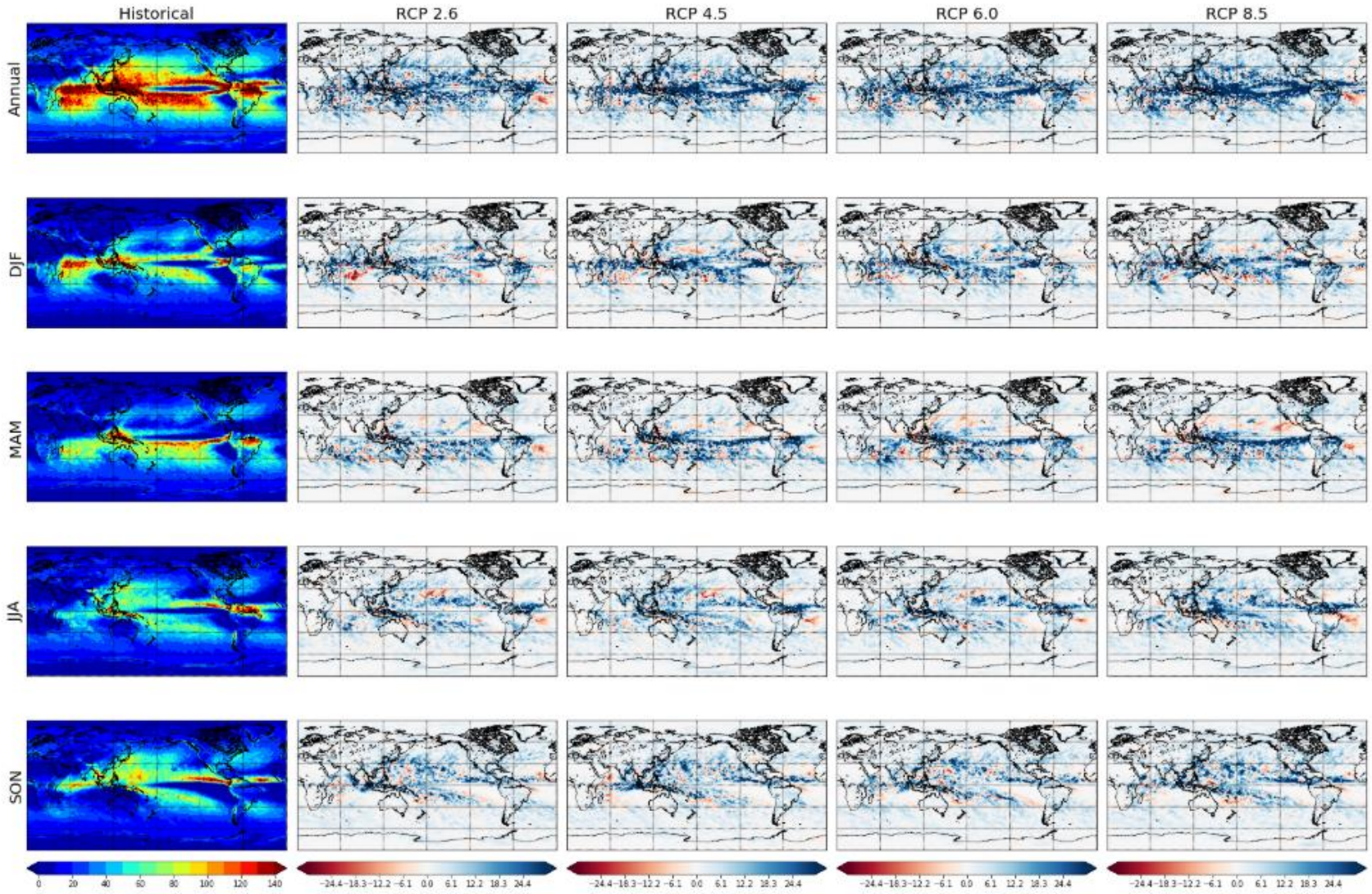

E.7 Median Maximum Daily Precipitation (2081-2100)

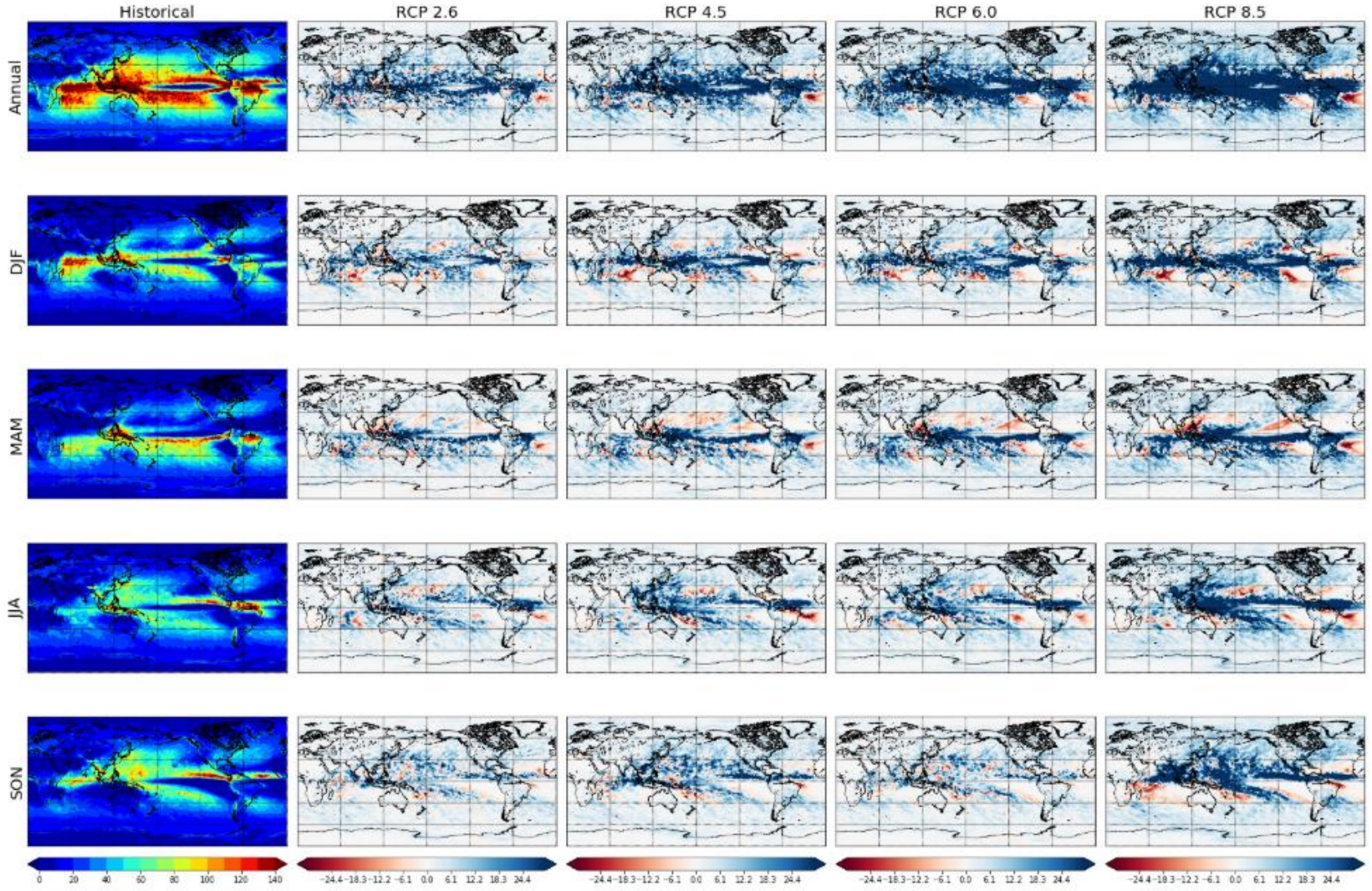

E.8 Average Median Maximum Daily Precipitation

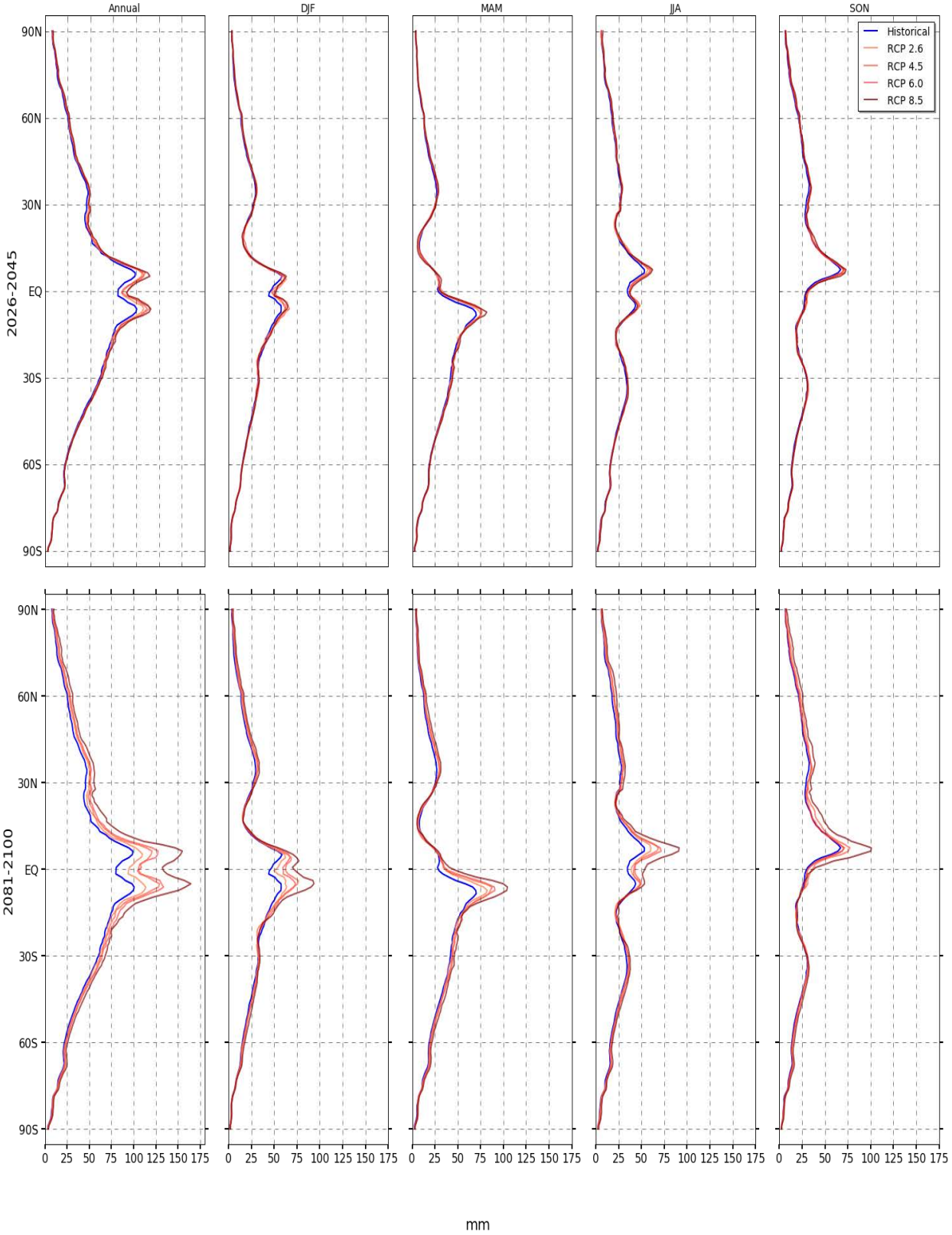

F. MRI-ESM1

F.1 Median Maximum Sub-Daily Precipitation Model-Observations

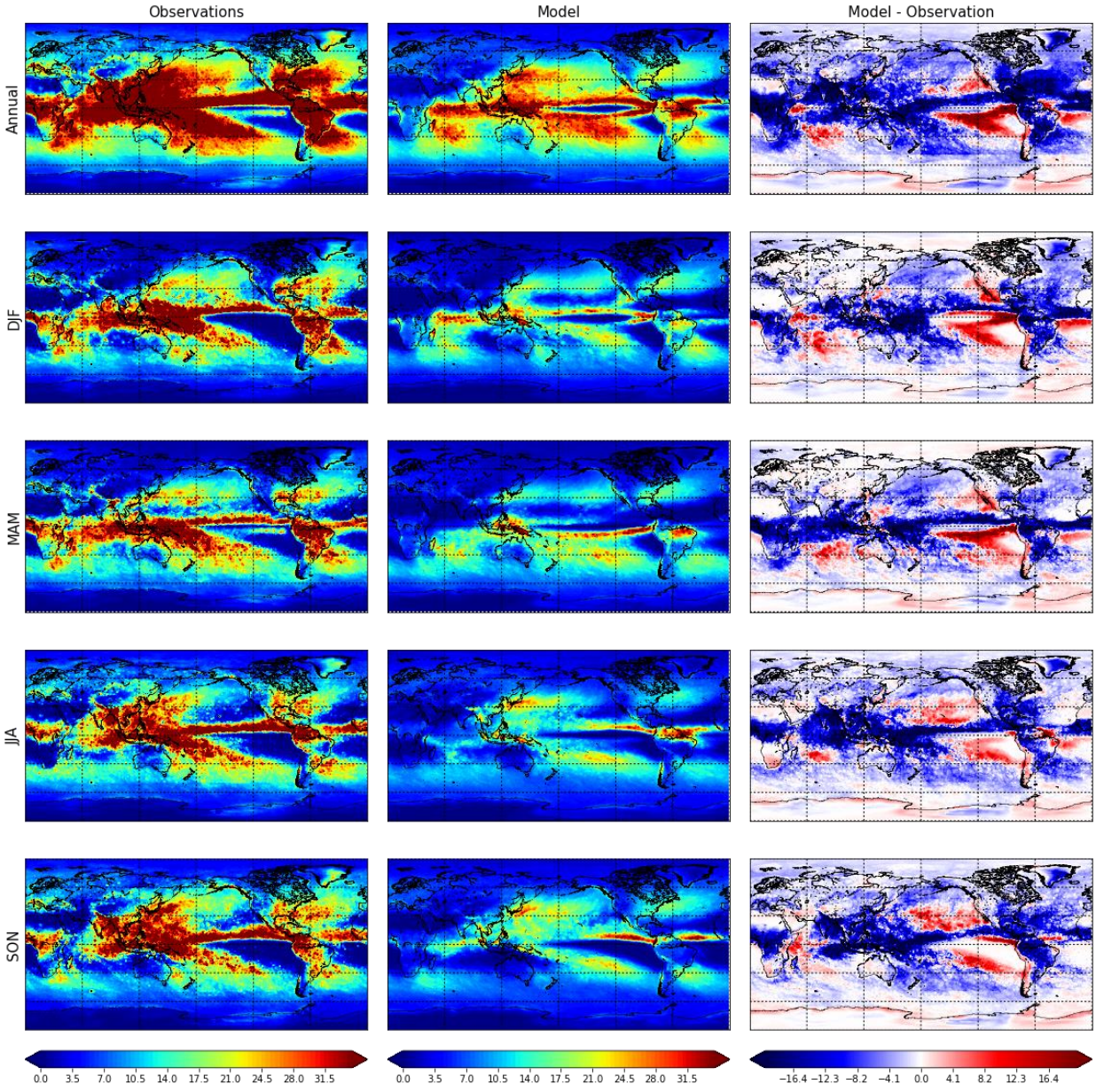

F.2 Median Maximum Sub-Daily Precipitation (2026-2045)

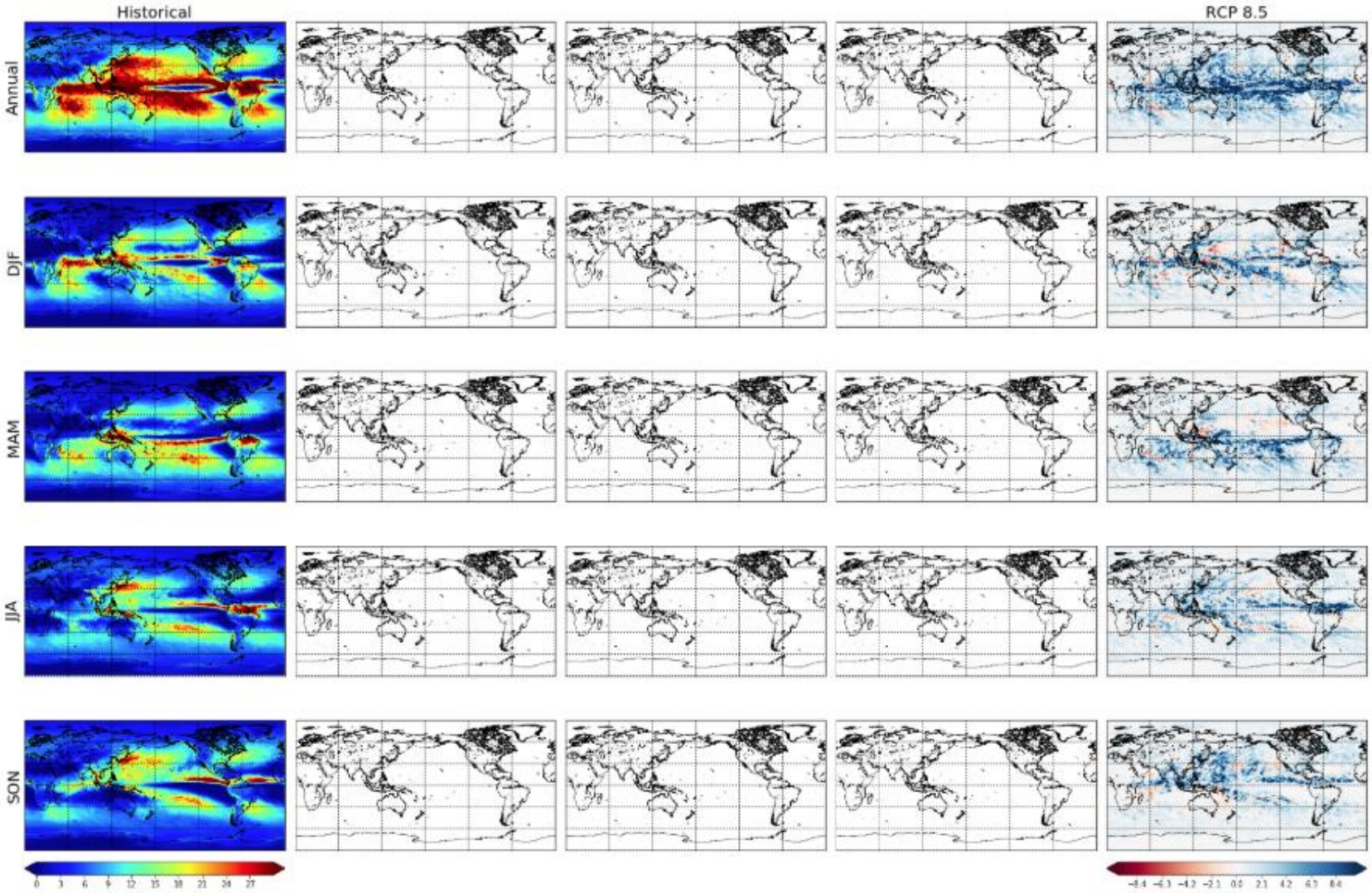

F.3 Median Maximum Sub-Daily Precipitation (2081-2100)

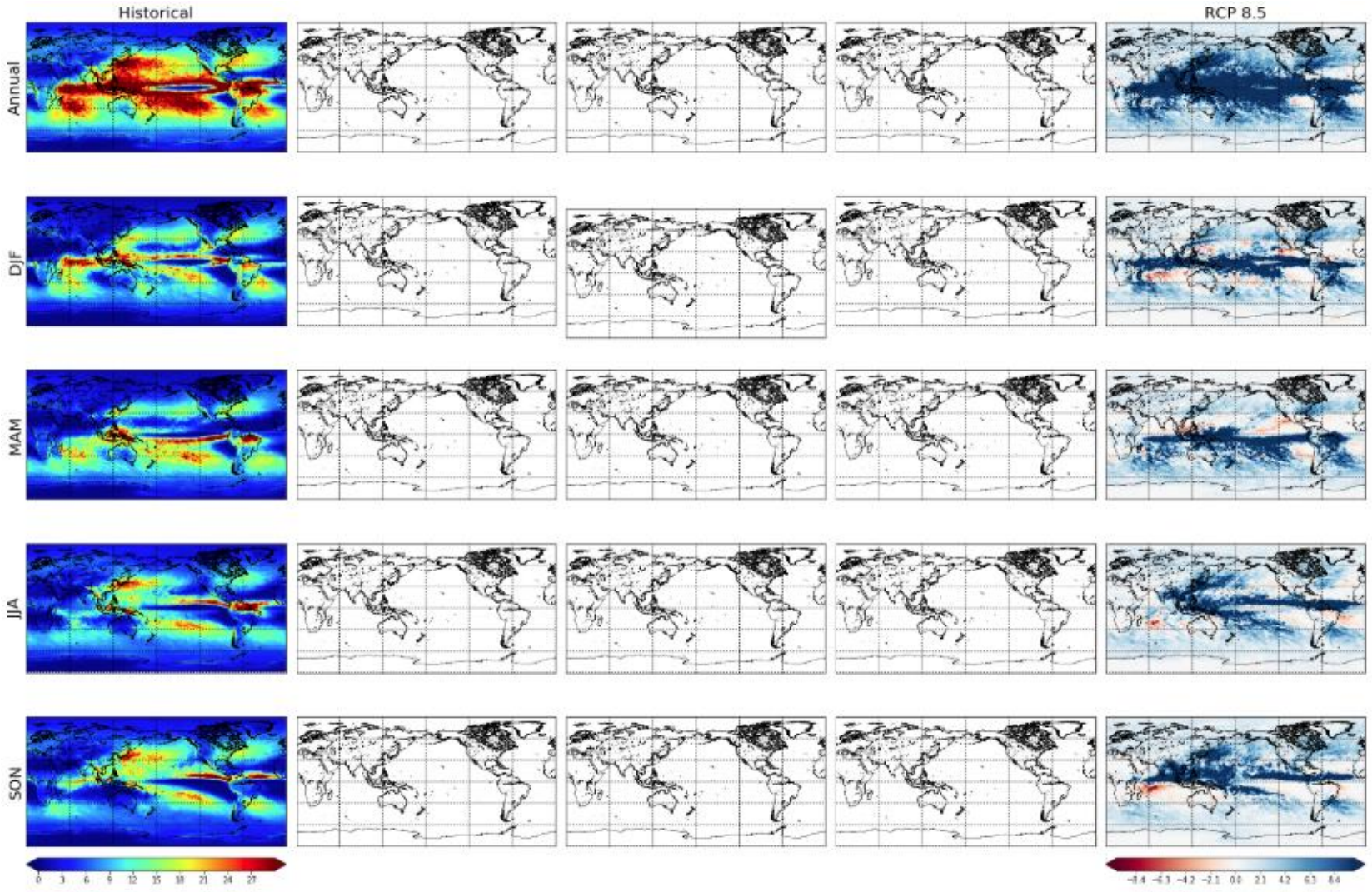

F.4 Average Median Maximum Sub-Daily Precipitation

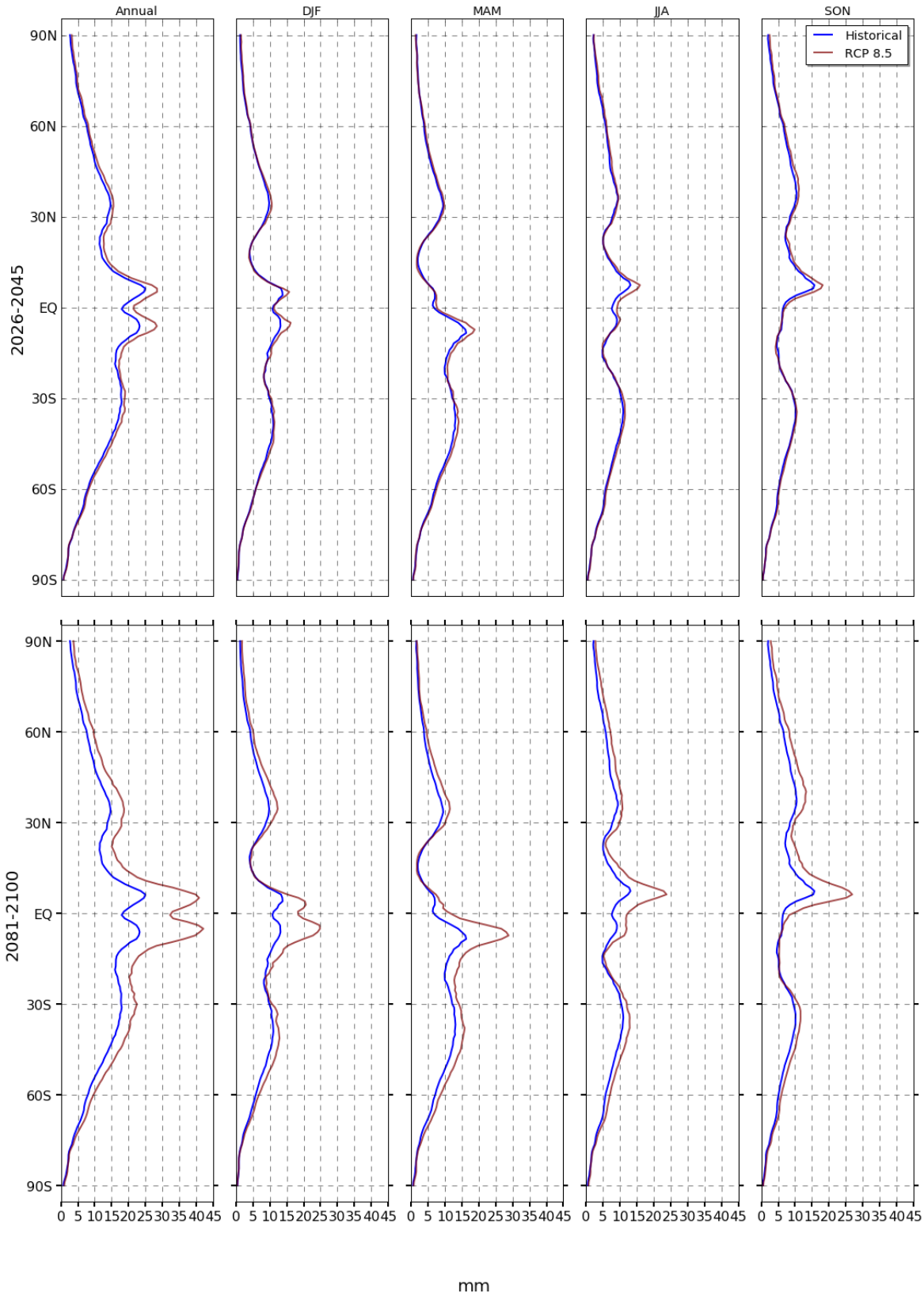

F.5 Median Maximum Daily Precipitation Model-Observations

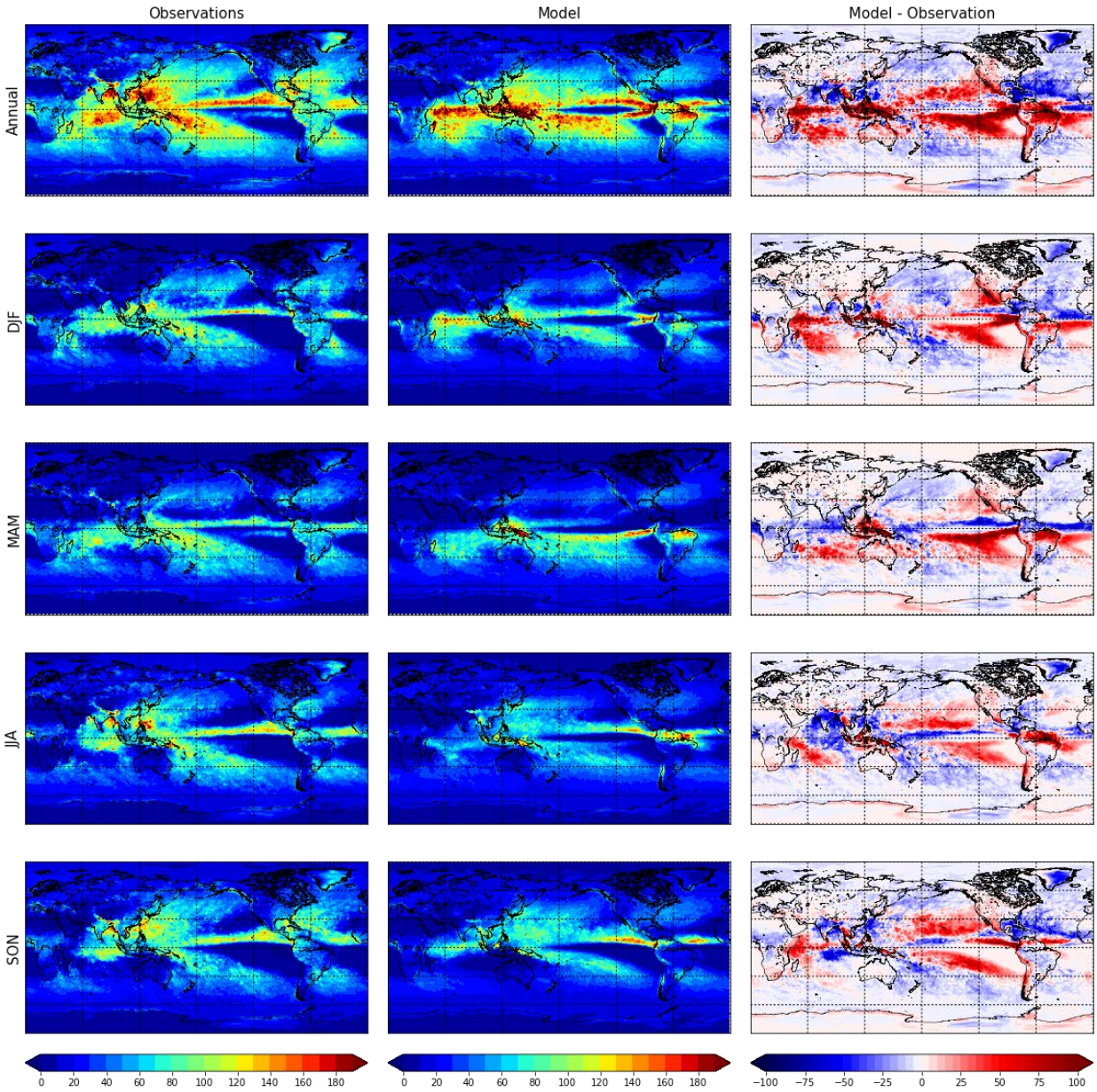

F.6 Median Maximum Daily Precipitation (2026-2045)

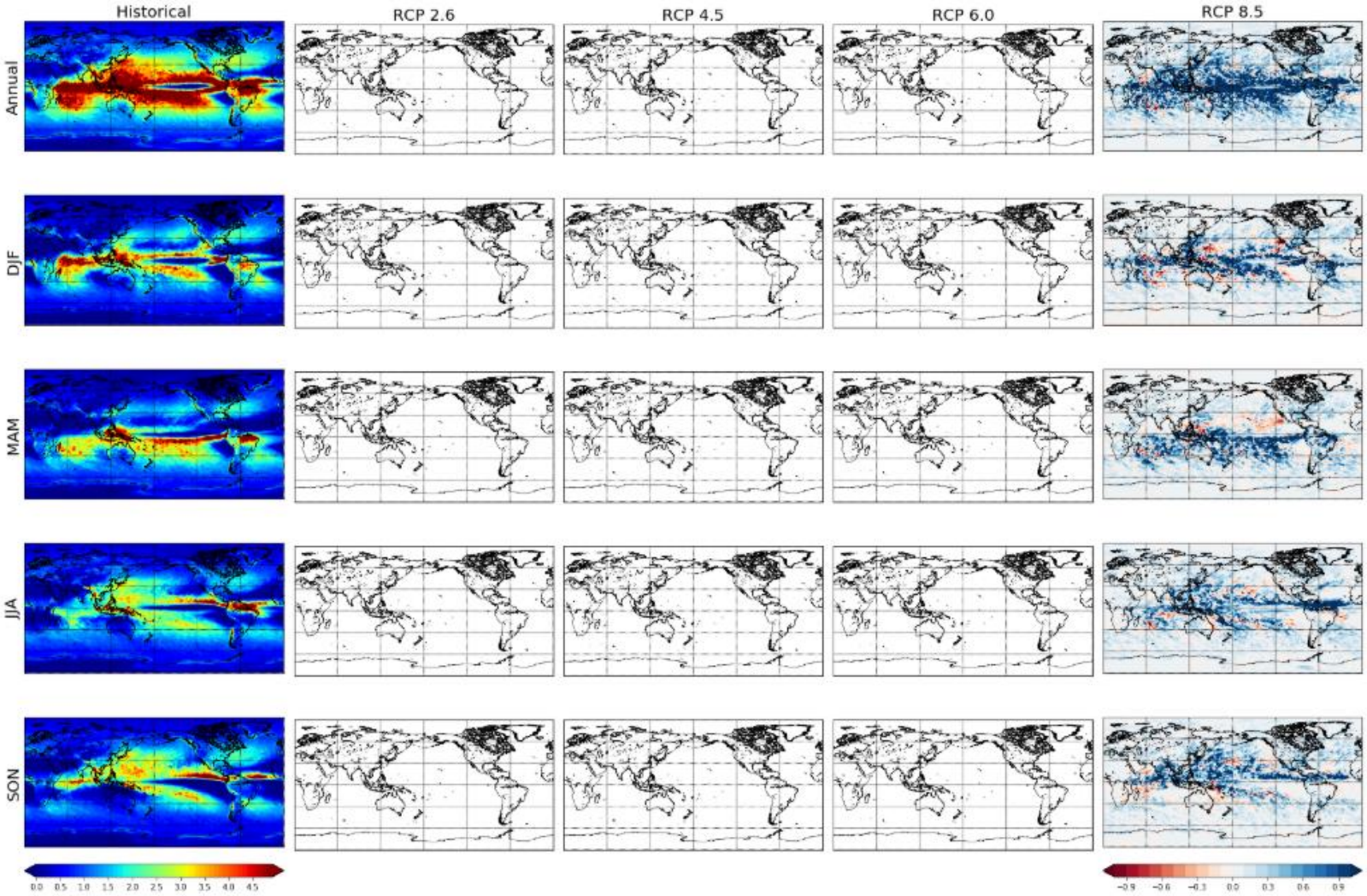

F.7 Median Maximum Daily Precipitation (2081-2100)

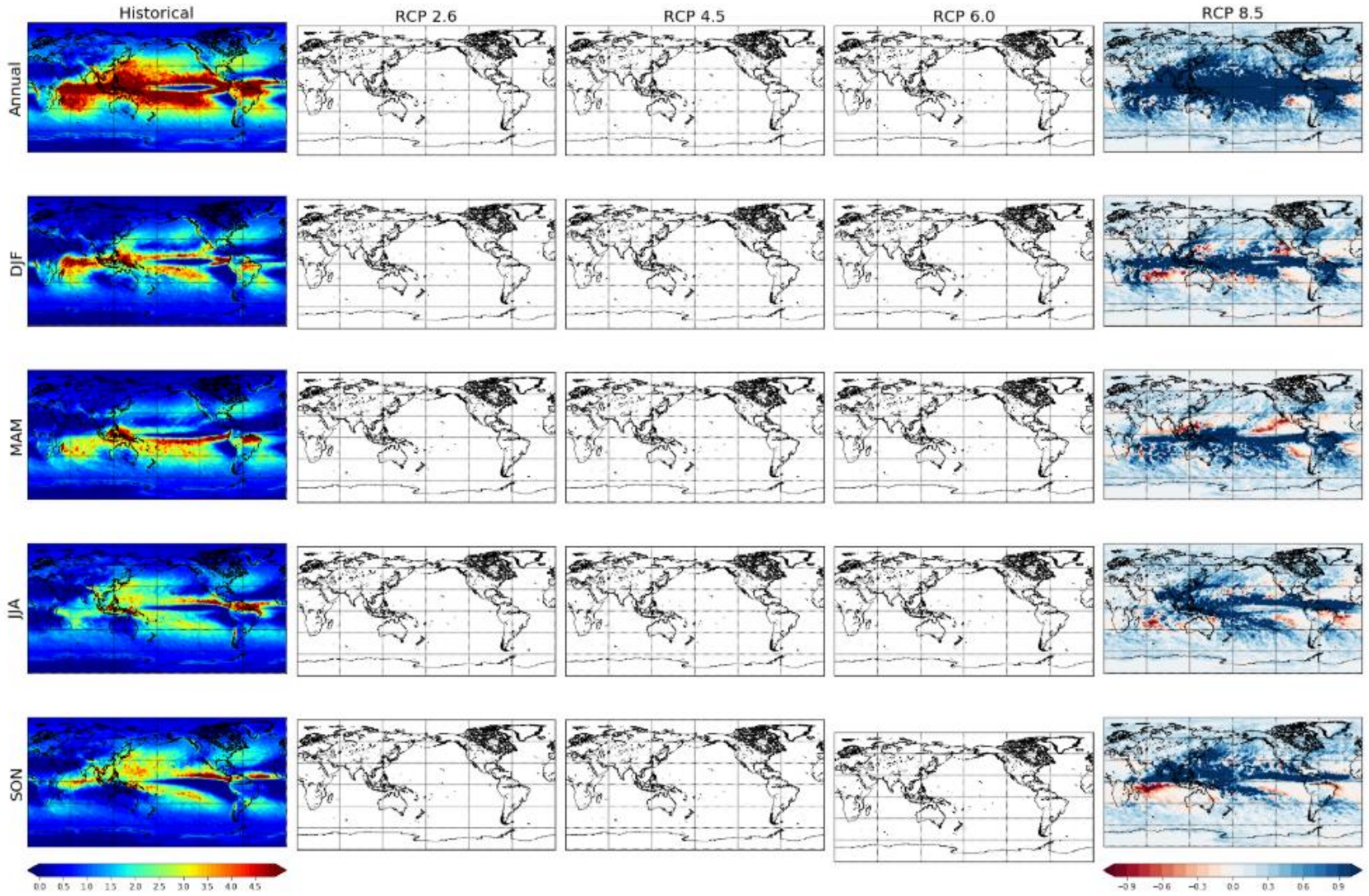

F.8 Average Median Maximum Daily Precipitation